PART II:

RV AKADEMIK LAVRENTYEV CRUISE 29

LEG 2

PUSAN - SEA OF OKHOTSK - PUSAN - VLADIVOSTOK

JUNE 27 - AUGUST 7, 2002

Table of contents

PART II: CRUISE REPORT LV29: SECOND LEG OF THE 29TH CRUISE OF RV *AKADEMIK LAVRENTYEV*, JUNE-AUGUST 2002

1. CRUISE NARRATIVE

Nicole Biebow and Ruslan Kulinich

After having completed the first leg RV *Akademik Lavrentyev* entered Pusan harbor again in the morning of June 27th. There, the video equipment and the multibeam echosounder were offloaded, and the German coring equipment, the sediment echosounder, the multinet and spares for the winch were onloaded. In addition, 5 German and 9 Russian colleagues left the ship, being replaced by new working groups.

We left Pusan harbor again at noon of June 28th in direction of the Okhotsk Sea. Those of us who had taken part in Leg 1 used the transit for finishing their cruise reports, while the new colleagues aboard equipped the labs and installed the new equipment. The scientific focus of the second leg was mainly paleoceanographic: we wanted to find out how the environment changed during the last several thousands of years and where these changes arose from. Therefore, we mainly wanted to take long cores in the key areas of the Okhotsk Sea, e.g. the estuary of the Amur River and along the straits into the Pacific Ocean. Furthermore, we planned to take many plankton samples, to dredge submarine volcanoes and to carry out seismic investigations in the Kurile Basin. The complete cruise track is shown in *Figure 1.1*; the working areas and stations are given in *Figure 1.2*.

During transit through the Japan See we stopped at 39.03.561´ N/ 133.00.650´ E for a sea bath at 21°C water and air temperature. The water depth was there 2,500 m. A bath in the ocean is a tradition on Russian research vessels, and all participants enjoyed it very much.

On July 1st, RV *Akademik Lavrentyev* passed La Perusa Strait and thereby reached the Okhotsk Sea. In the night from July 1st to 2nd, we began to work west of La Perusa Strait. At our first station we deployed the sediment echosounder SES-2000DS from Rostock University with which we were for the first time able to survey and sample sediments which continuously deposited without disturbance. In the beginning, there were problems with deploying the echosounder, because the mounting at the ship's side did not keep the echosounder in a stable position. As a result, the echosounder started strongly vibrating. Thanks to active help of the Russian crew and some improvisation we could solve the problem, and since then the echosounder worked well.
After having received spares for the deep-sea winch in Pusan and having made some modifications on it, the winch worked more or less fine, too.

The usual daily work on the paleoceanographic stations now was performed as follows: Firstly, we mapped the seafloor with the sediment echosounder. The Russian scientists ran their seismics at the same time. Secondly, we deployed the multicorer, the Russian and German gravity corers, CTD and a multinet for plankton sampling. From July 2nd to 4th we successfully carried out these works at three stations on the northwestern continental slope of the Kurile Basin at water depths from 2,500 to 1,000 m. All gravity core deployments were successful, and we recovered three 12 m long sediment cores with the German gravity corer which cover, according to first analyses, a period of 60,000 years. Subsequent to core deploying, the Russian and German colleagues together described and sampled the cores and determined their physical properties.

In the period of July 4th to 8th RV *Akademik Lavrentyev* slowly went north along the continental slope off Sakhalin. We successfully carried out two coring transects north of 52°N and 53°N at the continental slope off northeastern Sakhalin. Mainly the perfectly working sediment echosounder made it easy for us to choose favorable stations so that every

deployment of the 12 m long core was a success. Additionally, water and plankton samples were taken.

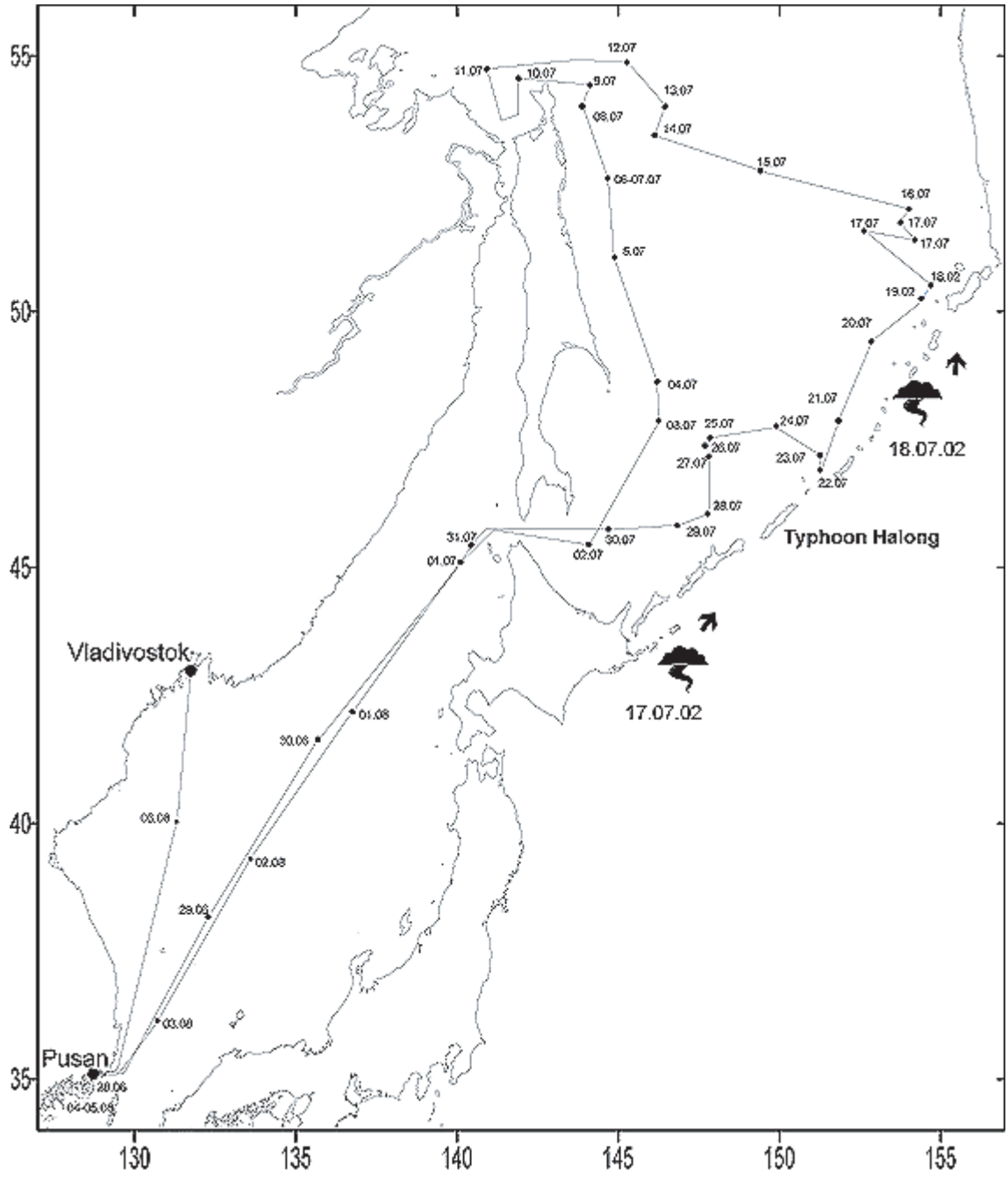

Fig. 1.1: *Ship's track of RV Akademik Lavrentyev 29th cruise, Leg 2, June - August 2002.*

After having finished the sediment core transects, we went around the northern tip of Sakhalin into the Sakhalin Gulf (Amur River estuary) on July 9th in order to take water and sediment samples there. Amur River is the largest source for fresh water and sediment of the Okhotsk Sea and the 4th largest Siberian river. Apart from that, Amur River is the only of the large Siberian rivers which does not flow into the Arctic Ocean. We were mainly interested in the effect the Amur waters have on sea-ice formation and productivity of the Okhotsk Sea. We mapped the area of the Amur River estuary two days and carried out extensive water sampling. The fact that Amur River transports large amounts of sediment into the Okhotsk Sea is visible even from the vessel, because the water here is of brownish color.

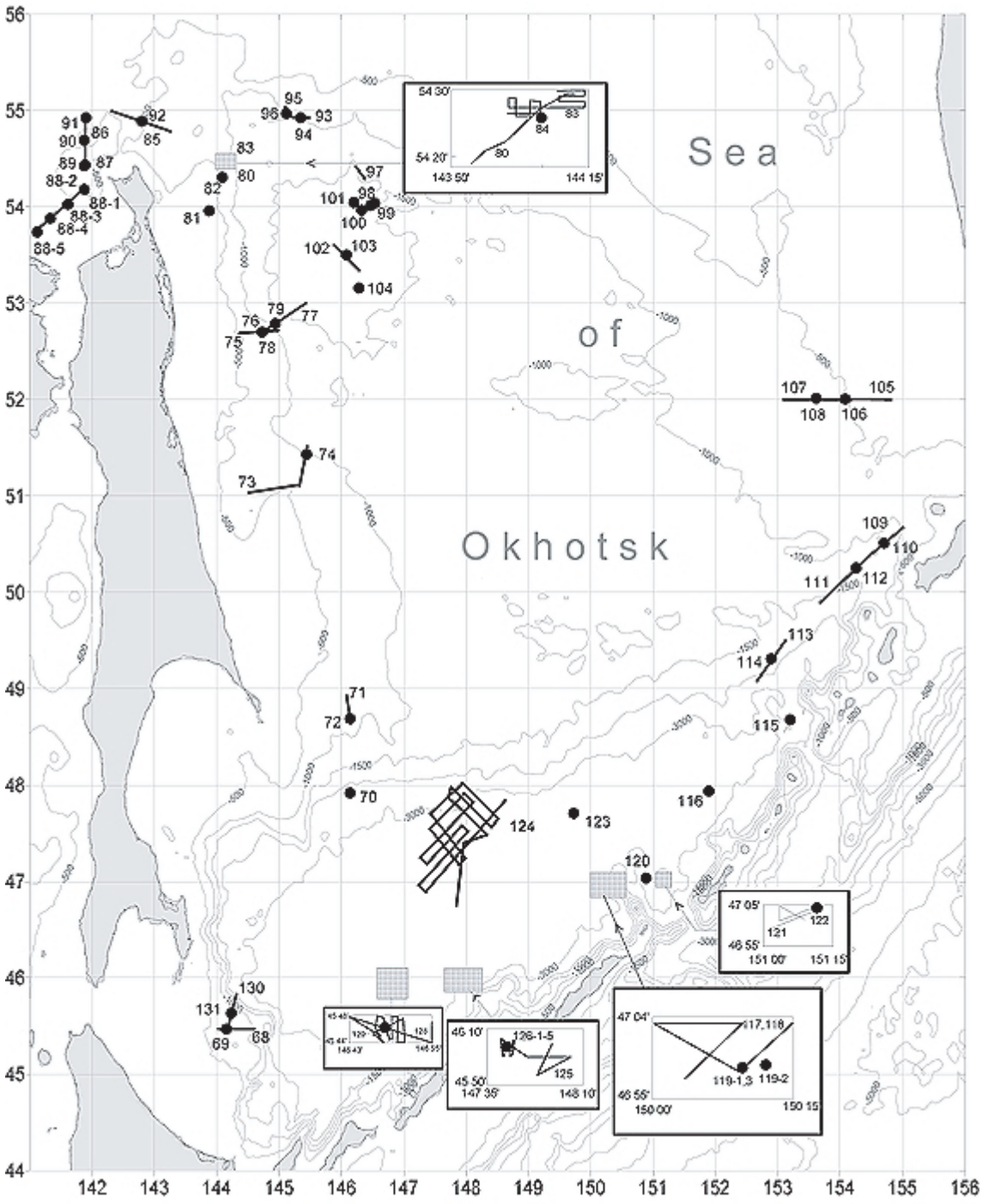

Fig. 1.2: *Locations of stations (filled circles), echosounding and seismic profiles (bold lines) and areas of detailed investigations (shaded rectangles) carried out during the 29th cruise of RV Akademik Lavrentyev, June - August 2002.*

Unfortunately, it quickly became clear that exclusively sand up to coarse gravel is deposited in the Sakhalin Gulf. Our attempts to directly sample the Amur sediments at three stations thus were unsuccessful as the cores could not penetrate the sand layers. We recovered only fist-sized pebbles. Fortunately, the coring equipment was not damaged.

From July 11th to 14th we worked again in the Derugin Basin at 54°00 N/ 146°26 E and sampled with sediment cores and dredges that barite area which we had mapped during the first leg by the video-sled OFOS. On July 13th a dredge recovered barite crusts and living vent clams which were directly conserved in alcohol. On July 14th we finished our work in the northwestern Okhotsk Sea with two stations in the deepest part of the Derugin Basin which is

characterized by a very low oxygen content in the bottom water. For the first time on this cruise, a 15 m long gravity core was successfully deployed. The multicorer, which did not work well up to that time, also worked fine after some modifications. In the evening of July 14th we left for Kamchatka, our next investigation area. We used the 36 hours transit to Kamchatka for an early "half time party" with our Russian colleagues and the crew. In traditional Russian style we celebrated with vodka, sausages and mandolin music until early morning.

On July 16th we reached the coast of Kamchatka and successfully completed the E-W transect begun during LV28 cruise with two coring stations at 500 and 600 m water depth at the continental slope off Kamchatka. Our attempts to core at shallower water depths, however, had to be cancelled, because according to echosounding records the sediment there consists mainly of sands. In the morning of July 17th we were forced to interrupt our program in order to seek shelter from the typhoon Halong coming with 35 knots per hour into our direction. Our attempt to seek shelter from it north of the Kurile island Paramushir had to be cancelled, too, because of a sudden change of direction of the typhoon. We therefore went west into the central Okhotsk Sea. There, we waited for one night at more or less calm sea and could then, in the morning of July 18th, continue our station work west of Paramushir Island. We successfully carried out there sediment, water and plankton sampling at three stations at water depths of 1,000-2,000 m.

After having completed the paleoceanographic work in the eastern part of the Kurile Basin we started dredging at the submarine Browton Ridge. During transit to this area we had a great view on the partly snow-covered volcanoes of the 5 Kurile islands Chirinkotan, Kharinkotan, Shiashikotan, Ekarta and Matua. From the 21st to 22nd of July we carried out volcanologic-petrological works in the Kurile Basin. The main investigation objective was the submarine Browton Ridge spreading from the central part of the Kurile Island Arc about 80 km northwest into the Kurile Basin. The highest rise of the ridge is represented by the small volcanic island Browton, and the submarine part of the ridge is at least partly formed of volcanoes, as well. The origin and the development of this ridge are up to now fairly unknown and probably cannot be explained only by the island arc volcanism of the Kurile Islands. Subsequent to extensive seismic and hydroacoustic mapping, 4 dredging tracks were carried out near Browton Island at the northwestern end of the ridge. This part of the ridge had not been successfully sampled before. During 3 dredging tracks rock material was recovered containing apart from up to 80 cm large dropstones (ice-rafted debris) a large variety of different, mainly old and already consolidated sediments. Additionally, manganese and fossil sponges were often dredged. It therefore can be assumed that the volcanic activity in this region had extincted a long time ago. The sediments will nevertheless allow to determine the minimum age of this structure.
Additionally to the ridge, a neighboring volcano was dredged, too. Due to the fact that also here only old sediment was recovered the dredging was cancelled in order to be continued subsequent to the planned seismic mapping at submarine volcanoes in the southwestern Kurile Basin.

On the way to the central Kurile Basin we sampled the deepest station of this cruise with 3,500 m water depth with the CTD, the plankton net and the multicorer. The oxygen anomaly in the bottom waters which had already been discovered on the MV *Marshal Gelovany* cruise in 1999 and which probably yields the influence of Pacific water masses could thereby be confirmed.

From July 24th to 27th we mapped the northern connection and transition of the spreading ridge discovered on the SAKURA cruise in 1999 to the continental slope in the central Kurile

Basin with seismic profiles. To our great delight the discovery of 1999 could be confirmed by the new profiles. Of special interest was the transition from the ridge to the northern slope of the Kurile Basin, because we found there an extensive zone of submarine volcanism. The discovery and confirmation of a spreading ridge in the Kurile Basin means that the basin did not, as formerly assumed, open in NW-SE direction as a consequence of the sinking of the Pacific plate under the Kurile Island Arc, but in E-W direction as a kind of "pull-apart" basin.

From July 28th to 29th we continued volcanologic-petrological investigations at Hydrographer Ridge and Loskutov seamount northwest off the Kurile island Iturup. These both submarine, up to 1,600 m high mountains are partly of volcanological origin and had so far not been investigated in detail. In total, 9 dredge tracks were carried out subsequent to hydroacoustic and seismic mapping. Apart from different kinds of sediment and dropstones (ice-rafted debris), fragments of submarine lava flows (pillow lava) were thereby recovered at Hydrographer Ridge. The little alteration of these basalts and basaltic andesites and their high content of different minerals allow extensive lab analyses by which we hope to gain interesting information about the origin of these volcanoes as well as about the structure of the Kurile Basin.

The last station of this cruise was carried out on July 30th in La Perusa Strait. There, the water and the sediment were once more sampled. We successfully deployed an 18 m long gravity core for the first time on this research vessel and thus broke our own record set in 1998.

On the evening of June 30th, RV *Akademik Lavrentyev* started its way back to Pusan. We used the transit for taking last samples, packing the equipment and writing cruise reports. In the night from August 1st to 2nd the ship stopped for several hours for fishing squid.
The very last station was then carried out on August 2nd at 4 p.m. local time in the Japan Sea at 39.19.9 N/ 133.28.03 E. To our great delight we were allowed to go once more offboard and take a bath in the ocean at 1,286 m water depth and a water temperature of 24°C. In the evening of the same day we were invited by our Russian colleagues to a farewell party with vodka, snacks and dancing until early morning.

Altogether, 131 stations were successfully carried out during the whole cruise LV29. Thereby, no equipment was lost and no banana recovered. The second part of the cruise was especially a great success for our colleagues from Rostock University who got to know during one of the last deployments of the sediment echosounder in the deep Kurile Basin that their echograms record a seafloor penetration of about 10 m at 3,200 m water depth. At the beginning of the cruise they had expected that the sediment echosounder can be deployed only up to 2,000 m water depth.

RV *Akademik Lavrentyev* arrived in Pusan in the evening of August 3rd. The next morning, a pilot was taken aboard and we proceeded into the port of Pusan and tied up at pier at 7:00 am local time. During daytime the German equipment was unloaded and the German scientists left the ship in the same evening. On August 5th RV *Akademik Lavrentyev* left Pusan again and made is way to Vladivostok harbor, where it tied up on August 7th.

2. HIGH-RESOLUTION ECHOSOUNDER PROFILING ON LV29 – TECHNICAL ASPECTS

Jens Wunderlich

2.1 Echosounders for high-resolution subbottom profiling

Echosounders for acoustic subbottom profiling use sound pulses generated by electrical transducers and send them to the seafloor. The seafloor and sediment layers reflect the sound waves. These reflections are received by the echosounder device, and an echo print is calculated. To get echo prints with high vertical and horizontal resolution the echosounding equipment should fulfill the following requirements:

- A narrow sound beam is needed to hit only a small part of the seafloor.
- If only one frequency is used, the sounded bottom area should be equal in size independent from the transmitted frequency.
- The transmitted sound pulses should be as short as possible without ringing.
- The use of stacking algorithms for enhancing the signal to noise ratio (SNR) requires high repetition rates.
- Beam stabilizing and steering as well as heave compensation is useful especially at greater water depths.

2.2 Linear and non-linear acoustics

Sediment echosounders use two different ways to generate the sound pulse, linear or non-linear (parametric) acoustics.
Linear echosounders generate the sound pulse of the desired frequency directly. The directivity depends on the ratio of the transducer dimension and the signal frequency. Therefore, a narrow beam at low frequencies requires large transducers. But such transducers are heavy and expensive.
Parametric echosounders transmit two signals of slightly different high frequencies at high sound pressures (primary frequencies f_1 and f_2). Because of non-linearity's in the sound propagation in the water column at high pressures, both signals interact and new frequencies arise. The difference frequency ($\Delta f = f_2 - f_1$) is low and penetrates the seafloor. The primary frequencies may be used for exact determination of water depths even in difficult situations, e.g. soft sediments.

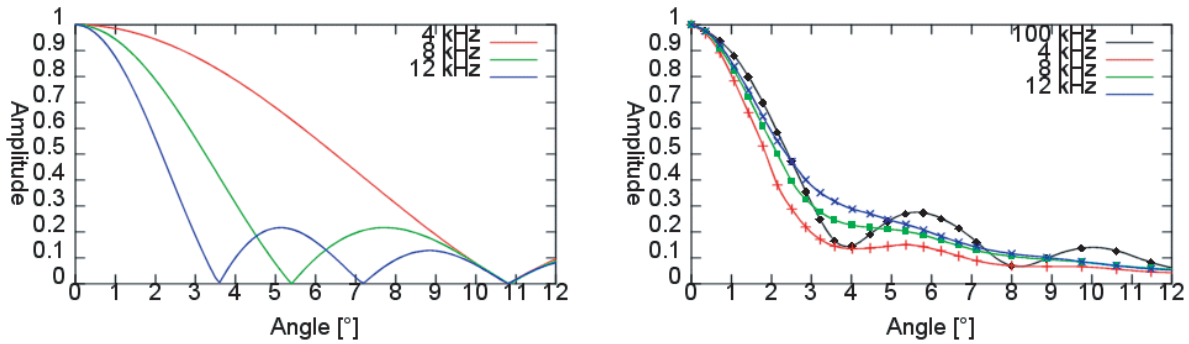

Fig. 2.1: *Beam pattern for linear (left) and parametric transducer at different frequencies.*

Parametric systems have a small beam width in spite of small transducer dimensions independent of the difference frequency. The beam width only depends on the primary frequency related to the transducer aperture, even for the secondary frequency. There are no significant sidelobes and you will get a constant directivity for different secondary frequencies. Therefore, the size of the sounded area is independent of the frequency used for bottom penetration.

Figure 2.1 shows in the right subfigure experimental data from a parametric transducer array with an active sound area of about 0.2 m x 0.2 m. All difference frequencies between 4 and 12 kHz (ratio 1:3) have nearly the same half power beam width as the primary frequency of about 100 kHz. The left subfigure shows the computed directivity of a linear transducer that is 10 times larger (2 m x 2 m). In this case, different radiated frequencies have different half power beam widths. Therefore, the sounded area will not be the same at different frequencies, and the echo prints cannot be compared.
The high bandwidth of parametric systems allows to generate very short sound pulses without ringing for a high vertical resolution.

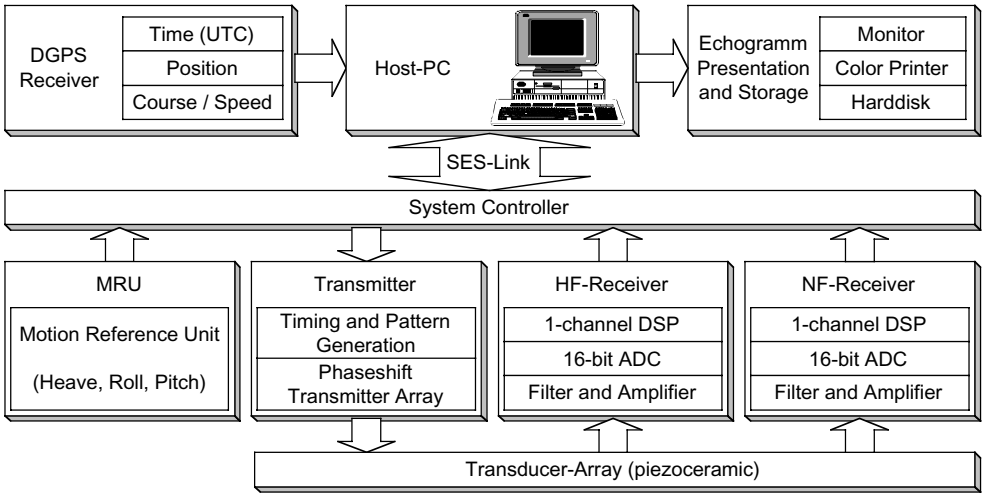

Fig. 2.2: *SES-2000 system architecture.*

2.3 Parametric Sediment Echosounder System SES-2000DS

During cruise LV29 the sediment echosounder system SES-2000DS, developed by the research group of underwater acoustics of the Rostock University, was used. The echosounder system SES-2000 was originally designed for shallow water to detect small buried objects and sediment structures at high three-dimensional resolution. The system was optimized to improve the power for greater water depths (SES-2000DS).
The echosounder system SES-2000DS consists of a main device, a host PC and a transducer array (*Fig. 2.2*). The main device comprises integrated transmitters, receivers and modules for analog and digital real-time signal processing. Analog to digital converters (ADC) are used for digitizing the receiver signal with 16-bit resolution at sampling rates of up to 200 kHz depending on the signal bandwidth.
A special link module connects the echosounder main device to the PC which is used for system controlling and data display. All received data are stored digitally on harddisk including GPS data and other important system parameters. The echosounder file format is device-specific, but may be converted into the standard SEG-Y format for postprocessing using conventional equipment. Analog data storage on a DAT-recorder is also possible, but was not used on cruise LV29.

Sound pulses are generated by a small piezoceramic phase shifted transducer array with 32 separately controlled elements (32 x 1 matrix). Electronic beam stabilizing and steering is possible in roll direction. Thus, all the ship movements are detected by a motion reference unit (MRU). This sensor, made by SEATEX (Norway), outputs the absolute roll, pitch and yaw, and dynamic heave. Roll and pitch values are used for electronic beam stabilizing. Echo prints are heave-compensated using the MRU heave value.

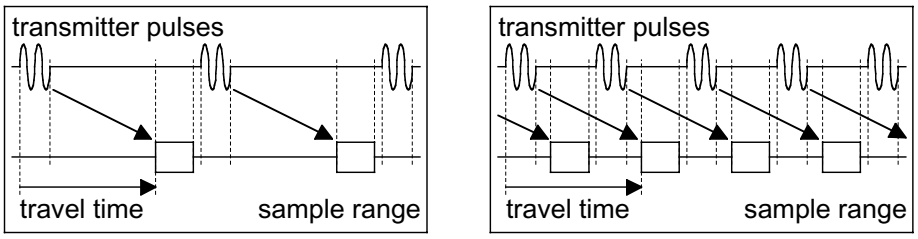

Fig. 2.3: *Transmitter regime at shallow water (left) and deep sea.*

High repetition rates are used to improve the signal to noise ratio and to raise the degree of probability to find small single objects and small bottom structures. At greater water depths a special regime is used to get higher repetition rates (*Fig. 2.3*).
A color echo print is generated immediately using 12 colors at a logarithmic scale. The echo print includes all important parameters, e.g. GPS position, time (UTC), pulse frequency, pulse length and echo stacking rate. All transmitter and recording parameters are controlled by software, designed for this purpose.

Table 2.1: *SES-2000DS main parameters.*

Water depth range	0.5 ... 3,000 m
Vertical resolution	up to 6 cm
Penetration depth (near the bottom surface)	up to 50 m
Transmitter power (electrical pulse power)	> 32 kW
Primary transmitter frequency	about 100 kHz
Secondary transmitter frequencies	4, 5, 6, 8, 10, 12 kHz
Transmitter pulse length	0.08 ... 1 ms
Repetition rate	1 ... 100 s^{-1}
Beam width	±1 x 2 deg @ 4...12 kHz
Beam steering range	± 16 deg roll
Transducer principle	piezoceramic
Separately controlled transducer elements	32
Transducer dimensions	ca. 20 x 40 cm^2
Transducer weight (in air, incl. 40 m cable)	ca. 70 kg

2.4 Installing the echosounder equipment

The echosounder equipment was installed on transit from Pusan to the working area. There is no hydroacoustic shaft available on RV *Akademik Lavrentyev*. Therefore, the transducer had to be mounted at the ship's hull using a long pipe (*Fig. 2.4*). Because of the high freeboard, there was no possibility to fix the mounting pipe near the water surface. This caused a lot of vibrations and noise. After the first profile, the mounting construction was slightly modified, and less noise was produced by the transducer itself. Good echo prints were produced up to a ship's speed of about 5 knots at calm sea.

Mounting the transducer inside an acoustic shaft would give a lot of advantages like less noise and the ability to use the echosounder all day, even during transit and at higher speed.

Fig. 2.4: *Pipe.*

2.5 Results

Profile data with a total length of about 480 nm (890 km) was produced. Echo print examples are shown in *Figures 2.5-2.7*. Depth values were computed from travel times assuming a constant sound velocity of 1,500 m/s. Variations of sound velocity due to water temperature, pressure or salinity were not taken into account. The data was plotted time-sequentially from the left to the right. Heave components were removed from the echo prints by an enhanced algorithm using the heave data delivered by the MRU.

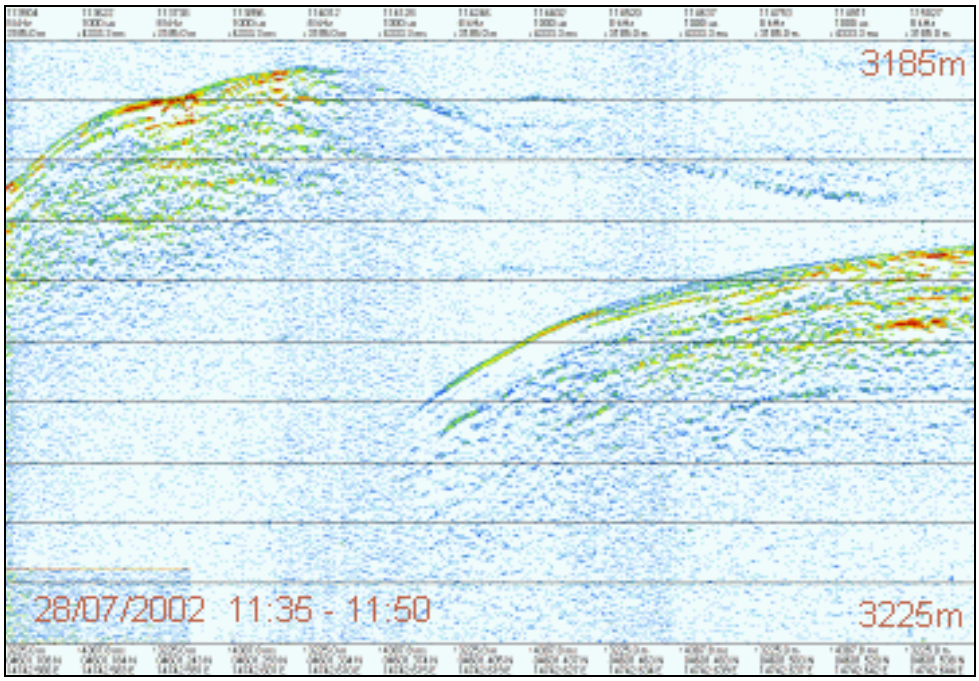

Fig. 2.5: *Echoprint example (Range 2,185 m … 3,225 m; Frequency 8kHz / 1ms).*

All received signals were stored digitally on a harddisk together with the GPS data and system parameters. The total volume of digitally stored echosounding information is about 8.8 GB.

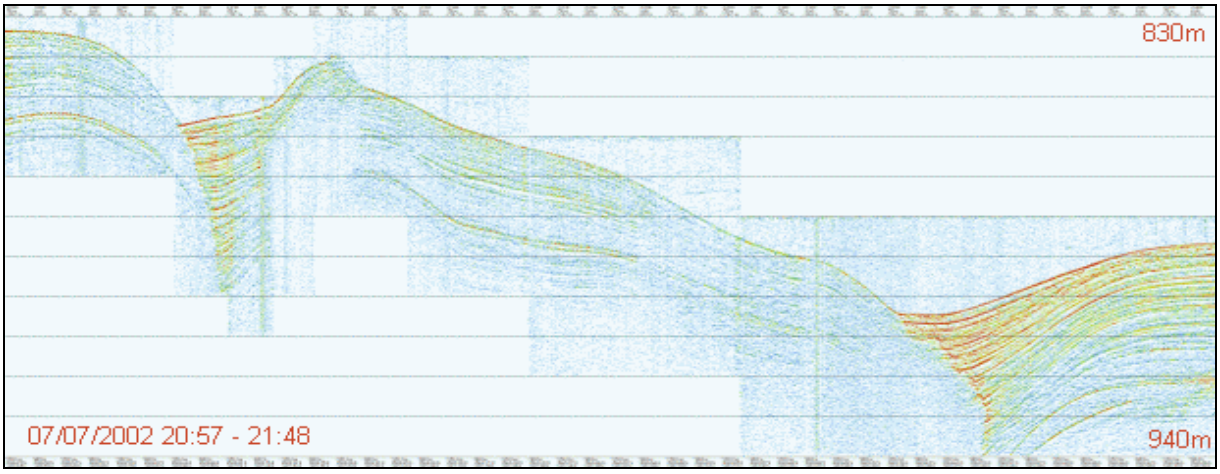

Fig. 2.6: *Echoprint example (Part of profile 7; Range 830 m … 940 m; Frequency 8kHz / 0.75ms).*

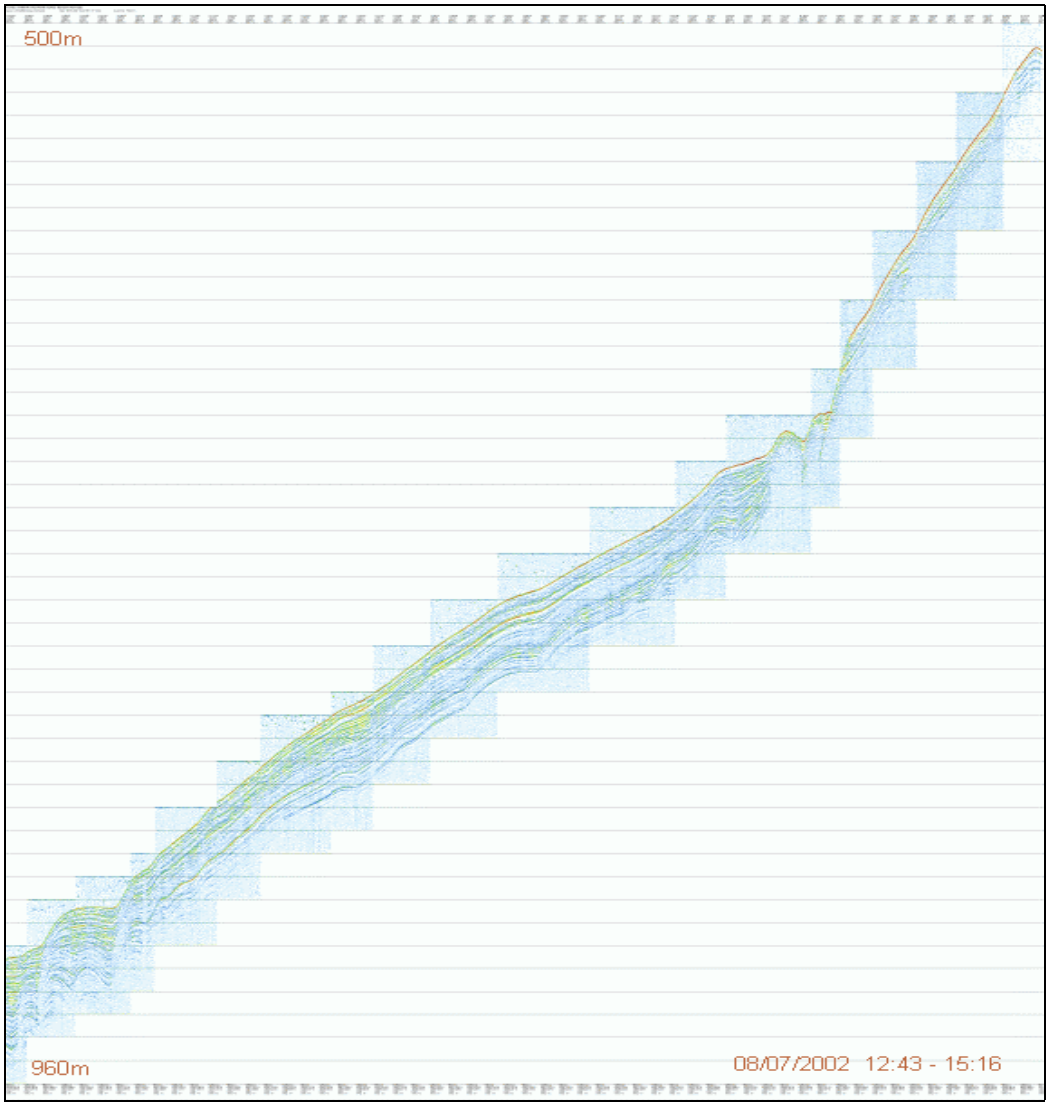

Fig. 2.7: *Echoprint example (Profile 14; Range 500 m … 960 m; Frequency 8kHz / 1ms).*

The investigated area included different regions with water depths between 50 m and 3,200 m. This means that there were very different conditions for applying the echosounder system. Different frequencies were used under varying conditions. Best results were received using 8 kHz especially at greater water depths. This frequency gave good penetration and good resolution and caused no additional noise at the ship's echosounder (ELAC) which operates at 12 kHz.

Tests showed that good echo prints are produced up to water depths of about 3,200 m assuming nearly flat bottom (*Fig. 2.5*). At water depths of about 700-1,500 m the SES-2000DS achieved a penetration up to 40 m. Even at steeper slopes a penetration of about 10-20 m was possible (*Fig. 2.6*).

The results at the slopes could be improved if beam steering was possible not only sideways but also in forward and backward direction. For this purpose, greater transducers are necessary which cannot be mounted at a pipe like on LV29, but they could be placed easily inside a hydroacoustic shaft. This would also lead to greater acoustical power available, and therefore the water depth range could be increased. The SES-2000DS echosounder system can be adopted in this way.

3. RESULTS OF HIGH-RESOLUTION SUBBOTTOM PROFILING

Thomas Lüdmann

For the detection of the uppermost strata of the sedimentary column a high-resolution subbottom profiler (SES-2000DS) from the University of Rostock was used. The main purpose of its deployment was to support the sediment sampling program by finding appropriate coring stations. In general, the device achieved a penetration of 30-25 m with an average resolution of ca. 25 cm depending on the selected frequency and pulse length of the source signal. During the cruise, 36 profiles with a total length of ca. 860 km were obtained (*Fig. 3.1*).

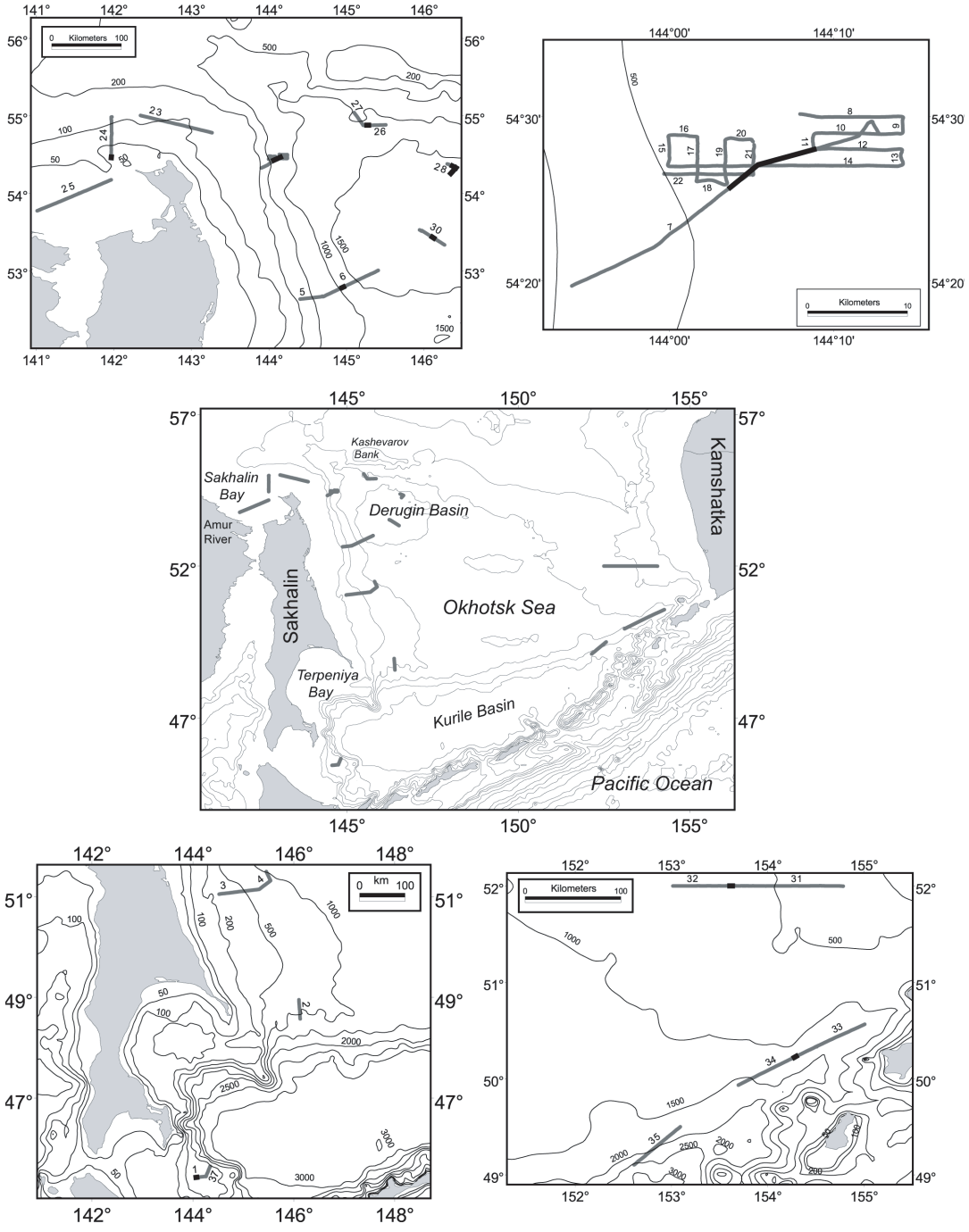

Fig. 3.1: *Maps exhibit the location of track lines (gray lines) of the sediment echosounder SES-2000DS. Black lines mark examples of profiles.*

A seismic facies analysis of the high-resolution reflection data allows to characterize the depo-environment and lithofacies of the sediments. Seismic reflection termination and configuration can be interpreted as stratification pattern of the depositional sequences. Hence, the attempt was made to use the amplitude, continuity and frequency information of the reflections in order to correlate the echograms with the lithology of the sediment cores (Payton, 1977; Emery & Myers, 1996). Therefore, we chose 6 locations which represent different types of depositional environments: La Perusa Strait, the central East Sakhalin continental slope, Sakhalin Gulf in the vicinity of the Amur River mouth, the North Okhotsk continental margin, the central Derugin Basin, the continental slope of southwestern Kamchatka and the slope of the Kurile back-arc basin.

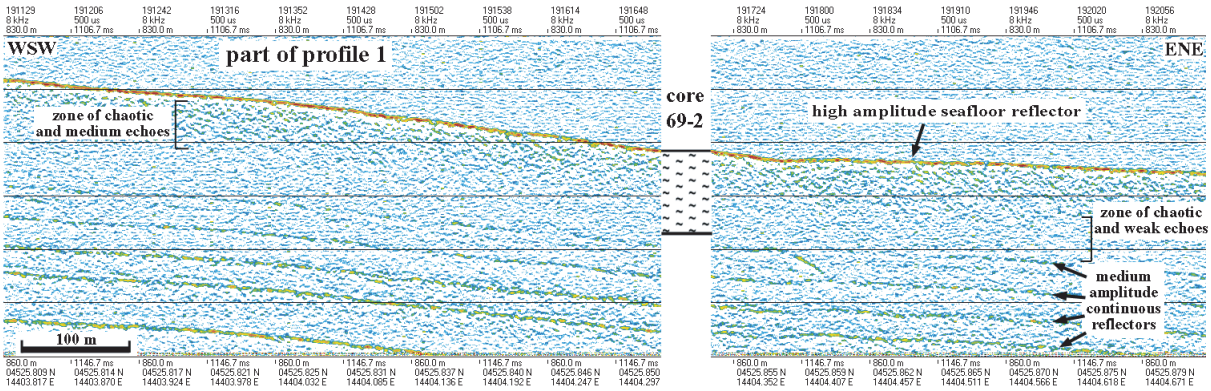

Fig. 3.2: *Part of subbottom profiler profile 1 (see Fig. 3.1 for location) near La Perusa Strait. Indicated is sediment core station LV29-69-2 (see Appendix 6 for detailed description) which is mainly composed of clay (see text for discussion).*

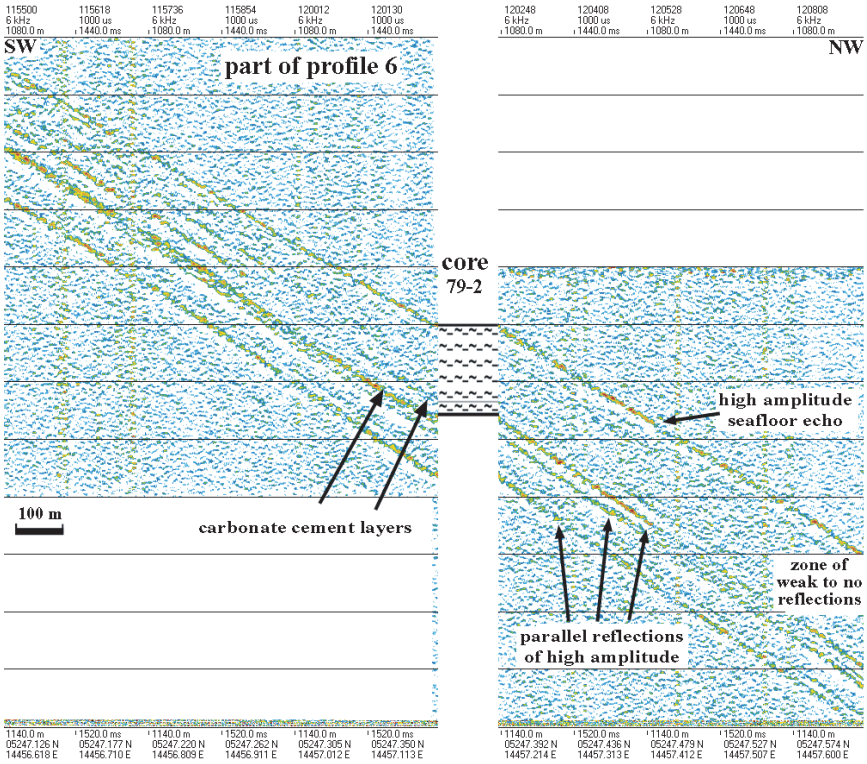

Fig. 3.3: *Part of sediment echosounder profile 6 (see Fig. 3.1 for location) at the central East Sakhalin slope. Sediment core station LV29-79-2 (see Appendix 6 for detailed description) is shown. The core is composed of silty clay, incorporated are layers of carbonate cement (see text for discussion).*

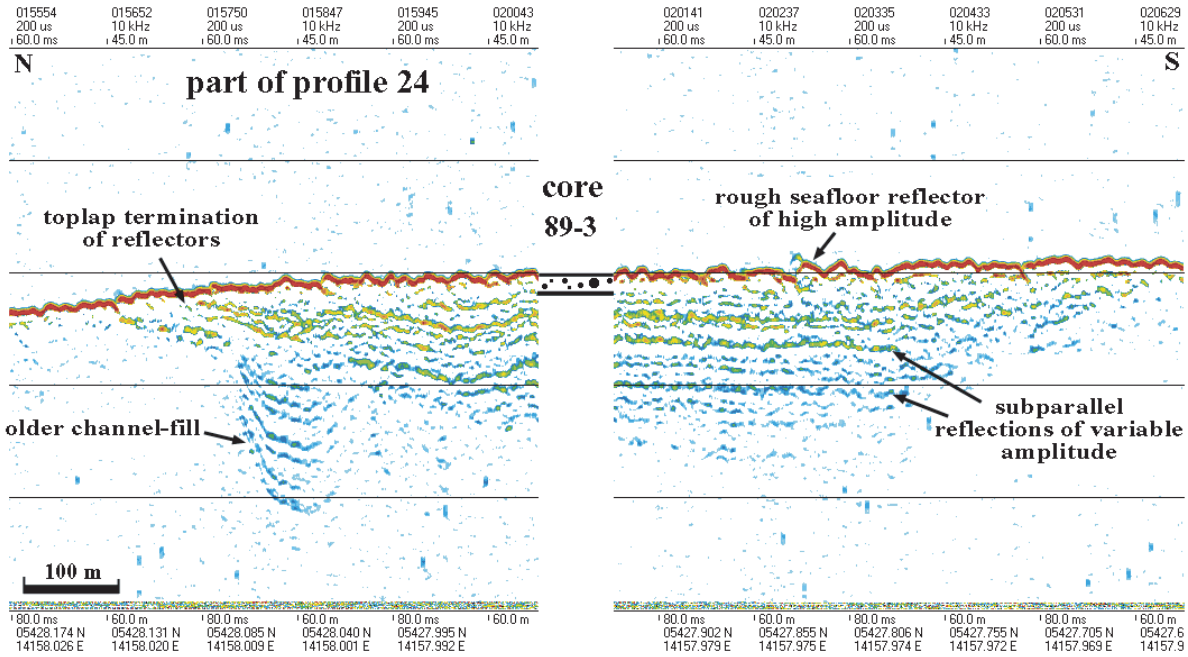

Fig. 3.4: *Part of subbottom profiler profile 24 (see Fig. 3.1 for location) in the Sakhalin Gulf near the Amur River mouth. Sediment core station LV29-89-3 (see Appendix 6 for detailed description) is indicated. The core is mainly composed of clay (see text for discussion).*

Gravity core LV29-69-2 (see Appendix 6 for detailed core description) was taken approximately 156 km eastward of La Perusa Strait at a water depth of ca. 868 m. The echogram at the coring station (*Fig. 3.2*) exhibits a strong seafloor reflector followed by a succession of subparallel reflectors of medium amplitude and high continuity. Intercalated are sections of apparent chaotic reflections of low amplitude and low continuity. Since this pattern is comparable to that of the background noise (see seismic signal above the seafloor, *Fig. 3.2*), it is only an effect of high signal amplification and therefore these zones should be correctly described as more or less reflection-free or transparent. The upper zone of structureless and weak reflectors directly beneath the seafloor has a thickness of 8-9 m, whereas the lower ones range between 2-5 m. Their internal reflection configuration points to layers which might be too thin to be seismically resolved or layers of the same lithology accumulated under uniform energy. The lithology of core LV29-69-2 supports the second interpretation, because the entire core is mainly composed of clay with increasing density downcore. The thin subparallel reflectors inserted below ca. 9 m are possibly attributed to beds of relatively coarse material. The carbonate concretions which are located in a core depth of ca. 650 cm are seismically not resolved. There is not a significant reflection at this depth. The high amplitude of the surface reflection is possibly due to the dispersed gravel in the surface layer. The subparallel reflections of medium amplitude below ca. 8.5 m might be due to thin sand-rich layers intercalated into the fine mud-rich hemipelagic sediments (see core LV29-69-3, Appendix 6).

The lower slope of central East Sakhalin in a water depth of ca. 1,100 m is characterized by parallel reflectors of high amplitude and high to medium continuity (*Fig. 3.3*). They are separated by segments of 1-3 m in thickness with weak to no reflections. A correlation of the seismogram with the lithology of sediment core LV29-79-3 demonstrates that the zones of weak echoes are related to the silty clay deposits and the high amplitude reflections are generated by dense carbonate cement beds (gray line in *Fig. 3.3* at ca. 686 cm and at the bottom of the core section at 780 cm).

In general, a high-amplitude bottom reflection with weak or no subbottom signals is characteristic for the shallow water (ca. 50 m) area of the Sakhalin Gulf (*Fig. 3.4*). Here, close

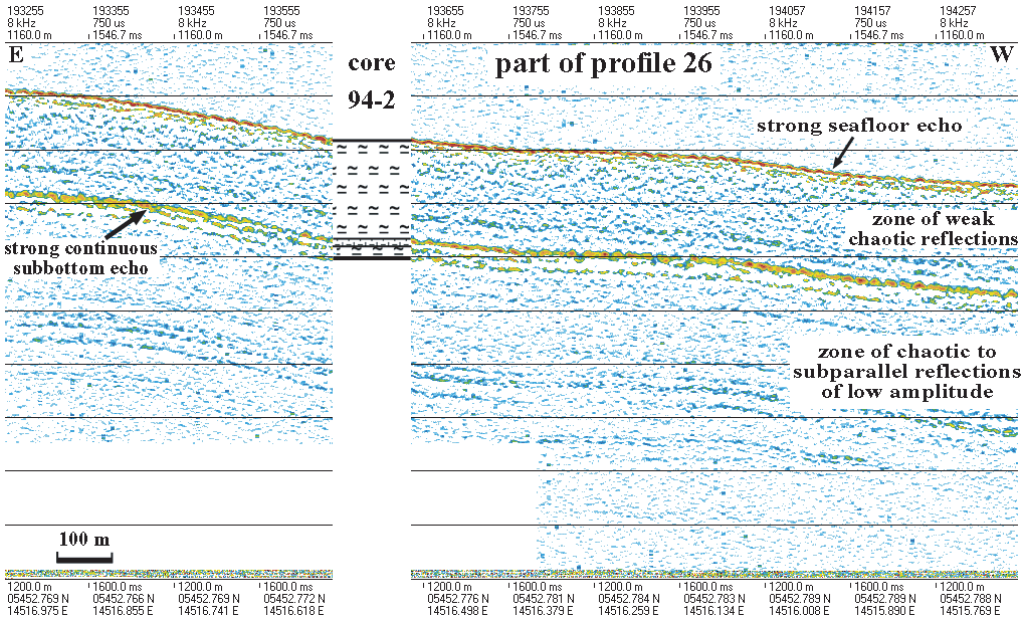

Fig. 3.5: *Part of subbottom profiler profile 26 (see Fig. 3.1 for location) at the North Okhotsk continental margin. Sediment core station LV29-94-2 (see Appendix 6 for detailed description) is shown. The core is mainly composed of clayey silt (see text for discussion). Strong parallel reflections might be generated by a prominent lithological change (see text for discussion).*

to the depo-center of Amur River, the uppermost strata consists mainly of coarse material. Samples of the surface sediments reveal unsorted clasts from fine sand to coarse gravel (core LV29-89-3). *Figure 3.4* shows one of the few places where pockets of well stratified sediments occur. The subparallel reflection of variable amplitude and medium continuity have a spacing of 50-30 cm. At the rim of the pocket the reflectors terminate with toplap against the surface layer indicating their former erosion. The channel-fill-like structure has a width of 1 km and a depth of 5 m. At the northern rim of the pocket a smaller channel filled with ca. 3 m of sediments is unconformably overlaid.

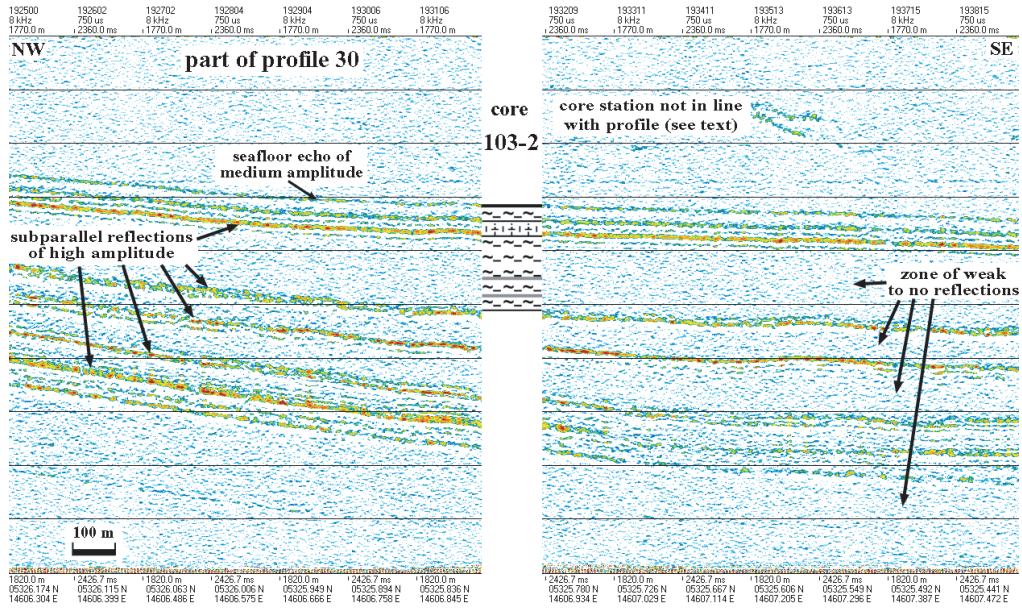

Fig. 3.6: *Part of sediment echosounder profile 30 (see Fig. 3.1 for location) in the central Derugin Basin. Sediment core station LV29-103-2 (see Appendix 6 for detailed description) is indicated. The core is mainly composed of silty clay with two turbiditic layers (gray lines) near the base (see text for discussion).*

It may represent an older channel which was later truncated by the upper broader channel. The internal reflection pattern of the sediment pocket is typical for a fluvial environment of variable energy.

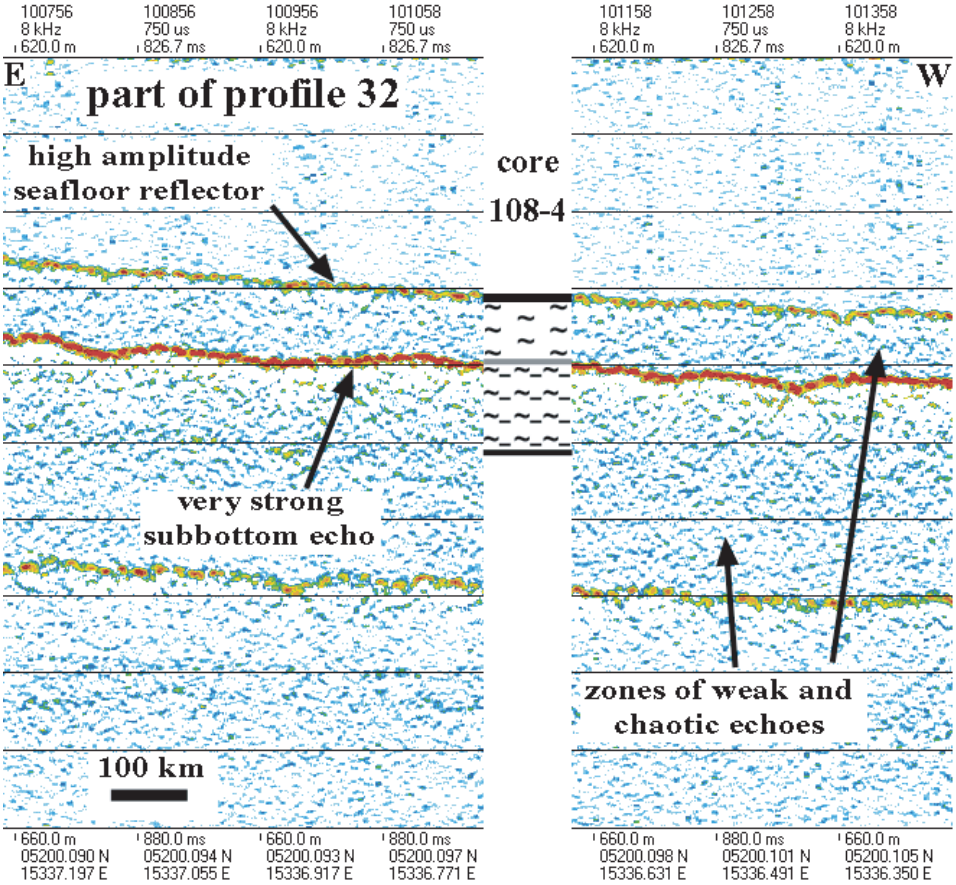

Fig. 3.7: *Part of subbottom profiler profile 32 (see Fig. 3.1 for location) at the lower slope off southwestern Kamchatka. Sediment core station LV29-108-4 (see Appendix 6 for detailed description) is shown. The core is mainly composed of silty clay and an ash layer at about ca. 315 cm (gray line) which is seismically expressed by a subparallel very high amplitude reflection (see text for discussion).*

The seismic image from the lower slope of the North Okhotsk continental margin south of the Kashevarov Bank (ca. 1,170 m, *Fig. 3.5*) illustrates a section of about 25 m with parallel reflections interbedded by broad zones (ca. 8 m) of weak echoes. The surface reflector exhibits a strong amplitude which assigns to coarse bottom sediments of a sandy silt composition with dispersed pebbles and sand lenses (core LV29-92-2 in *Fig. 3.5*, see also Appendix 6*)*. Chaotic reflections of low amplitude characterize the subjacent zone with several discontinuous subparallel reflectors at its base. Subsequently a 2 m thick band of medium amplitude reflectors occur, followed by a zone of weak chaotic to subparallel echoes. The chaotic reflections correspond to clayey silt layers intercalated by a 10 cm thick layer of clay-silt-sand material with lenses of pebbles and sand. This lithological change produced a strong subbottom echo at ca. 740 cm (*Fig. 3.5*).
Profile LV29-30 located in the central Derugin Basin (*Fig. 3.6*) shows a pattern of several continuous parallel surface reflectors of medium amplitude comprising the topmost 3 m of the deep-basin deposits. Below these layers, a more or less transparent zone with a thickness of ca. 7-8 m occurs. It is replaced downwards by an alternation of parallel reflectors of medium amplitude and zones with weak or no echoes of 2-3 m thickness. The weak seafloor reflection may be due to the soft silty clay which thereafter pass into sandy silty clay with dense green diagenetic interlayers at ca. 150 cm, producing parallel high-amplitude reflections. The

subsequent silty clay deposits (from 286 cm to the bottom of the core) are seismically not expressed, whereas the two turbiditic sequences (at ca. 685 and 850 cm) are marked by prominent reflections. Unfortunately, the core station is located more to the west, beside the seismic track, therefore the correlation especially of the turbiditic layers with the observed strong subbottom reflectors seems to be questionable. However, the seismic profile shows (*Fig. 3.6*) that the sediment section above these reflectors markedly thins to the northwest and that they become shallower.

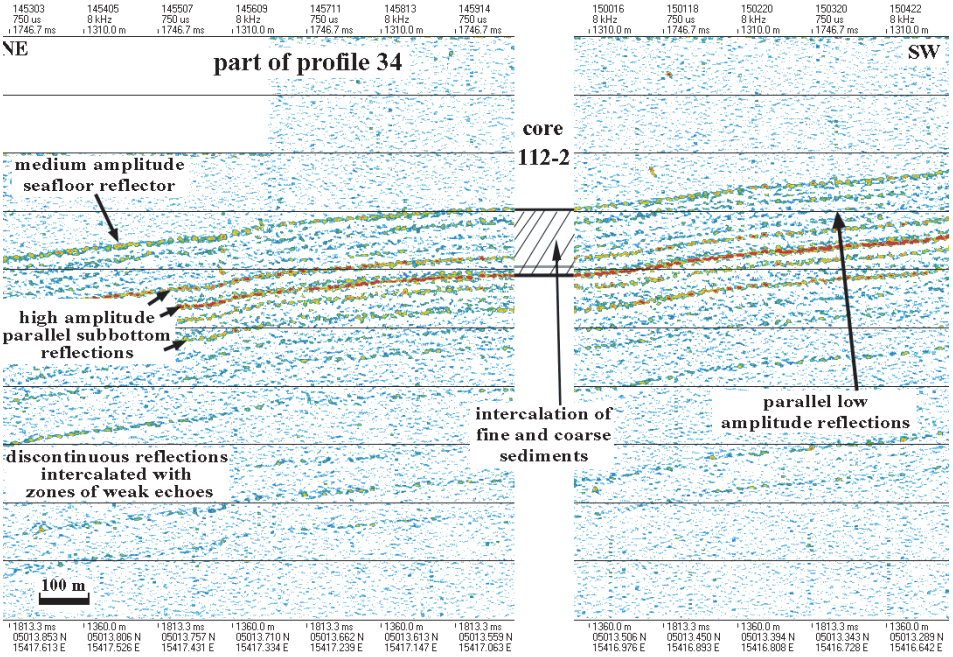

Fig. 3.8: *Part of sediment echosounder profile 34 (see Fig. 3.1 for location) west of Paramushir Island near Fourth Strait. Sediment core station LV29-112-2 (see Appendix 6 for detailed description) is indicated. The core consists of an intercalation of fine and coarse sediments (parallel low-amplitude reflectors) and ash layers (gray line, strong parallel echoes) (see text for discussion).*

At the lower slope off southwestern Kamchatka (ca. 630 m, *Fig. 3.7*) undulating continuous isolated reflectors with medium to high amplitude appear. They are separated by thicker zones of weak chaotic echoes. 3-4 m below the seafloor a subbottom reflector with a remarkable high amplitude occurs. This reflector represents a volcanic ash layer (core LV29-108-4, see Appendix 6 for detailed description) which is characterized by a marked density contrast of the volcanic minerals to the neighboring silty to clayey sediments. The zone of weak and chaotic echoes reflect the more or less homogeneous clayey sediments.

The echogram west of Paramushir Island near Fourth Strait (*Fig. 3.8*) reveals a series of subparallel wavy reflections with a wave length of ca. 500 m and an interval of about 1 m. They comprise the uppermost 15 m of the sedimentary column. Below it, reflectors of medium amplitude occur intercalated with zones of very weak echoes. The parallel low-amplitude reflections (*Fig. 3.8*) correspond to an alternating lithology of fine and coarse sediments (core LV29-112-2, see Appendix 6 for detailed description). High amplitude subbottom echoes are probably generated by volcanic ash layers.

In summary, the seismic facies analyses demonstrate that the zone of weak to no echoes correspond to more or less homogeneous fine sediments. In the Okhotsk Sea, this sediment type is represented mainly by silty to clayey hemipelagic deposits at the continental slopes and in the deep basin. Reflectors of high amplitude and continuity correspond to volcanic ash layers or to carbonate-cemented sediments. Near the Kurile Islands, the seismogram is dominated by parallel reflectors which indicate a more variable depo-environment with an alternating input of fine to coarser material and volcanic ashes.

4. WATER COLUMN STUDIES

Anatoly Salyuk, Valery Sosnin, Anatoly Obzhirov, Galina Pavlova, and Nicole Biebow

4.1 Introduction

Water column sampling was carried out using a rosette water sampling system consisting of a Sea-Bird-32 twelve position system with Niskin Bottles (10 l) and CTD probe Sea-Bird-911 with standard temperature, pressure, conductivity sensors and also sensors for oxygen light transmission, altimeter and bottom contact. The CTD was lowered to 3 m above the seafloor at stations shallower than 100 m and to 8 m at deeper ones. Water sampling was started at maximum depths and the samples were taken during upcasts. The interval of water sampling depended on the purpose of investigation, and the water depths varied during observations from 5 to 500 m.

A total of 29 stations were carried out during Leg 2 of LV29. Water samples were collected for pH, alkalinity, methane, δO^{18} and δC^{13} isotopes, calcium, and deuterium. All data is tabulated in Appendix 3.

The second leg started under conditions of unusually active tropical cyclones. They came one by one from the tropics to East Asia and the Japan Islands. Such an unusual early beginning of the typhoon activity in Asia is in good agreement with an anomaly in the atmospheric circulation of the Northern Hemisphere this year. But only one of the typhoons ("Halong", July 17th-18th, 2002) passed just through the Kurile Islands and disturbed routine observations. So, in spite of the cyclonic activity far south, a high atmospheric pressure field predominated over the Okhotsk Sea and in general weather conditions were convenient for all kinds of observations.
Ice conditions in the sea have changed and the sea-ice fields in the Tugur area disappeared after July 5th. Sometimes ice conditions in the Tugur region remain until August.
During this stage of the expedition oceanographic observations were carried in the NW Sakhalin area (Sakhalin Gulf), in the deepest part of the Derugin Basin, West Kamchatka and the Kurile Basin.

4.2 Amur River and NW Sakhalin area

The region is characterized by shallow water depths. The minimum depth of observations was 22 m in the mouth of the Sakhalin Gulf. The salinity field in the gulf is strongly influenced by the Amur River outflow (16.91 at the sea surface of station LV29-88-1). Amur River plays an important role in delivering dissolved and suspended organic matter into the western part of the Okhotsk Sea. Due to this, the water color was dark green and even black. There were a lot of ground-grown grasses at the sea surface. The light transmission of the water column was the lowest for all observed areas. Besides the suspended material, we suppose the Amur outflow to be responsible for the appearance of the methanotrophic but pathogenic bacteria *Listeria monocytogena* in the western part of the sea and around Northeast Sakhalin.
The vertical structure of the water column consists of two layers. An upper warm layer with a temperature up to 12.89°C is located in the uppermost 10 m and is divided from the lower one by a very sharp thermocline and strong halocline. The properties of the bottom layer (temperature: -1.69°C, salinity: 33.27 and a very high density up to 26.83) reflect winter conditions (*Fig. 4.1*, station LV29-88-1). The whole water column is oxygen-rich (~7-8 ml/l) up to the seafloor (more than 100 m).

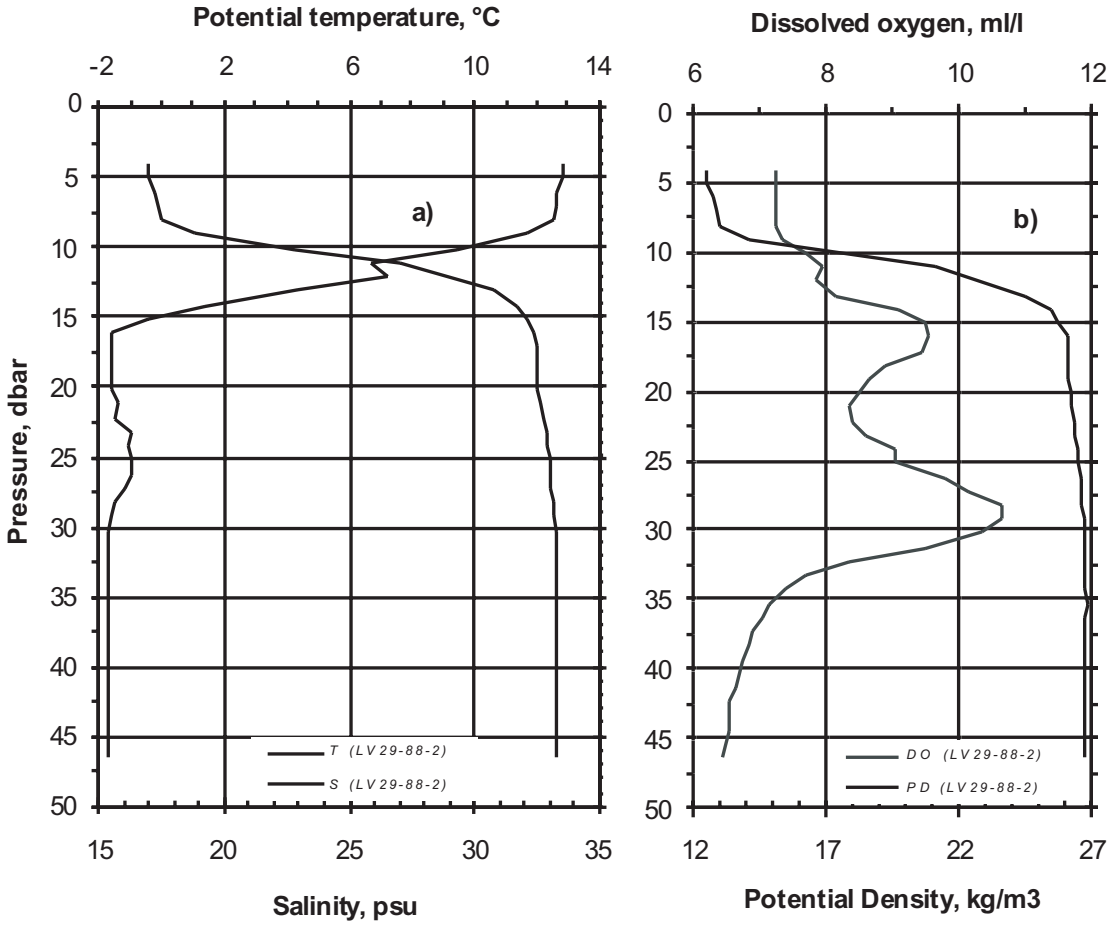

Fig. 4.1: *Potential Temperature and Salinity (a) and Dissolved Oxygen and Potential Density (b) at station LV29-88-2.*

The water column of this area shows no signs of vertical mixing and, moreover, seems to keep the winter properties in a stable way in comparison with the water column of the East Sakhalin shelf area. This is not surprising, as the ice conditions in the region disappeared only from July 5th on. Additional stability of the water column is derived from the Amur fresh-water input and the melting of sea ice.

The East Sakhalin shelf and slope area is characterized by relatively high temperatures in the cold subsurface layer (-0.4 - 0.7°C) and frequent intrusions with negative temperature values at intermediate depths and near the bottom (station LV29-76, -81). In our opinion, these cold intrusions originate from dense water northwest and west off Sakhalin. They occur as a result of sinking and diapycnal entrainment of shallow shelf waters with winter properties along the continental slope in the vicinity of Cape Elizabeth and a mixing with the surrounding waters with a subsequent lateral transport southward along the slope. During summer, the volume of dense shelf waters is much less than in winter and, as a consequence, the vertical scale of intrusions is less in summer time than in winter.

4.3 Derugin Basin

Two CTD stations were carried out in the deepest part of the Derugin Basin (stations LV29-103 and -104) (*Fig. 4.2*, station LV29-104). Both stations showed the lowest values of dissolved oxygen in near-bottom layers amounting to ~0.30 ml/l. In comparison with the observations during the first leg in the “Barite Mounds” area (0.5-0.6 ml/l), this is twice less.

Such low oxygen values in the deepest part of the basin indicate stagnant conditions which are also reflected in the representative sediment cores (see Appendix 6). Besides, in contrast to the barite mineralization area, the oxygen minimum layer was missing in both stations.

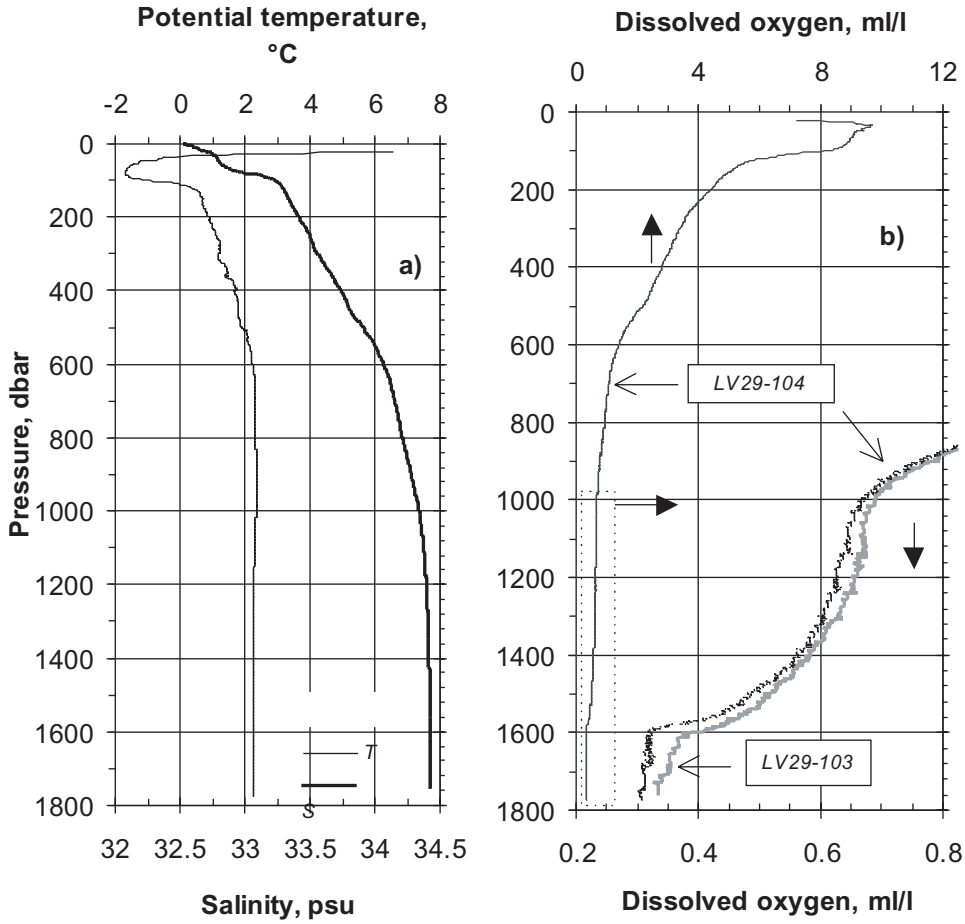

Fig. 4.2: *Potential Temperature and Salinity (a) at station LV29-104 and Dissolved Oxygen (b) at stations LV29-103 and LV29-104.*

4.4 Kurile Basin

The eastern part of the Okhotsk Sea in the vicinity of the Kurile Straits was covered by 7 CTD stations. Observations were made in the deepest part of the basin - up to 3,334 m depth (stations LV29-116, -120, -123) - as well as on the northern slope of the basin with lower depths. This area is under strong influence of tidal currents of diurnal period coming from the North Pacific through the deep and also shallow Kurile Straits. It is well known that the Okhotsk Sea is a region with strong tidal currents. This is due to the wide and shallow shelf in the northern part and also due to the near-resonant trapping nature at diurnal frequency. The tide amplitude is maximal in Penzginskaya Bay (13.9 m) and in the Tugur area (9.7 m). Tidal currents, especially diurnal, are dominant also in and around the Kurile Straits, and their speed is up to a few knots. For example, a maximum tidal current of 11 knots was observed in Nadezhda Strait. In Srednego, Severgina, Kreniczina, and Diany straits the tidal speed reaches 10.4, 9.4, 9.0 and 8.8 knots, correspondingly. In all other straits, the minimum current speed amounts to 6 knots. Due to astronomic reasons, the maximum tides and tidal currents take place in June-July and in December-January.

Tidal currents in and around the Kurile Straits are expected to play a major role in water exchange processes between the Okhotsk Sea and the North Pacific and also in internal water mixing. The diurnal cycle of CTD observations made by one of the authors in Friza Strait in the summer of 1989 revealed a mixing of the whole water column resulting in a homogeneity up to the seafloor in the middle part of the strait in one phase of the tidal cycle. There is no doubt that this leads to a cyclic mixing of the water masses in this area.
In the southern part of the sea (Kurile Basin) an anticyclonic circulation of several eddies with diameters of 100-150 km was observed which are often recorded by hydrographic data and by satellite imaging. The eddies appear each year, developing in summer and decaying in winter. Although eddy-like motions are dominant in the Kurile Basin, the mean eastward flow with a speed of 0.1 m/s still exists.

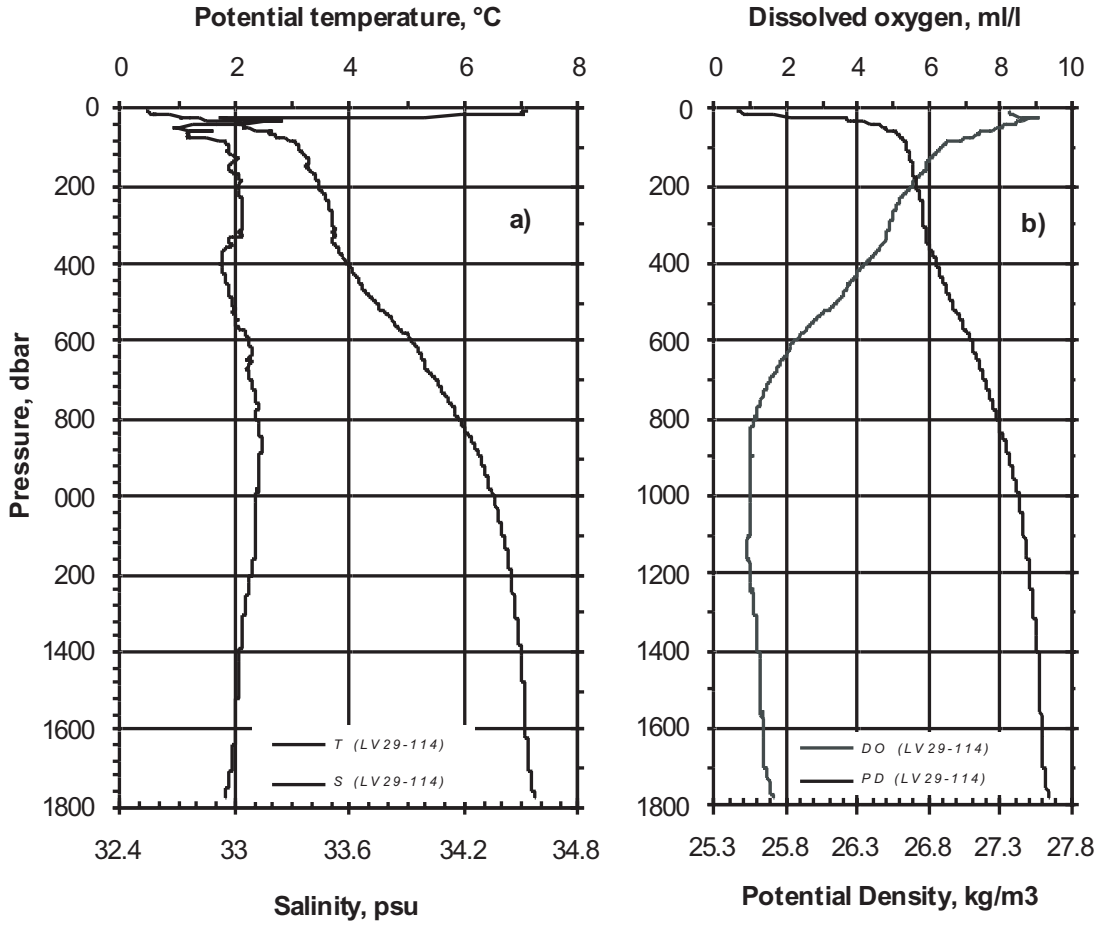

Fig. 4.3: *Potential Temperature and Salinity (a) and Dissolved Oxygen and Potential Density (b) at station LV29-114.*

All CTD stations in this area have the following characteristic features: relatively high (up to 1.8°C) temperatures in the cold subsurface layer, a smooth lower boundary and a huge amount of small intrusions up to 1,600 meters depth. For example, at station LV29-114 (*Fig. 4.3*, station LV29-114) a well pronounced but very small dichothermal layer was observed caused by intrusions of warm water on its lower boundary. Besides, a lot of intrusions of different vertical scales can be observed at intermediate depths up to 1,000 m. Even in the oxygen minimum zone which coincides with the intermediate temperature maximum, there is a local increase of the oxygen value connected with intrusions of colder waters.
An increase of the oxygen concentration value was also observed corresponding to a relatively sharp temperature decrease in the near-bottom layer at 70 m depth.

CTD station LV29-115 is, on the contrary, characterized by a massive cold subsurface layer (up to 600 m) with high values of temperature (1.8°C) but with a lot of small intrusions. Of course, such a vertical distribution indicates a very intensive mixing at these depths.
The next deep station (station LV29-116) (*Fig. 4.4*, station LV29-116) is also characterized by numerous intrusions, and signs of internal mixing can be seen up to 1,600 m. Additionally, there is an intrusion of cold and oxygen-rich waters at the depths of the intermediate temperature maximum.
A very strong interleaving of the water column was observed at the station in the central part of the basin which is located farest from the straits but which contains a lot of very sharp intrusions beneath the cold subsurface layer. As a rule, sharp intrusions indicate the very beginning and the first phase of internal mixing processes.

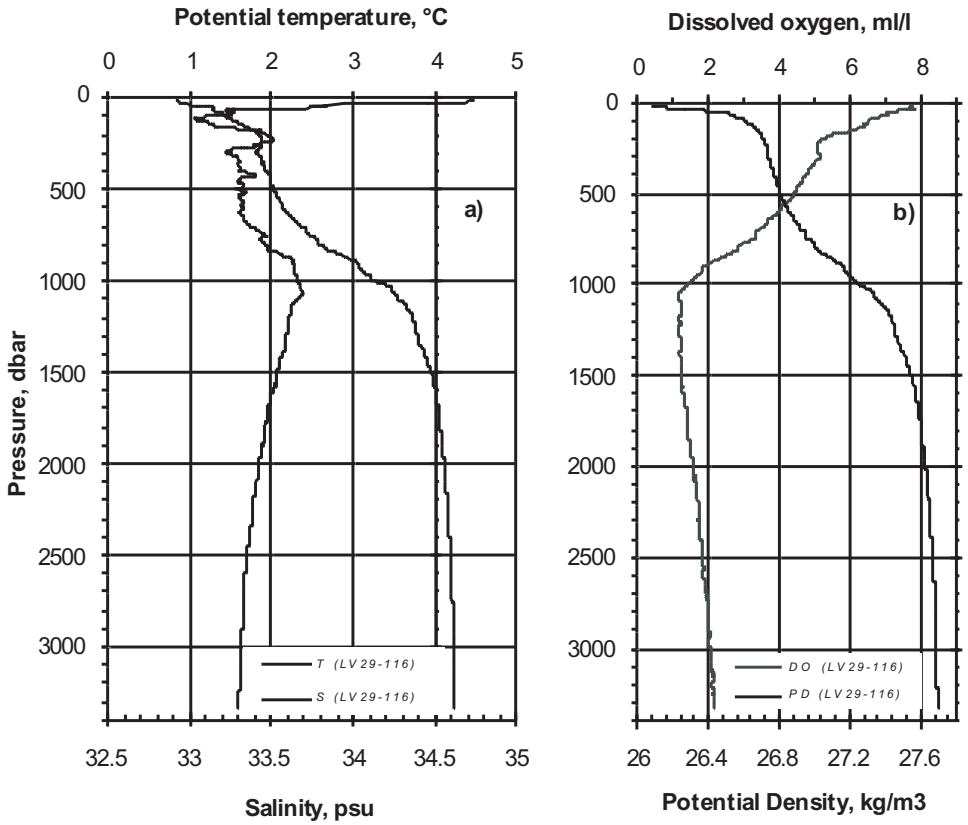

Fig. 4.4: *Potential Temperature and Salinity (a) and Dissolved Oxygen and Potential Density (b) at station LV29-116.*

It is suggested that the Okhotsk Sea surface waters migrate from the Kurile Basin into the North Pacific Ocean through the deepest of the straits, Bussol Strait (sill depth 2,300 m), and several shallower straits in the southern part of the Kurile Island Arc. A two-way flow is supposed to exist in Bussol Strait: the outflow from the Okhotsk Sea was found in the upper layers of the western side of the strait, while the Pacific inflow entered the Okhotsk Sea in the eastern part of the strait down to depths of 1,700 m. Strong tidal mixing occurs in the straits. In some phases of the tide, the whole water column up to the bottom could be homogeneous (Friza Strait). Thus, Pacific waters flowing into the Okhotsk Sea at different levels and in various stages of transformation strongly influence the vertical thermohaline structure in the eastern part of the sea.
Obviously, our observations in the deep Kurile Basin demonstrate that the waters originating from the Pacific are enriched with respect to oxygen (station LV29-120, -114). This data supports the role the North Pacific plays in the ventilation of the deep Okhotsk Sea. The same results were obtained during the MV *Marshal Gelovany* cruise in 1999.

5. THE CARBON DIOXIDE SYSTEM IN THE OKHOTSK SEA

Galina Pavlova, Anatoly Salyuk, Valery Sosnin, Nicole Biebow, and Lester Lembke

5.1 Sea water sampling and analysis

On this cruise, we studied the carbonate system (pH, Total Alkalinity, dissolved calcium) in the water column (CTD stations) and in the bottom waters (MUC stations). *pH* measurements were carried out by means of a cell without liquid junction (Tishchenko et al., 2001). *Total Alkalinity (TA)* was analyzed by Bruyevich`s method (Bruyevich, 1944). Samples for *dissolved calcium* (*Ca*) were preserved with hydrochloric acid and will be analyzed by Tsunogai's method (Tsunogai, 1968) in the shore-based laboratory at POI. Various carbonate parameters were in situ computed by a combination of the measured parameters according to a generally accepted scheme. A detailed description of the methods and designations used in the text are given in Chapter 7, Part I of this Report. *Biological productivity* was estimated using the "biological" term of apparent oxygen utilization (AOU_b), which was calculated using the data for dissolved oxygen and measured parameters of the carbonate system (Tishchenko et al., 1998). A negative value of AOU_b implies that the oxygen production by photosynthesis surpasses the oxygen consumption by respiration and oxidation of organic matter. A correction factor for *dissolved oxygen* (O_2) CTD data was applied to draw near the Winkler method data.

5.2 Results and Discussion

The carbonate chemistry data was obtained at 29 CTD and 17 MUC stations for three main areas of the Okhotsk Sea: the Sakhalin slope (stations LV29-69, -72, -76, -79, -81, -82, -84, -94, -103, -104), Sakhalin Gulf (stations LV29-87, -88-2, -88-3, -88-4, -88-5, -90, -91) and Kurile Basin (stations LV29-70, -110, -112, -114, -115, -116, -120, -123). Stations LV29-92, -106, -108 and -131 were located separately. The complete list of the measured and calculated carbonate parameters for CTD stations is given in the Appendix 3 and for MUC stations in *Table 5.1* in this chapter.

5.2.1 Slope of Sakhalin Island (depth 370-1,800 m)

The CTD stations investigated at the slope of Sakhalin Island were divided into two groups using the common features of the carbonate parameters distribution:
1. South-north transect along Sakhalin (stations LV29-69, -72 , -76 , -79 , -81, -82 , -84 , -94, depth 370-1,100 m)
2. Derugin Basin (stations LV29-103, -104, depth 1,800 m)

5.2.1.1 South-north transect

Figure 5.1 displays vertical profiles of selected carbonate parameters and shows a clear separation of some water properties for the stations along the transect.
A minimum normalized Total Alkalinity (NTA) value (2.372 mmol/kg) was found at about 220 m with little variation along the transect. It is related to the biogenic $CaCO_3$ formation in water layer 0-220 m. The greatest decrease in NTA for this layer by 53 µmol/kg was observed at the northern end of the transect (station LV29-82) compared to 10 µmol/kg at station LV29-72. Therefore, the intensity of biogenic $CaCO_3$ formation increases towards the north of the Sakhalin slope. Below 220 m, NTA increases steadily with depth due to dissolution of

biogenic carbonate. This implies that $CaCO_3$ is accumulated in the sediments of the Sakhalin slope up to a water depth of 1,100 m.

***Tab. 5.1**: Carbonate parameters for bottom water samples (MUC, CTD).*

Station	Depth m	Temp °C	Salinity	pHt in situ	*TA* mmol/kg	DIC, mmol/kg	CO_3, mmol/kg	pCO_2, µatm	Lc	La
MUC69	845			7.6	2.36	2.348	0.044	997	0.75	0.52
CTD69	837	2.313	34.165	7.532	2.359	2.367	0.038	1177	0.66	0.46
MUC70	1988			8.017	2.211	2.033	0.115	250	1.21	0.97
CTD70	1984	1.945	34.566	7.599	2.406	2.367	0.052	786	0.56	0.45
MUC72	1121			7.551	2.385	2.38	0.042	1066	0.64	0.46
CTD72	1113	2.375	34.373	7.531	2.382	2.383	0.04	1119	0.61	0.44
MUC76	627			7.89	2.23	2.139	0.075	483	1.39	0.94
CTD76	618	2.147	34.037	7.556	2.338	2.345	0.038	1154	0.71	0.48
MUC84	753			7.666	2.255	2.227	0.048	830	0.85	0.58
CTD84	747	2.205	34.1063	7.544	2.349	2.356	0.038	1160	0.68	0.47
MUC89	46			8.011	2.069	1.981	0.071	375	1.69	1.06
CTD87	45	-1.696	33.351	7.829	2.284	2.246	0.053	650	1.27	0.8
MUC92	99			7.887	2.274	2.218	0.061	556	1.41	0.89
CTD92	87	-1.671	33.33	7.894	2.283	2.224	0.062	548	1.44	0.91
MUC94	1123			7.556	2.39	2.384	0.043	1058	0.65	0.46
CTD94	1113	2.379	34.371	7.505	2.388	2.397	0.038	1195	0.58	0.41
MUC103	1748			7.443	2.409	2.42	0.036	1215	0.43	0.33
CTD103	1739	2.368	34.436	7.431	2.409	2.423	0.035	1251	0.42	0.32
MUC104	1762			7.5	2.41	2.404	0.041	1057	0.49	0.38
CTD104	1751	2.368	34.436	7.436	2.408	2.421	0.036	1230	0.42	0.33
MUC108	617			7.572	2.324	2.327	0.039	1107	0.74	0.5
CTD108	608	2.19	33.868	7.559	2.322	2.328	0.038	1141	0.72	0.48
MUC110	1215			7.584	2.393	2.376	0.046	968	0.67	0.49
CTD110	1205	2.298	34.449	7.531	2.393	2.391	0.041	1098	0.6	0.43
MUC112	1373			7.533	2.395	2.389	0.042	1057	0.57	0.42
CTD112	1367	2.253	34.474	7.519	2.393	2.391	0.041	1090	0.56	0.41
MUC114	1764			7.599	2.412	2.378	0.051	828	0.59	0.46
CTD114	1755	1.938	34.567	7.556	2.417	2.396	0.046	920	0.54	0.42
MUC116	3292			7.504	2.416	2.372	0.05	741	0.32	0.3
CTD116	3277	1.835	34.623	7.503	2.417	2.374	0.05	743	0.32	0.3
MUC123	3329			7.508	2.418	2.372	0.051	729	0.32	0.3
CTD123	3322	1.898	34.611	7.494	2.418	2.376	0.05	755	0.31	0.29
MUC131	762			7.572	2.358	2.357	0.041	1089	0.72	0.5
CTD131	749	2.286	34.134	7.52	2.353	2.367	0.037	1231	0.65	0.44

pCO_2 is much lower in the surface water than in the atmosphere at all stations. Extremely low values (190-220 µatm) were observed in the northern part of the transect (station LV29-76 – LV29-84). They are associated with increased photosynthesis processes (and organic-debris formation) in the north of Sakhalin Island. Below the photic zone, organic debris is oxidized to carbon dioxide. The pCO_2 value increases with depth to maximums of more than 1,000 µatm, which is comparable to pCO_2 values in intermediate and deep water layers in the North Pacific (Broecker et al., 1982).

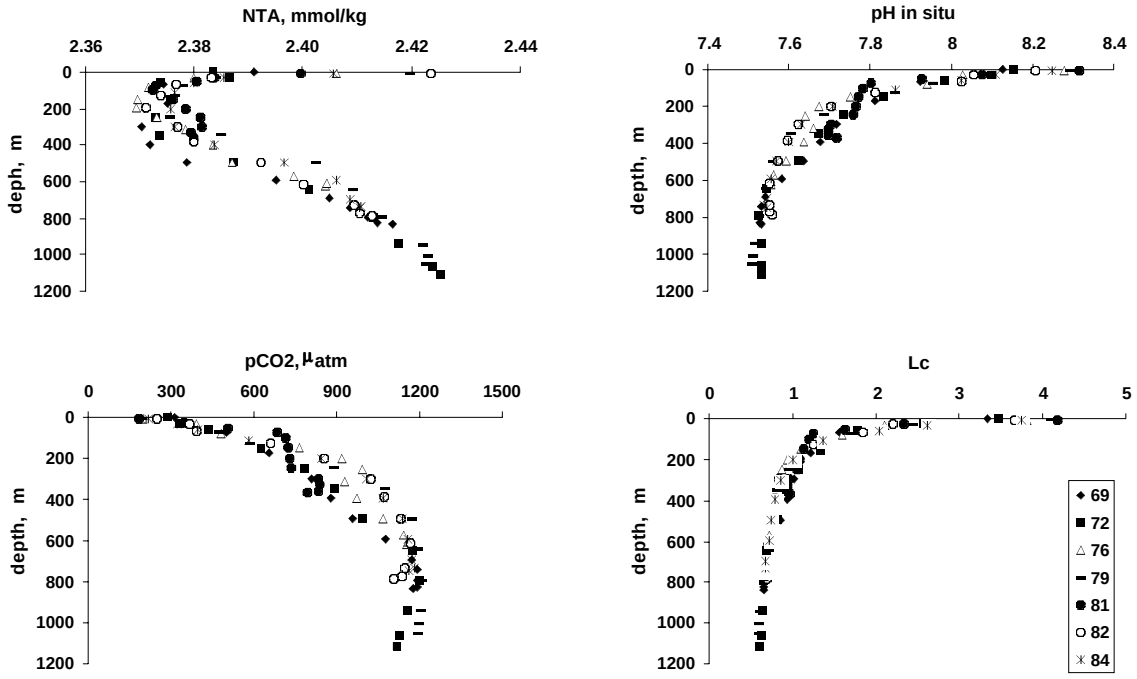

Fig. 5. 1. *Vertical profiles of normalized total alkalinity (NTA), pH in situ, partial pressure of CO_2 (pCO_2) and saturation degree of calcite (Lc) at a slope of Sakhalin Island.*

The investigation of the carbon dioxide system along the Sakhalin slope showed that the northern part of the slope is more productive in biogenic material than the southern one. These results coincide with the distribution of dissolved organic matter in the waters (Agatova et al., 1996) and in the sediments (Bruyevich, 1956) of the Okhotsk Sea.

5.2.1.2 Derugin Basin

Numerous observations of the water column in the Derugin Basin, including our own investigations of several years, showed that the water structure here is very homogeneous below 1,000 m. Hydrochemical data obtained in Leg 2 provided new informations with regard to the Derugin Basin.

Stations LV29-103 and -104 are located in the Derugin Basin at a depth of approximately 1,760 m. The vertical profiles of selected carbonate parameters for these stations and for station LV29-19, sampled at a shallower depth (1,684 m) in Leg 1, are shown in *Figure 5.2.* As it is clear from the figure, the vertical profiles of the water properties are found to be nearly identical from the surface to approximately 1,600 m. The carbonate parameter distribution in the water column for this group of stations is not described here, because detailed investigations of the carbonate system for 17 stations of the Derugin Basin were carried out during Leg 1.

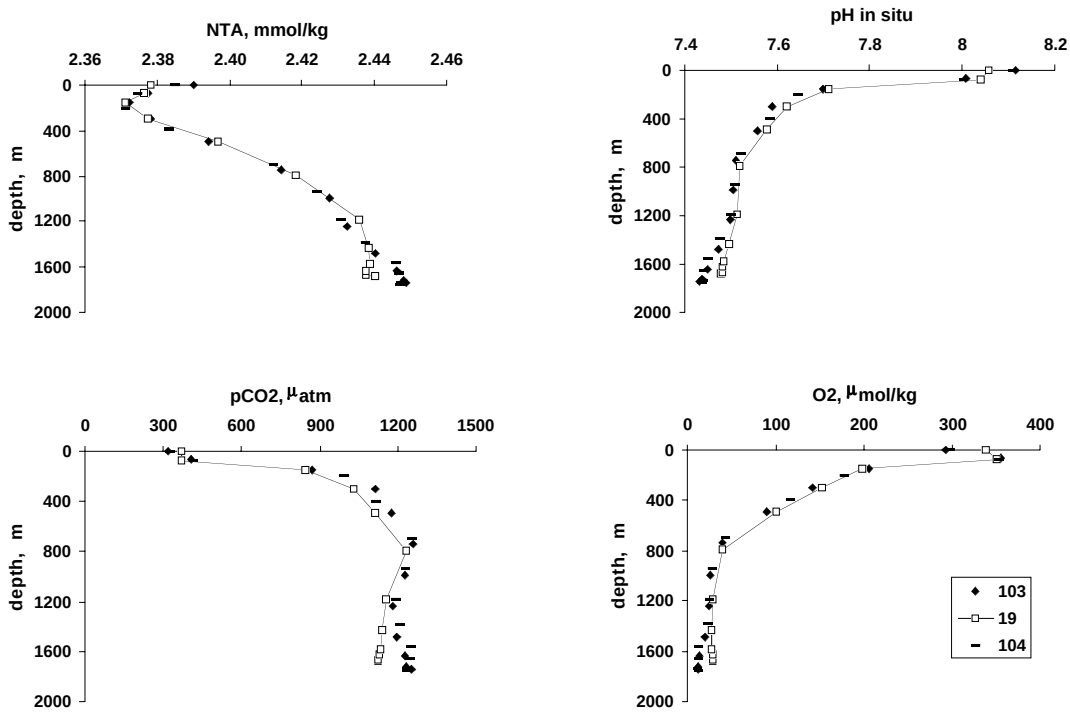

Fig. 5.2: *Vertical profiles of normalized total alkalinity (NTA), pH in situ, partial pressure of CO_2 (pCO_2) and dissolved oxygen content (O_2) in Derugin Basin.*

As a striking feature of the new locations (stations LV29-103 and -104), the existence of a water column layer with very low oxygen contents located 200 m above the seafloor was observed. Such a low oxygen content had never been measured before in the Okhotsk Sea. Oxygen concentrations of 14 µmol/kg and of 13 µmol/kg were found in the bottom water of station LV29-103 and -104, respectively. They were accompanied by an increase in alkalinity (by 10 µmol/kg) and a decrease in pH (*Fig. 5.2*).
We believe that carbonate dissolution in the bottom water is responsible for the alkalinity increase. The question arises what processes affect an enhanced carbonate dissolution within a zone with low oxygen concentration. The dissolution of carbonate can be favored by conditions that create high levels of CO_2 and low pH values, and these processes seem to be sufficient to lead to carbonate dissolution. The remineralization of organic matter by oxygen and nitrate leads to very high CO_2 partial pressures (and therefore low pH) in the oxygen minimum zone. The question arises whether the denitrification starts before the oxygen is fully depleted. We believe that the substantial lack of oxygen in this zone may initiate the consumption of nitrate for the oxidation of organic carbon. Most probably a combined effect of oxygen utilization and denitrification led to the carbonate dissolution in the study region.
We also believe that the bottom water at stations LV29-103 and -104 might be influenced by the underlying sediments. Both cores contained anoxic sediments with a strong H_2S odor. The change in the pH value in the bottom water depends on the extent of removal of generated hydrogen sulfide in the underlying sediments (Ben-Yaakov, 1973). Probably, the hydrogen sulfide remaining in sea water decreased the pH value at these stations.

Obviously, additional investigations, including H_2S and nutrient measurements in the sea water and in the pore water, are required to understand this interesting region in the Derugin Basin.

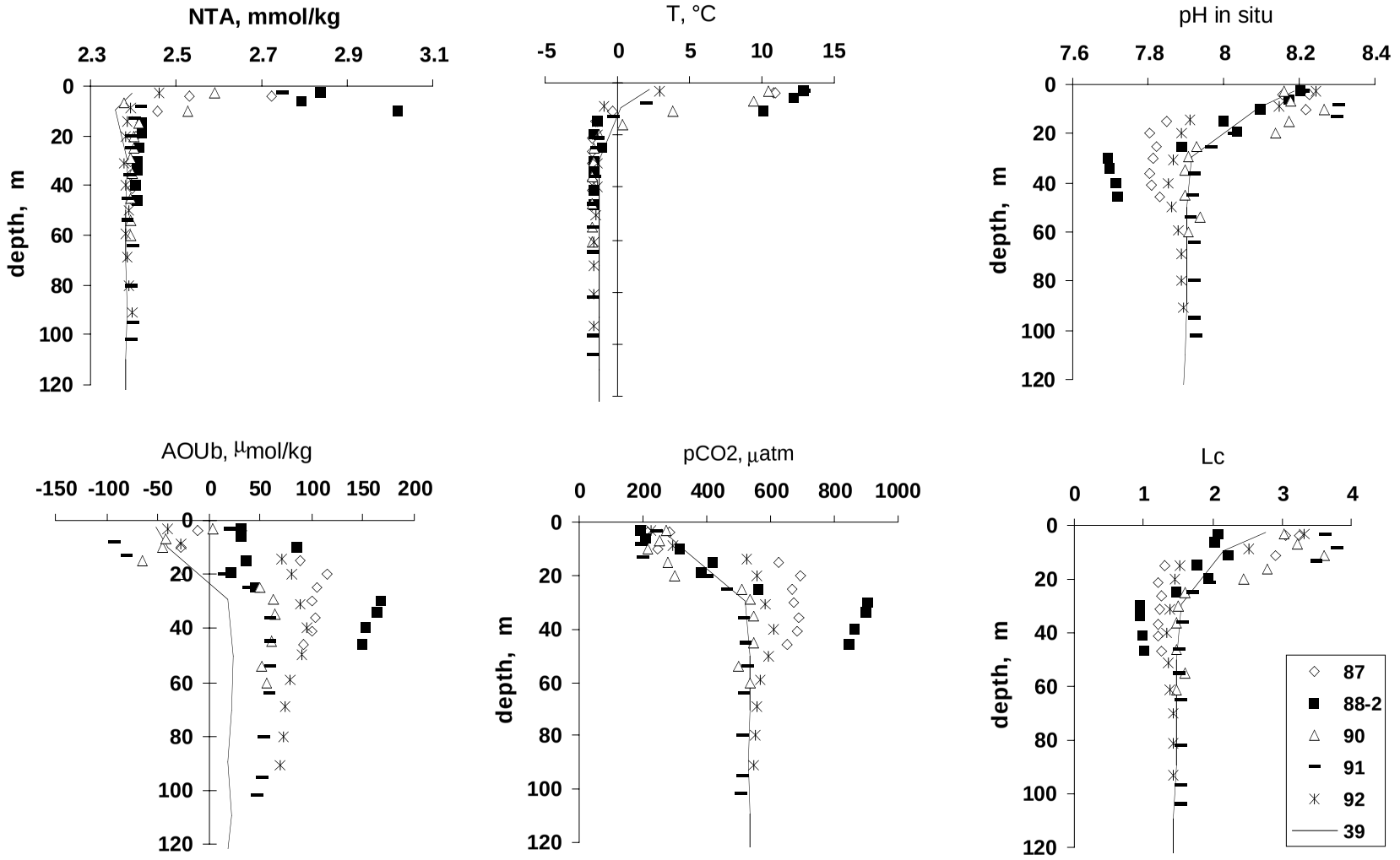

Fig. 5.3: *Vertical profiles of normalized total alkalinity (NTA), temperature (T), pH in situ, "biological" term of apparent oxygen utilization (AOUb), partial pressure of CO_2 (pCO_2) and saturation degree of calcite (Lc) at a South-North transect across the Sakhalin Gulf.*

5.2.2 Sakhalin Gulf

The spatial distribution of carbon dioxide equilibrium species is presented for 7 locations in the Sakhalin Gulf. A south-north transect (transect 1) comprising 4 sites (stations LV29-88-2, -87, -90, -91) along 142°E in combination with an east-west transect (transect 2) also consisting of 4 sites (stations LV29-88-2, -88-3, -88-4, -88-5) along 54°N were carried out to study the carbonate system of the Sakhalin Gulf and to investigate the influence of Amur River on the major components of the Okhotsk Sea waters. In this section, they are compared with stations LV29-39 and -92 on the northern Sakhalin shelf. The surface water properties for station LV29-92 varied more than those for station LV29-39 due to the inflow of fresh waters from Amur River.

Figures 5.3 and *5.4* display vertical profiles of measured and calculated hydrochemical parameters in the sea water for transect 1 and transect 2, respectively.

The high input of alkalinity from Amur River contributes to the observed spatial gradients in carbonate chemistry at the surface and at all depths for both study areas of the Sakhalin Gulf. In contrast to this, the fresh-water influence was observed at station LV29-92 only in the upper 10 m. The surface NTA values are highly variable. They are higher in the east (3.016 mmol/kg, station LV29-88-2) and in the north (2.749 mmol/kg, station LV29-91) than in the west (2.537 mmol/kg, station LV29-88-5). It seems likely that the area along the eastern shore was influenced by the Amur River input to a higher degree than the area along the western shore.

The behavior of selected carbonate parameters showed a significance of photosynthetic activity on the carbon dioxide equilibrium in the Sakhalin Gulf. pCO_2 is one of the most sensitive parameters for small variations in the sea-water properties caused by photosynthetic activity. Therefore, in order to obtain a detailed pCO_2 profile in the water column, we measured TA and pH every 5 m from the surface to the bottom and computed pCO_2 values using these measured properties.
Photosynthetic carbon dioxide consumption at the surface results in reduced levels of carbonic acid (pCO_2 decreasing to only 200 μatm), an increase in pH to 8.2-8.3, and increased concentrations of carbonate ions, leading to a higher degree of calcium carbonate saturation (Lc = 3.4-3.8). The pCO_2 profiles show (*Figs. 5.3* and *5.4*) that pCO_2 decreases with depth and reaches its minimum value in the subsurface layer at 10-23 m, which coincides with a negative maximum of AOU_b. Most probably, this observed pCO_2 minimum reflects both the consumption of CO_2 by photosynthesis and the observed sharp temperature gradient, which decreases the sea-water temperature from 10°C at the surface to -0.3°C in subsurface waters. At station LV29-88-4, where the temperature gradient was not that sharp (within 5°C), a pCO_2 minimum was not observed in the subsurface water. The distribution of the properties pH, AOU_b, and Lc at station LV29-88-2 did not indicate an active photosynthetic process. This corresponds to the observations made in the mixing areas of the Okhotsk Sea (Bruyevich et al., 1960), where the surface water is not oxygen-supersaturated despite the abundance of phytoplanktic biomass.
If we assume that the atmospheric CO_2 concentration was close to 350 µatm at the time of the cruise, the difference of pCO_2 between the atmosphere and the sea surface of the Sakhalin Gulf was more than 100 μatm, thus indicating that the basin represented a sink for atmospheric CO_2 in July 2002. We may conclude that the high input of alkalinity from Amur River contributes to the observed spatial gradients in carbonate chemistry and thus directly influences the equilibrium conditions. The direct chemical influence on the carbon dioxide equilibrium was compared with the indirect impact of nutrient-stimulated photosynthetic uptake of carbon dioxide. Thereby, the carbonate

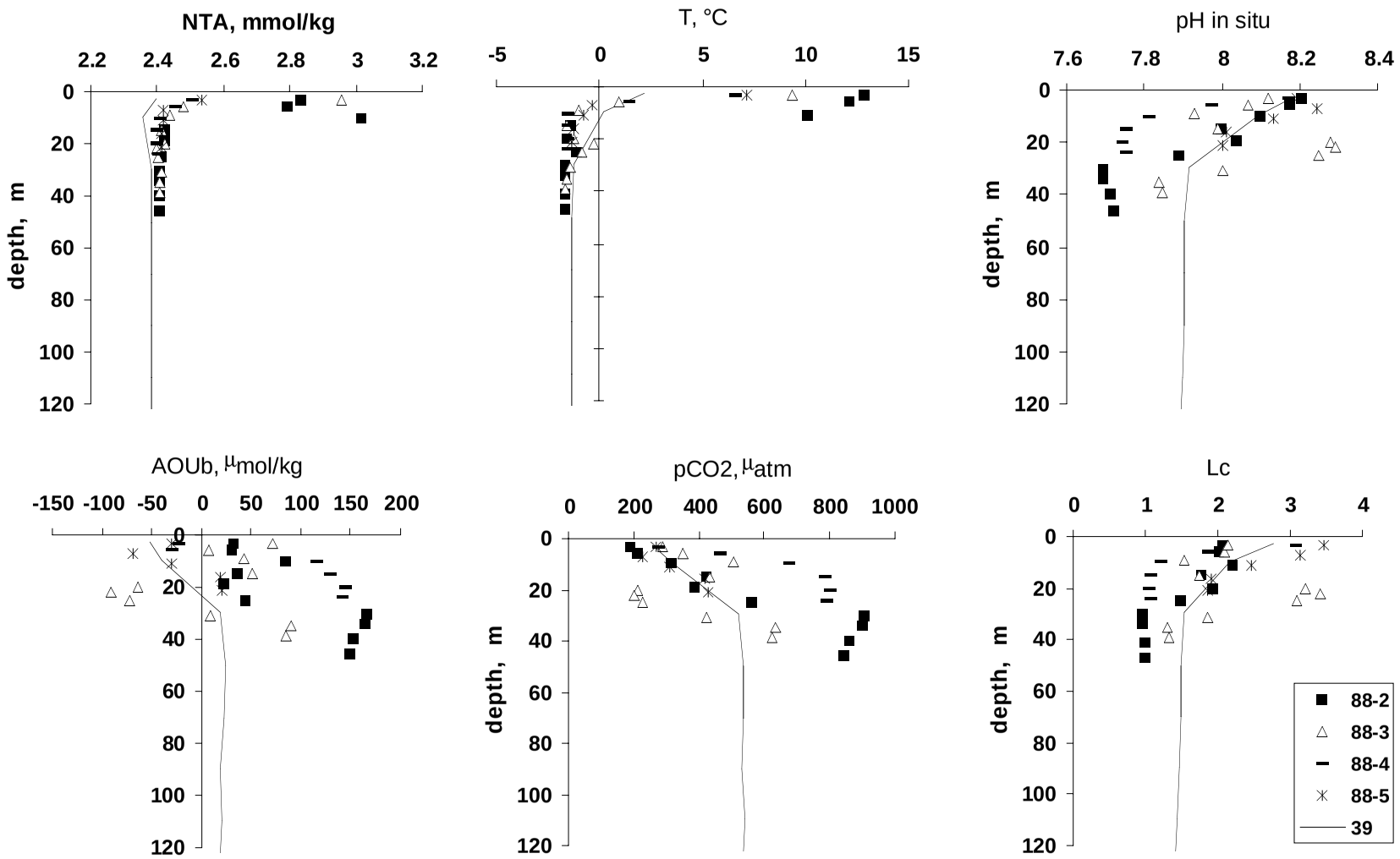

Fig. 5.4: *Vertical profiles of normalized total alkalinity (NTA), temperature (T), pH in situ, "biological" term of apparent oxygen utilization (AOUb), partial pressure of CO_2 (pCO_2) and saturation degree of calcite (Lc) at a East-West transect through the Sakhalin Gulf.*

chemistry investigations in the Sakhalin Gulf yielded a great sensitivity of the carbonate system with respect to biological as well as physical-chemical influences.

Future sample analyses for dissolved calcium will reveal the Amur River influence on the major components of the Okhotsk Sea.

5.2.3 Kurile Basin

The distribution of inorganic carbon equilibrium species is given for 8 stations representing the deepest part of the Okhotsk Sea, the Kurile Basin. Carbonate parameters (pH, Total Alkalinity and dissolved calcium) measurements covered the eastern (stations LV29-110 and -112) and the western (station LV29-70) slopes of the basin, the Kurile Straits areas via which the Okhotsk and Pacific waters exchange (stations LV29-114, -115, -120) and the deep Kurile Basin (stations LV29-116, -120, -123).

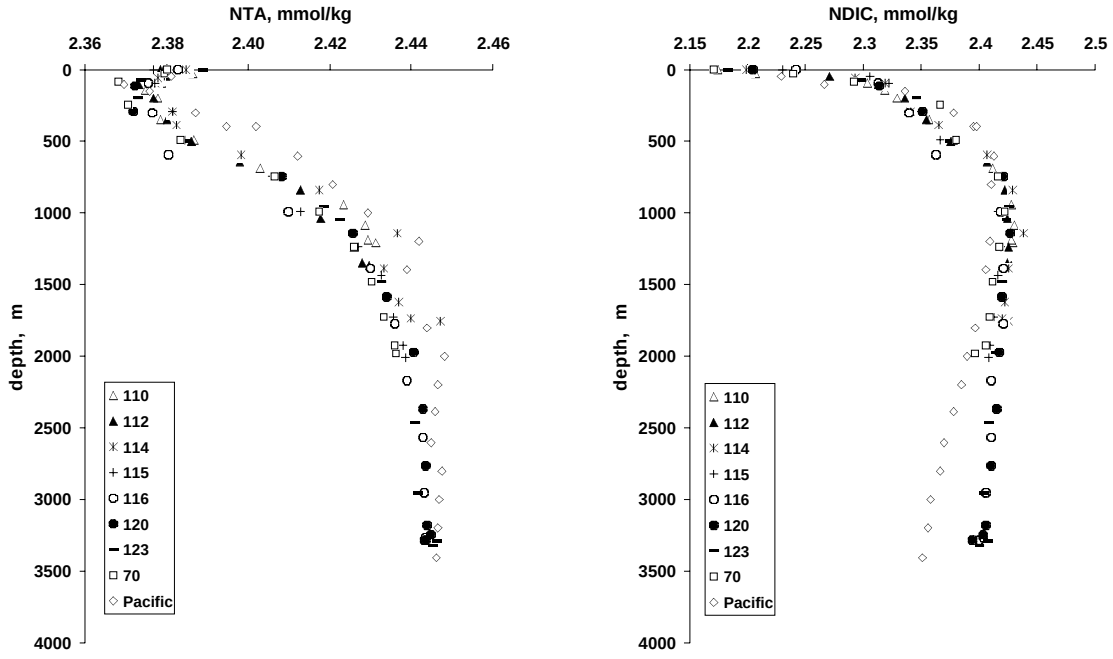

Fig. 5.5: *Depth scatter plots of normalized total alkalinity (NTA) and dissolved inorganic carbon (NDIC) in the Kurile Basin and the northwestern Pacific.*

The distribution of carbonate parameters in the surface layer reflects the spatial variability of the entire study area. Despite the summer photosynthetic activity, the highest values of pCO_2 (about 400 µatm) were observed at stations LV29-115 and -116 located in the Kruzenshtern`s Strait area. This can be explained by intensive vertical mixing and rising of deep, CO_2-rich water to the surface. In the surrounding waters, pCO_2 was less; and extremely low values were observed at the slopes of the Kurile Basin (300 µatm).
The distribution of carbonate parameters in the water column is almost homogeneous in the entire study area and may be summarized as follows. The consumption rate of dissolved $CaCO_3$ from sea water exceeds the rate of carbonate dissolution at water depths of 100 m due to biogenic $CaCO_3$ formation. Below 100 m biogenic calcium carbonate is dissolved, but accumulated in the sediments of the Kurile Basin up to a water depth of 1,200 m. The surface waters are highly supersaturated with respect to calcium carbonate. The saturation horizons

for calcite and aragonite are at 350 m and 100 m, respectively. Thus, the Kurile Basin waters are undersaturated with respect to calcium carbonate below 350 m and highly undersaturated (Lc <0.5) beneath a depth of about 2,000 m.

One of the most intensively discussed question during the investigation of the Kurile Basin, the process of the bottom water renewal, is not clear in detail. We compared two regions, the Kurile Basin and the open Pacific. Station 3 (44°59.90 N; 152°48.43 E) located in the northwestern Pacific Ocean was used to characterize the waters of the open Pacific. This station was performed for summer season in 1993; Total Alkalinity and dissolved inorganic carbon in the water column were measured using Bruyevich`s method (Bruyevich, 1944) and the coulometric method (Johnson et al., 1985), respectively. Since precipitation and evaporation affect the distribution of alkalinity and dissolved inorganic carbon, we chose to present and compare the data at the same salinity (NTA, NDIC).

Scatter plots of NTA and dissolved inorganic carbon (NDIC) for the entire study area in the Kurile Basin and for station 3 in the open Pacific are shown in *Figure 5.5*.
As it can be seen from the figure, the NTA profiles of the Kurile Basin and the open Pacific are substantially similar suggesting a possible water exchange between these two regions.
Scatter plots of NDIC show that the sea-water properties in the open Pacific and in the Kurile Basin are identical up to a depth of about 2,000 m. Below this depth, NDIC decreases with depth in the open Pacific by 40 µmol/kg, whereas in the Kurile Basin by 10 µmol/kg. The observed offset perhaps resulted from the difference between measured (open Pacific) and calculated (Kurile Basin) NDIC data. But the same distinct difference in the dissolved inorganic carbon content between the Kurile Basin and the open Pacific was also reported by Bychkov et al., 1996 for both measured profiles.
For station LV29-116, -120, and -123 (depth >3,000 m) an additional decrease in NDIC by 10 µmol/kg, resulting in a NDIC value of 2.394 mmol/kg, was found in a thin (about 30 m thick) near-bottom layer. Pacific waters with the same NDIC value (2.395 mmol/kg) were observed at approximately 2,200 m depth (the sill depth of Bussol Strait). This supports the idea of new Pacific waters intruding into the Kurile Basin through Bussol Strait (Salyuk et al., 2001). Thus, the process of bottom water renewal continues.

5.2.4 Bottom water study

The study of the carbonate system in the bottom water is very important for the understanding of geochemical processes in the underlying sediments. As parameters like the concentration of carbonate ions and the saturation degree of calcium carbonate indicate $CaCO_3$ preservation in the sediments, the carbonate parameters of the bottom water layer are also very useful for different diagenetic model calculations.

Bottom water samples were taken by 17 multicorer (MUC) deployments and were analyzed for pH and TA. Various carbonate parameters were in situ computed by the combination of the measured parameters according to a generally accepted scheme. A complete list of measured and calculated concentrations is given in *Table 5.1*. For comparison, the properties of the bottom water from CTD measurements, carried out at the same stations, are also listed in *Table 5.1*. The differences in depth between the MUC samples and the samples from the deepest horizons of CTD amounted to no more than 1-12 m.

Alkalinity is a good indicator for the bottom water as far as this parameter is very stable there. Striking differences in the TA values of the two sample groups were observed at stations LV29-70, -76, -84, -89. Obviously, the low alkalinity values of the MUC samples do not reflect the bottom water properties, but are artifacts produced by multicorer sampling.

Probably, sea water from shallow depths was trapped in the tubes overlying the sediment/water interface. Therefore, MUC stations LV29-70, -76, -84 and -89 were excluded from the further description.
Figure 5.6 shows the coincidence (within experimental uncertainty) between MUC and CTD Total Alkalinity values for the other 13 MUC stations.

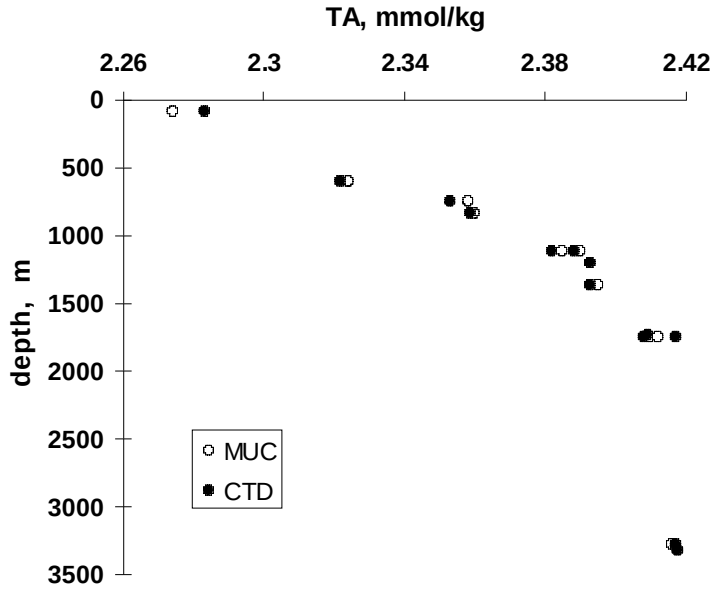

Fig. 5.6: *Comparison between total alkalinity (TA) values in bottom water for MUC and CTD stations.*

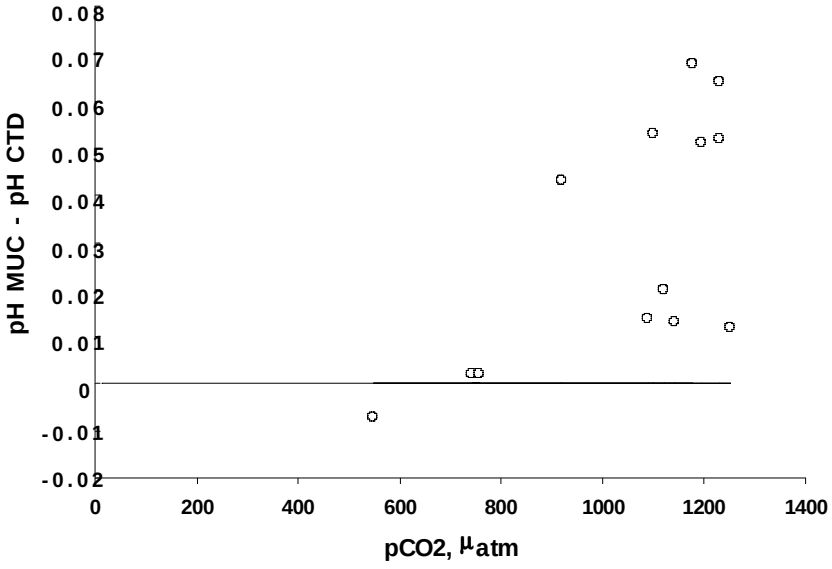

Fig. 5.7: *Difference between in situ pH values in bottom water for MUC and CTD samples versus partial pressure of carbon dioxide.*

The comparison of the pH values for this group of samples showed that pH of bottom water is higher in the MUC than in the CTD (*Fig. 5.7*). As it is clear from the figure, pH_{MUC} - pH_{CTD} values depend on the partial pressure of CO_2 in the bottom water. They do not exceed 0.01 pH

unit (the error of pH measurements is ±0.003 pH unit) when the pCO_2 values in the bottom water are less than 800 µatm, but they considerably increase (up to 0.07 pH unit) when pCO_2 is >1,000 µatm. Obviously, the increased pH value in MUC samples is a result of a loss of CO_2 from the bottom water to the atmosphere during the opening of the multicorer tubes and sampling of the bottom water. The loss is more intensive in samples with a very high CO_2 content.

We believe that the CTD carbonate parameters data reflects the in situ bottom water properties more correctly.

6. METHANE INVESTIGATIONS

Anatoly Obzhirov

6.1 Introduction

The first leg of cruise LV29 was devoted to gas-geochemical investigations and the second leg mainly to paleoceanological objectives. Gas investigations were an important task on both legs, because they provide informations about the methane distribution in the water column of different areas of the Okhotsk Sea. This is necessary to better distinguish between background and anomalous methane values and to use methane as a tracer for the sources of methane and for the direction of moving water layers. This is important for both gas-geochemical parameters of the water layers and for paleoceanological reconstructions. Apart from that, methane was measured in the sediment cores of 3 stations to compare the methane distribution in the sediment in different areas inside and outside of the fields of methane anomalies in the water column.
The main goal of methane investigations was to use methane like a tracer to distinguish water masses and to study the Sakhalin Gulf area and the Kurile Basin in more detail.

6.2 Method

Water samples were taken from the Niskin Bottles of the CTD-rosette. Gas was extracted from water by a vacuum line and analyzed by a chromatograph. Methane and heavy hydrocarbon values were measured. Standard gas produced in the USA was used for calibration. Gas in the sediments was studied by the Head Space method.

6.3 Results

6.3.1 Methane distribution in the water column

Methane measurements in the water column were carried out at 29 CTD stations. 2 stations were located at the western slope of the Kurile Basin, 7 at the Sakhalin slope, 4 at the northern Derugin slope, 5 in the Sakhalin Gulf, 2 in the northern Derugin Basin, 2 at the Kamchatka slope and 8 in the Kurile Basin. The methane distribution is given in Appendix 4.

6.3.1.1 Western slope of the Kurile Basin

Stations LV29-69 and LV29-131 were carried out at the western slope of the Kurile Basin located near station GE99-1 (Biebow et al., 2000) and in the open part of La Perusa Strait. The methane distribution in the water column of stations LV29-69 and GE99-1 is very similar – background concentrations at the surface (60-70 nl/l) and maximum concentrations in the subsurface layer (about 200-250 nl/l, depth 70-80 m). High methane concentrations (100-150 nl/l) were observed at 400 m and 700 m depth as well as in the bottom waters. The methane concentration at station LV29-131 increases in the near-bottom layer (225-433 nl/l, depth 749-692 m). This is possibly an indication for a mixture of different water layers with the upper layer containing a subsurface methane maximum originating from the Kurile Basin and the bottom layer with maximum methane concentrations from Aniva Bay. The methane anomaly in the bottom waters (more than 400 nl/l) of station LV29-131 may be caused by methane migrating from oil-gas-bearing sediments via a fault zone into the water column or by transport with water masses from the northern shelf and slope of South Sakhalin where methane flares and anomalous high methane concentration were found in the bottom waters.

6.3.1.2 Sakhalin slope

7 CTD stations were carried out along the Sakhalin slope (Appendix 4). Stations LV29-70 and LV29-72 are located in the northwestern Kurile Basin and on the Sakhalin slope at depths of more than 1,000 m. Methane is nearly equally distributed in the water column of both stations with a background concentration (45-50 nl/l) at the surface, a subsurface maximum (90-200 nl/l) and background values in deeper water layers (20-40 nl/l).
Stations LV29-76, -79, -81, -82, and -84 are located on the northeastern Sakhalin slope. As usual for this area (Biebow & Hütten, 1999; Biebow et al., 2000; Chapter 6, Part I of this Report) methane anomalies were found here especially in bottom waters (500-3,000 nl/l), whereas the content at the surface does not exceed background concentrations (50-80 nl/l). The concentration decreases (200-300 nl/l, station LV29-79) at depths greater 1,000 m. A large methane anomaly (15,000 nl/l) was measured at station LV29-81 in the intermediate water layer (depth 200 m). Perhaps, there is a flare near this station, and methane-containing waters migrate from the flare to station LV29-81. Methane sources in this area are oil-gas-bearing sediments and decomposing gas hydrates (see Biebow & Hütten, 1999; Biebow et al., 2000; Chapter 6, Part I of this Report).

6.3.1.3 Sakhalin Gulf

Stations LV29-88-2, -88-3, -88-4, and -88-5 are located in the Sakhalin Gulf. The methane distribution in the bottom water of this area was already studied in 1985 (Obzhirov, 1993). A comparison of the methane concentrations in the bottom waters obtained in 1985 and on this cruise shows similar values: there is a methane anomaly (200-300 nl/l) in the bottom water of the eastern part of the Sakhalin Gulf and a concentration at background level (60-70 nl/l) in the western part. A great methane anomaly (930 nl/l, depth 6 m) was measured in the surface layer of station LV29-88-3. The surface layers at all stations in this area contain high methane concentrations (115-650 nl/l), as well. The sources of methane and the reason for higher methane concentrations in the surface layers in comparison to the bottom water are still unclear. Oil-gas deposits are frequent on the Sakhalin coast and in the eastern part of the gulf. Methane can get into the bottom water from oil-gas-bearing sediments and into the water column from coastal oil-gas deposits. The high methane concentration at the surface possibly formed as a result of a mixture of water masses of Amur River and the Sakhalin Gulf. The methane distribution in the eastern part of the Sakhalin Gulf is similar to that on the shallow northeastern Sakhalin shelf.

6.3.1.4 Northern part of the Okhotsk Sea

Stations LV29-87, -90, -91, -92, -94 are located in the northern part of the Okhotsk Sea. Station LV29-87 is located between the Sakhalin Gulf and the open Okhotsk Sea. The methane distribution in the water column is here similar to that of station LV29-88-2, but the concentration is twice less. There is a methane anomaly (280 nl/l, depth 10 m) in the subsurface layer and a background concentration in the bottom layer. In northern direction (stations LV29-90, -91 and -94), background methane concentrations were observed in the water column with the exception for station LV29-92 where a high methane value (450-550 nl/l) was detected extending from the bottom (91 m) up to 60 m depth. Here, methane possibly emanates from oil-gas-bearing sediment and migrates via fault zones into the water.

6.3.1.5 Derugin Basin

Stations LV29-103 and LV29-104 are located in the deeper part of the Derugin Basin. The methane content is at background level over the whole water column from the surface to a depth of 1,400 m. A slightly increased methane content (100-150 nl/l) was found in the bottom water of station LV29-103, whereas the concentration in the bottom water of station LV29-104 is 10 times less (background concentration). But the water layer at 1,400-1,600 m depth of LV29-104 contains an about 3 times higher methane concentration (30 nl/l) than the bottom layer. Maybe this water layer with a thickness of about 200 m at station LV29-104 is stagnant.

6.3.1.6 Western slope of Kamchatka

Stations LV29-106 and LV29-108 are located on the western slope of Kamchatka. These stations were conducted to continue the station profile of cruise LV28 (Biebow & Hütten, 1999, stations LV28-40 – LV28-43) from the Sakhalin slope to the Kamchatka slope. The methane values in the water column of these stations do not exceed the background concentration and equal those obtained on cruise LV28 (stations LV28-42, -43).

6.3.1.7 Kurile Basin

Stations LV29-110, -112, -114, -115, -116, -120, -123 are located in the Kurile Basin. A regularity in the methane distribution of all these stations are decreasing methane concentrations from the sea surface (50-150 nl/l) to a depth of 1,000 m (7-15 nl/l) with this value being constant down to the bottom (depth 3,300 m). An exception from this was observed at station LV29-110 where the intermediate water layer (depth 700-900 m) contains a small methane anomaly (90 nl/l). An explanation could be that the water layer intruded into the area of station LV29-110 from the Paramushir slope where a high methane value was measured in a gas hydrate-bearing area. Methane measurements in the water column of stations GE99-6, -7, -8 carried out in 1999 (Biebow et al., 2000) yielded similar values with the exception of station GE99-7 containing a higher methane concentration (70 nl/l) in the bottom water. Here, methane possibly emanates from a fault zone connected with the acoustic basement rise (see Chapter 12). Another observed regularity is a subsurface methane maximum (150-250 nl/l, depth 100-150 m) in the water column of almost all areas of the Kurile Basin, especially in its western part.

6.3.1.8 Discussion

High methane concentrations of 1,600 nl/l at the seafloor depth of 367 m to 14,600 nl/l at 199 m depth were measured at station LV29-81. The methane distribution is here similar to that of "Giselle flare" where gas hydrates were found. This could mean that the sediments in the area of station LV29-81 (Sakhalin slope) possibly contain gas hydrates.
Another new area (station LV29-92) with an increased methane concentration of 528 nl/l at the seafloor depth of 91 m to 438 nl/l at 59 m depth was discovered on the northern shelf of the Derugin Basin. Methane emanates here probably from oil-gas deposits in the sediment via a fault zone.
Water layers intruding from the oil-gas-bearing area at the Sakhalin coast or from Amur River are supposed to be the source of the unusually high methane concentrations (600-900 nl/l) in the 10 m thick surface water layer in the eastern part of the Sakhalin Gulf. The methane flux goes here directly into the atmosphere and thereby may influence the primary productivity of this area and change biological tracers used for paleoceanographic purposes.

The low methane concentrations at the seafloor of the Derugin Basin (station LV29-104) of 7-8 nl/l from a depth of 1,754 m up to 1,650 m indicate that a methane flux caused by microbiological processes is almost missing. Methane was also measured in the core recovered at this station (Appendix 4): the concentrations vary from 0.003 mM/kg at 200 cm to 0.4-0.5 mM/kg at the depth interval 600-870 cm.
At the Sakhalin slope high methane concentrations in the water column were measured in an area where the concentrations in the core are less than at station LV29-104. This means that here, the methane anomalies in the water column are created when methane emanates from destabilizing gas hydrates, oil-gas deposits and is transported there by water layers from other areas (intruded water).
The bottom waters of the Kurile Basin contain very low (5-10 nl/l) methane concentrations. Deep Pacific Ocean water masses usually have the same concentration. It is supposed that the water layer of the deep part of the Kurile Basin consists of Pacific water masses from the seafloor depth of 3,300 m to a depth of about 700-500 m, while the upper water layer from 700-500 m to the surface consists of Okhotsk water. The methane anomaly (70 nl/l at 3,300-2,800 m depth) in the bottom water of station GE99-7 shows that there is also a source of methane in this area. Methane is here supposed to come from the interior of the basement rise via a fault zone.
The methane anomaly measured at station LV29-131 possibly intruded into this area with the current from the Sakhalin shelf and slope. Methane was measured here in a sediment core (see Appendix 4) yielding a similar concentration as in the core of station LV29-104. A background value (0.0001 mM/kg at 15 cm) was found in the core surface and a high methane concentration at the base of the core (0.4-0.7 mM/kg at interval 750-830 cm). In contrast to station LV29-104 where the bottom water contained very low methane concentrations (7-8 nl/l), a methane anomaly (about 400 nl/l) was measured in the bottom water of station LV29-131. This means that methane migrated into the area of station LV29-131 from the sediment via a fault zone or was transported into this area by water layers from the north, but that it is not of microbiological origin.

6.3.1.9 Conclusions

The results of methane measurement are the following:
1. There is a high methane anomaly in the water column of the Sakhalin slope (station LV29-81) providing evidence of the existence of gas hydrates in this area.
2. The high methane anomaly in the bottom water of the northern shelf of the Derugin Basin indicates that this area possibly is oil-gas-bearing.
3. The high methane anomaly in the surface layer (10 m thick) of the eastern part of the Sakhalin Gulf shows that the methane flux now emanates into the atmosphere.
4. The low methane concentration in the water column of the deep Kurile Basin (about 3,300-1,000 m water depth) serves as tracer for the presence of Pacific water masses.
5. The anomaly of methane in the bottom water of the western slope of the Kurile Basin marks the migration of water layers from the southern Sakhalin shelf and slope into this area.

6.3.2 Methane distribution in sediment cores

Methane was measured in the cores of stations LV29-78, -104, -112, -131 in order to compare the methane concentration in the cores from areas with and without methane anomalies in the bottom water and in core intervals in which gas is visible.
The results are presented in Appendix 4. The methane concentrations of different areas are almost the same. At the sediment surface (15 cm) the concentration is low (about 0.0001mM/kg). It slowly increases to a depth of about 200 cm up to 0.001 nM/kg, but then

increases very sharply below interval 200 cm reaching 0.4-0.7 mM/kg at interval 600-800 cm. This regularity in the methane distribution changes in the gas hydrate-containing sediment core where a methane anomaly (3-4 mM/kg, Appendix 4) was observed in the gas hydrate layer.
In the sediment of the core from station LV29-104 a black-colored layer was found at a depth of about 700-800 cm. This layer contains high methane concentrations (0.4-0.5 mM/kg) which are, however, not different from that in layers of another color (gray) in other cores (for example at station LV29-131).

6.3.2.1 Conclusions

1. There is a regularity of the methane distribution in sediment cores: a low (background) methane concentration (about 0.0001mM/kg) in the surface layer and a high concentration (0.4-0.5 mM/kg) at the base of the core (600-800 cm).
2. The concentration of methane in the bottom water does almost not depend on the methane concentration in sediment cores, because microbiologically produced methane concentrates in the lower layers of the sediment and, due to the influence of the biological filter, does not rise to upper sediment intervals.

7. PLANKTON SAMPLING

Andrea Abelmann and Tanja Pollak

Based on comprehensive plankton and surface sediment studies accomplished during KOMEX I, we were able to define radiolarian "key species and assemblages" to reconstruct Pleistocene changes in the water mass structure and biological productivity system of the Okhotsk Sea. For further paleoceanographic studies, which will focus on cores from the Sakhalin shelf, the Kamchatka slope and the western Kurile Basin, our plankton and sediment data sets were enlarged in Leg 2 of cruise LV29.

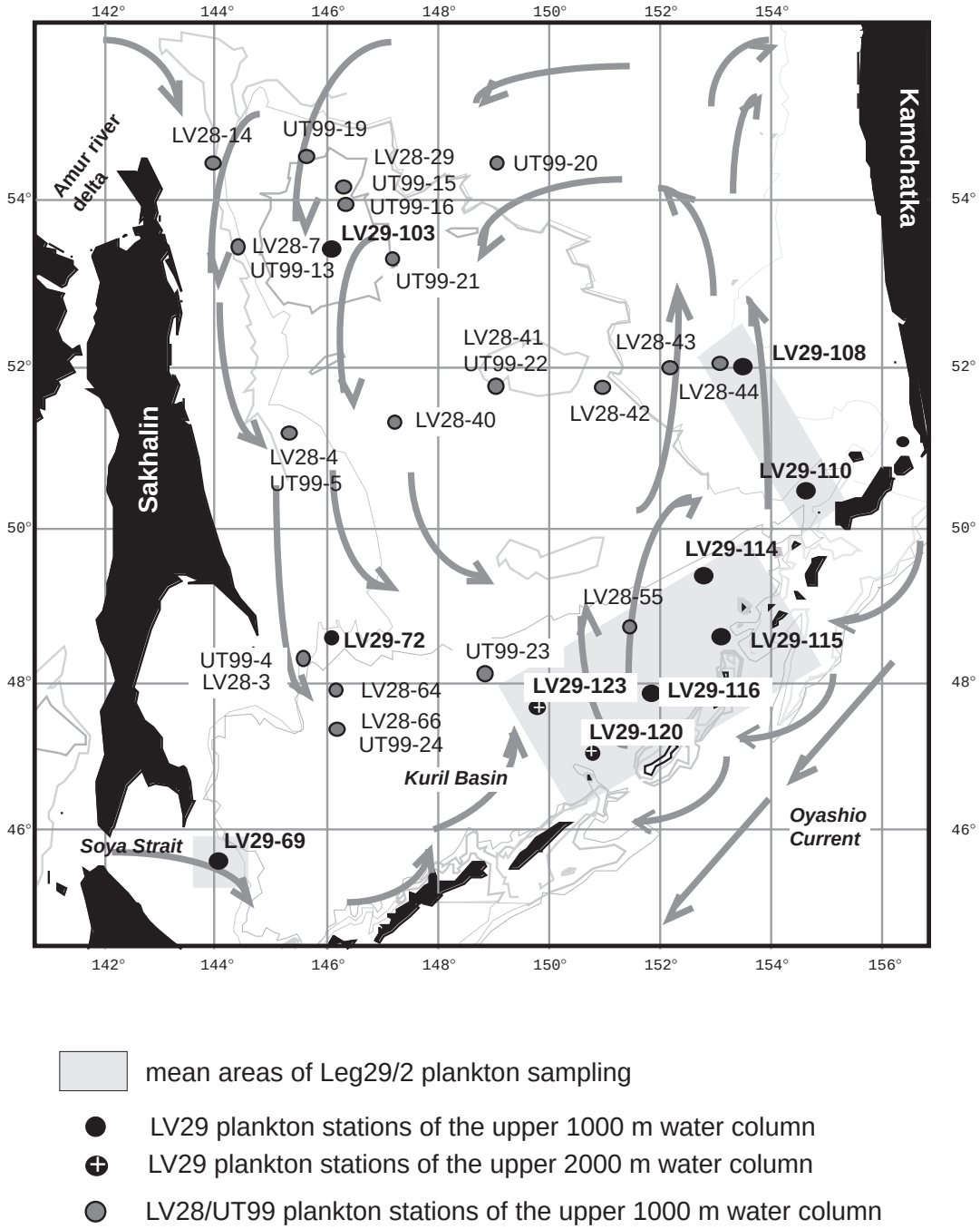

Fig. 7.1: *Locations of plankton stations sampled during Leg LV29/2 and previous cruises within KOMEX.*

7.1 Water column studies

Baseline for reconstructing the paleobiological system is the exact knowledge of the autecology of living radiolarians. On LV29 cruise we focussed our plankton sampling on the Kamchatka slope area, transects from the inner Kurile Basin towards the North Pacific and the Soya inflow area (*Fig. 7.1*). The goal of these investigations is to define
1) the boundary conditions of the biological system between the Okhotsk Sea and the North Pacific and
2) the import of taxa via the Kamchatka current (from the North Pacific) and the Soya Current (from the Japan Sea) into the Okhotsk Sea.

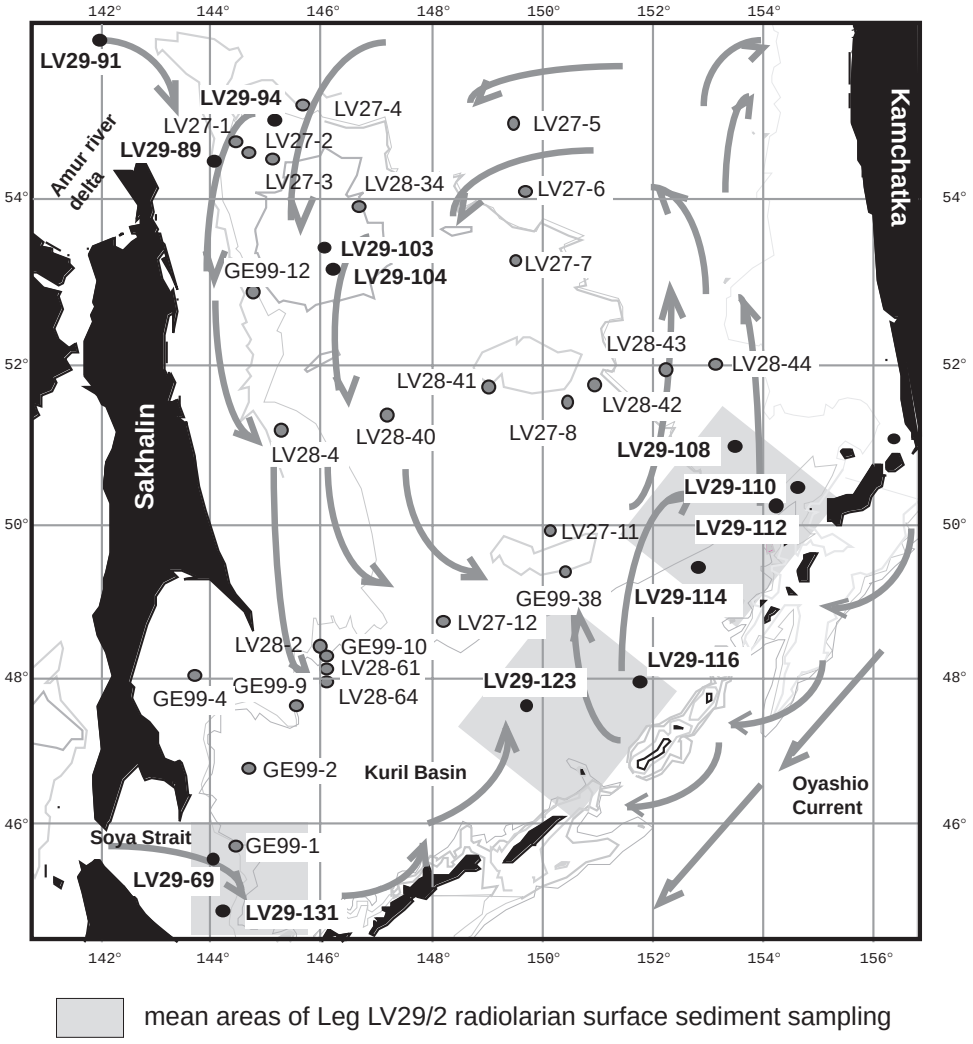

Fig. 7.2: *Locations of radiolarian surface sediment samples collected during Leg LV29/2 and previous cruises within KOMEX.*

We used an opening/closing net (Type MPS 92 B, "Hydrobios" Kiel, Germany), which consists of five nets, each 2.5 m long, with a mesh size of 55 µm fixed to a steel frame. This frame has a 50 x 50 cm large opening and is equipped with a motor and an electronic system for opening and closing the nets as well as a depth-measuring device. Both are connected with the board instrument, which displays the actual depth and which allows to open and to close the nets in specific water depths during heaving of the net. Each net ends with a sample beaker, equipped with a net window of 41 µm mesh size. Generally, we sampled five depth intervals in the upper 1,000 m of the water column according to the water mass distribution in combination with a CTD survey at each station. At two stations the water column was

sampled twice down to 2,000 m, including 9 different depth intervals. Depth intervals of each station are given in Appendix 5. Samples were preserved with a 2% dilution of formaldehyde.

The nets were towed vertically at low speed of 0.5 m s^{-1} (slacking) / 0.3 m s^{-1} (heaving) at all stations to avoid net clogging. The volume of water filtered was measured with calibrated flowmeters, which were installed at the inside of the mouth of each net. Thus, we could record the water passing through each net and for each depth interval. The application of flowmeters situated within the nets allows the quantification of the biological record, but also to recognize if the net has been clogged in areas of high productivity.

The differences between the flow meter values (the flow meter rotation values are proportional to the water volume flown through the net) after (F = final value) and before (S = start value) deployment multiplied by the opening diameter of the net frame (0.25 m^2) (A) and the impeller gradient (0.3 m) (P) defines the water volume (V) in m^3 flown through each net (Appendix A5).

$$V\ [m^3] = (F-S) \times P \times A$$
$$= (F-S) \times 0.3 \times 0.25$$
$$= (F-S) \times 0.75$$

7.2 Surface sediment studies

In contrast to plankton studies, which provide a spot-like information on the vertical distribution of taxa, surface sediment records provide a latitudinal signal integrated over a longer time period. To enlarge our radiolarian surface sediment dataset, needed as a reference for our paleoceanographic investigations, surface sediments were taken from various sites within the Okhotsk Sea, with emphasis on the Kamchatka area, the Kurile Basin and the Soya inflow area (*Fig. 7.2*). The sampling was done with a multicorer (MUC), which provides undisturbed sediment surfaces. For the radiolarian investigations the upper 0-1 cm were taken and preserved in formaldehyde. At most stations, we sampled one core in 1 cm slices to document the youngest sediment record, which may lack in the downcore record of the gravity cores.

8. PALEOCEANOLOGY AND SEDIMENTATION

Sergey Gorbarenko, Anatoly Botsul, Nicole Biebow, Lester Lembke, Anatoly Astakhov, Thomas Lüdmann, Alexander Derkachev, Natasha Nikolayeva, and Anatoly Salyuk

8.1 Introduction

Based on previous results of the RV *Akademik Lavrentyev* and MV *Marshal Gelovany* expeditions LV27, LV28 and GE99, we planned to clarify several important paleoceanographic problems in the Okhotsk Sea during the late Quaternary on cruise LV29:

8.1.1 Interaction of Amur River with oceanography and sedimentation in the Okhotsk Sea

We will further investigate the variability in Amur River runoff and influx of suspended material (development of Amur sediment drift). The prime area of investigation is set along a transect from the northern Sakhalin slope via the Derugin Basin to the Sakhalin Gulf.
Remarkably high sedimentation rates on the Sakhalin slope allow us to obtain high-resolution records to reconstruct rapid past changes of surface water conditions, supply of terrigenous matter and primary productivity during the Late Pleistocene – Holocene. The determination of these factors will help us to understand climate variability in the late Quaternary. Furthermore, we intend to clarify the varying production of North Shelf Density Water (NSDW) and the interconnected formation of Okhotsk Sea Intermediate Water (OSIW).
Our ongoing studies aim at the connection of marine productivity and terrigenous matter proxy records on the one hand with datasets from terrestrial climatic changes in the Amur drainage basin area and the surrounding Siberian hinterland. We try to evaluate the significance and impact of highly variable factors as precipitation, temperature, sea-ice cover in the Okhotsk Sea, their possible feedback mechanisms with the atmosphere and inherent ocean-continent interactions

8.1.2 High-resolution time scale study of the Pacific water inflow variability and the influence on paleoceanography

The sources of water masses in the Okhotsk Sea are from intermediate water layers of the NW Pacific (NPIW) and thence, also the newly formed OSIW is the product of mixing of the NSDW and inflowing Pacific water (Freeland, 1998). Today sea water masses below 800-1,000 m show parameters comparable to the Pacific via the deep Kurile Straits. Thus, oceanographic changes in the subarctic Pacific during Quaternary climate changes entail strong impacts on the Okhotsk Sea paleoceanography and -productivity. The areas of investigation are a southwest Kamchatka continental slope transect and a deeper profile on the eastern section of the Kurile Basin's slope. Our studies should provide a preliminary assessment of the Pacific water inflow changes into the Okhotsk Sea during the Quaternary and a connection with global climate and North Pacific paleoceanography. The changes derived from NPIW in the dichothermal layer; intermediate water production and the history of deep water ventilation will be studied in their response to climate change.

8.1.3 History of water exchange with the Japan Sea – La Perusa Strait's influence on the Okhotsk Sea paleoenvironment during the Quaternary and Holocene

The shallow depth of the La Perusa Strait sill (water depth 53 m) is a crucial key in regulating the warm subtropical water of the warm and saline Soya Current inflow from the Japan Sea into the Okhotsk Sea during glacioeustatical sea level changes.

Critical places for carrying out this part of our investigation are the southwestern part of the Okhotsk Sea close to La Perusa Strait and the deep profile from the northwestern Kurile Basin to the south Sakhalin slope. The influence of the relatively saline, dense Soya water on the OSIW formation will be studied during this part of work, as well.

8.2 Material and methods

During cruise LV29 the following steps of sediment sampling and processing were performed:

8.2.1 POI approach
8.2.1.1 Sampling

1. Sediment recovery was conducted with the POI Gravity Corer (SL-R): max. length 11 m, weight 850 kg, with an inner tube diameter of 145 mm. Polyethylene tubular film was inserted into the core before deployment. The attained sediment was removed from the corer in the PE foil. The Hydrostatic Corer (hydrocorer, HYC) with 126 mm in diameter and 6 m in length was used at vent areas with authigenic minerals and for gas hydrate sampling. The hydrocorer was also used for coring of harder sandy sediments. During Leg 2 of LV29 the total core recovery with the Gravity Corer and the Hydrostatic Corer added up to ca. 127 m. Aboard, a total of 114 m core was opened, described, measured and sampled in the matter described below.
2. Sediment cores were splitted. One half was used for sediment description, measurements and sampling, the other half was stored for archive.
3. Measurements of humidity and magnetic susceptibility were carried out every 2 cm by a microwave meter (MWM-8) and magnetic susceptibility meter (IMV-2) in direct contact with the sediment which is covered by cling wrap. Sampling every 20-50 cm for measuring sediment humidity and density according to the weight method as described below.
4. Sampling for micropaleontological (diatoms, radiolarians, foraminifers), granulometric (every 10 cm) and geochemical (every 5-10 cm) investigations.
5. Visual core description, sampling, preparation and the preliminary study of smear slides with microscope POLAM L-211.
6. Preliminary mineralogical investigations of volcanic ashes.
7. Separation and microscopic study of authigenic minerals, calcite, nodules and calcite-baritic crusts.

8.2.1.2 Mechanical properties of sediments

The analysis of sedimentary mechanical properties was mainly performed to establish a lithostratigraphy of the Quaternary sediments. In addition, the mechanical properties are necessary to calculate sediment accumulation rates. Since it is difficult to preserve the sediments natural humidity, humidity measurements were directly carried out aboard the ship immediately after core cutting.
Two methods were used: the standard weight method and humidity measurements with the MWM-meter. The first method includes sampling of 50 cm^3 of non-disturbed sediment, subsequent drying at 105°C temperature, and weighing before and after drying. On the basis of these data, the density of the natural sediment (D), the density of the mineral base (Dp), the volume humidity (Wv), and the weight humidity (Ww) were calculated applying the following equations:
$D = Po / V;$

DP = P / V;
Wv = (Po - P) / V x g x 100%;
Ww = (Po - P) / Po x 100%,
where Po and P are the sediment sample weight before and after drying; V - sample volume (cm^3); g - slime water density (g/cm^3) (1.00).

8.2.1.3 Magnetic susceptibility of sediments

Records of magnetic susceptibility mainly reflect the content of ferromagnetic minerals in the sediments. During the cruise measurements of magnetic susceptibility were obtained with the following method:
Cores retrieved with the POI gravity corer were measured with a sensor directly at the sediment surface. Magnetic susceptibility and humidity values were obtained every 2 cm alongcore. Magnetic susceptibility was measured in CGS-units using the microwave moisture meters MWM-8.

8.2.2 GEOMAR Approach

The KIEL Gravity Corer System was used for sediment sampling. The system consists of hot-dip galvanized steel tubes (575 cm length each, 125 mm diameter) connected by simple nail sockets and is equipped with a coretop penetration weight of 2 tons. The system is used with rigid PVC-liner tubes for sediment recovery allowing the permanent assessment of original sediment in the liner. During Leg 2 of LV29 the total core recovery with the KIEL Gravity Corer added up to 144 m.

Aboard, a total of 115 m core was opened, described, measured and sampled in the matter described below:

1. Cores were cut into segments of 1m length, and labeled following recommendations of Holler (1995)
2. Measurement of magnetic susceptibility: We used a Bartington loop sensor (MS2C) with a control unit (MS2) directly connected to a PC-laptop for data storage. The ring-shaped sensor generates a low-intensity magnetic field (f = 565 Hz), which is altered in its frequency by the sediment put into the loop depending on the amount of ferromagnetic minerals in the core section measured. Sampling interval was 1 cm.
3. Cores were split vertically and divided into work (W) and archive (A) halves. Sediment in the liner segments was leveled and covered with cling film.
4. The archive half was color-scanned with a handheld Minolta CM 2002 Spectrophotometer in 1 cm sample spacing according to the method outlined in Biebow & Hütten (1999).
5. X-radiographs were continuously taken from the work half of the cores (modified after Holler, 1995; Rehder, pers. comm.).
6. 5cc (10cc) syringe samples were taken at 5 cm (10 cm) intervals for subsequent land-based analysis of physical properties (pp-samples). Syringes were closed with caps and sealed with TEMFLEX tape. Sealed syringes were welded airtight in evacuated PE foil bags to minimize loss of pore water content. During the cruise, samples were stored refrigerated at 4-6°C.
7. Visual core descriptions were carried out on the archive halves of core segments. Classification of sedimentary texture and lithology generally follows modified recommendations of the ODP program (Sachs et al., 2000). Classification of randomly occurring dropstones is described by Powers (1982), grain sizes of the terrigenous fraction are classified as recommended by Shepard (1954).

8. A total of 337 smear slides was taken from the cores in order to corroborate the on-board visual core descriptions. Initial analysis (estimates of grain size distribution and components) was carried out at GEOMAR, Kiel using a Leitz Laborlux 12 POL S polarization microscope with a 100 x - 500 x magnification according to grain size composition.

8.2.3 Sediment stratigraphy and age model

In order to get an initial sediment stratigraphy and preliminary age models of the cores, we used the following proxies: visual sediment description, semi-quantitative analysis of smear slides, color spectra, magnetic susceptibility, water content, dry bulk density and tephrachronology. For stratigraphic interpretation of these datasets we follow the multi-proxy stratigraphy developed for Okhotsk Sea sediments based on oxygen isotope stratigraphy, AMS radiocarbon datings, sediment color and magnetic susceptibility records, calcium carbonate/opal content and tephrachronology (Gorbarenko et al., 1998; Biebow & Hütten, 1999; Biebow et al., 2000; Gorbarenko et al., 2002).

8.3 Results

8.3.1 Northwestern Kurile Basin - south Sakhalin slope profile

Stations LV29-70 and LV 29-72 are located at intermediate water depths of 2,325 and 1,380 m, respectively.

8.3.1.1 SL-R (LV29-70-2, LV29-72-2)

Records for these cores (*Fig. 8.1* and Appendix 6) show that both have sedimentation patterns typical for this part of the Okhotsk Sea and a rather clear stratigraphy and age model after correlation to existing records (Gorbarenko et al., 2002). Diatomaceous sediment with a base age of 6-8 kyr covers the upper 60 and 170 cm in cores LV29-70-2 and LV29-72-2, respectively. According to MS records, biogenic opal and carbonate content (smears slides description), the MIS 1/2 boundary is placed in LV29-70-2 and LV29-72-2 at a depth of 120 cm and 340 cm, respectively. With regard to ash layer K2 with an age of 26 kyr (Gorbarenko et al., 2002), MS records and the main component composition the boundary of MIS 2/3 can be determined at a depth of 370 cm and 545 cm in both cores. A gray ash layer at a depth 727 cm in core LV29-70-2 was preliminary identified by mineralogy as Spfa-1. Thus, the lower parts of both cores likely belong to MIS 3.

8.3.1.2 SL-G (LV29-70-3, LV29-72-3)

Records of magnetic susceptibility (MS) and color spectra allow us to set up a preliminary age model for the two cores LV29-70-3 and LV29-72-3, though our results remain preliminary and need further proof by independent proxy data.

LV29-70-3

Diatomaceous ooze extends down to 237 cm, thereby decreasing in total diatom abundance downcore. This upper section is interrupted by a brief setback at 166-180 cm with decreased diatom content and slightly elevated MS values that might represent a climatic rebound and the establishment of high biogenic productivity hereafter (i.e. visibly high diatom content in sediments). Later works for refined stratigraphic control will show if this offset correlates with global climatic signals like the commonly known early Holocene Northern Hemisphere climatic collapse at around 8,200 yrs BP. According to that, the sub-

sequent excursions in the MS signal (*Fig. 8.1*) might mark the terminations Ic, Ib and Ia at ca. 238 cm, 256 cm and 295 cm, respectively, with the Bølling-Allerød period between

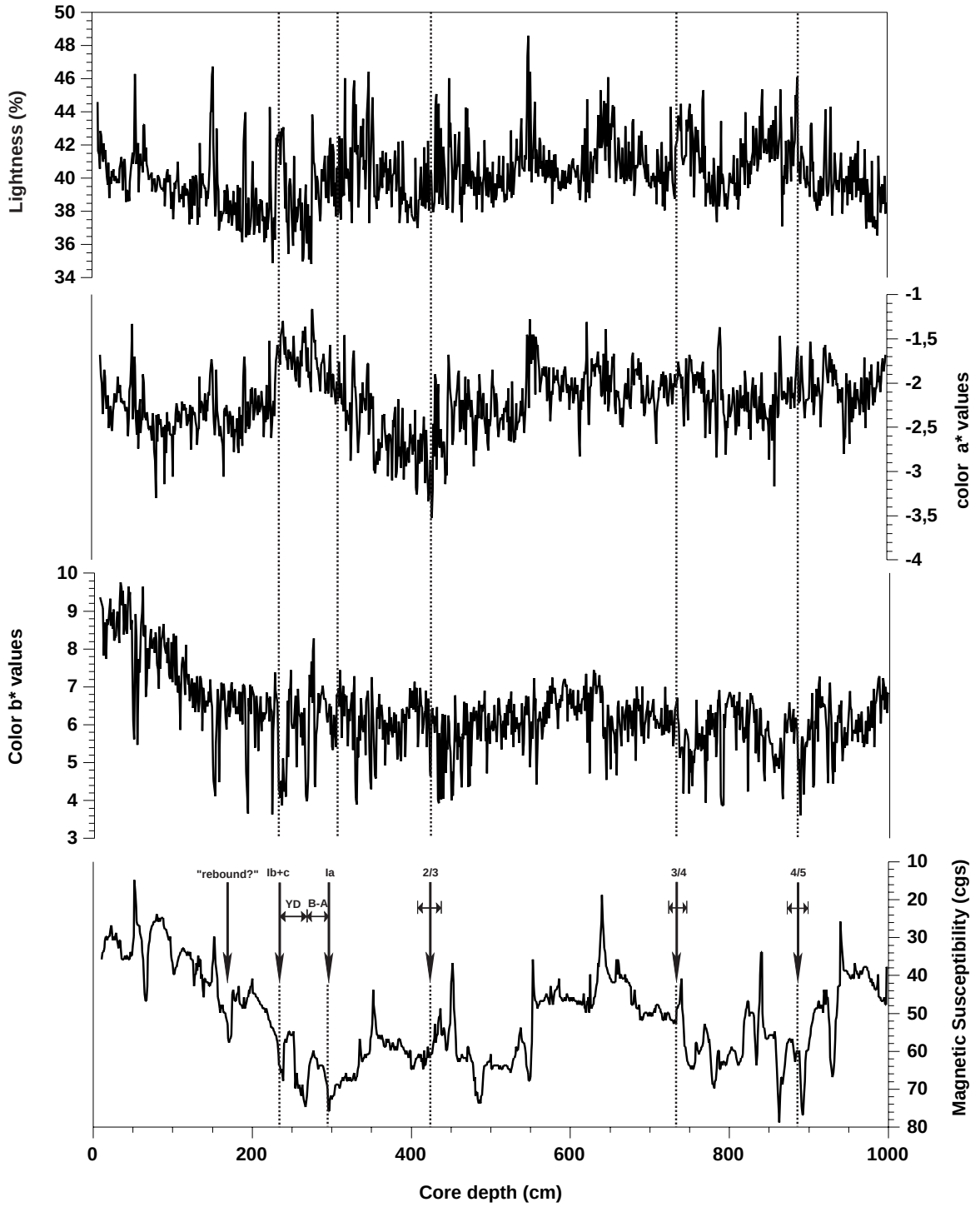

Fig. 8.1: *LV29-70-3, from top to bottom, Lightness of color reflectance spectra, Color spectrum of red-green chroma, Color Spectrum of yellow-blue chroma and magnetic susceptibility.*

the latter depth and ca. 270 cm. The MIS 2/3 transition occurs around 439 cm core depth with a slight decrease in MS values, accompanied by a notable increase in diatom content between 366-439 cm. Our findings are endorsed by the occurrence of cm-large lenses of volcanic ash (identified as K2 ≈ 26 ka) in core LV29-70-4 at a core depth of 483.5 cm and eventually ash layer Spfa-1 (≈40 ka), forming a 3-4 mm thick sandy layer at a depth of 706.5 cm. The MIS 3/4 boundary we prefer to leave rather unascertained, we believe it to

occur around 732-745 cm as we see there a decrease in diatom abundance and increased MS values. From 880 cm downcore, slightly higher contents of biogenic silica (diatom fragments mostly) and lower MS values might point to a change towards ameliorating climatic conditions. Further high-resolution studies of biogenic opal content, terrigenous supply and extended stratigraphic framework will elucidate if LV29-70-3 really reaches MIS 5 at its basal part.

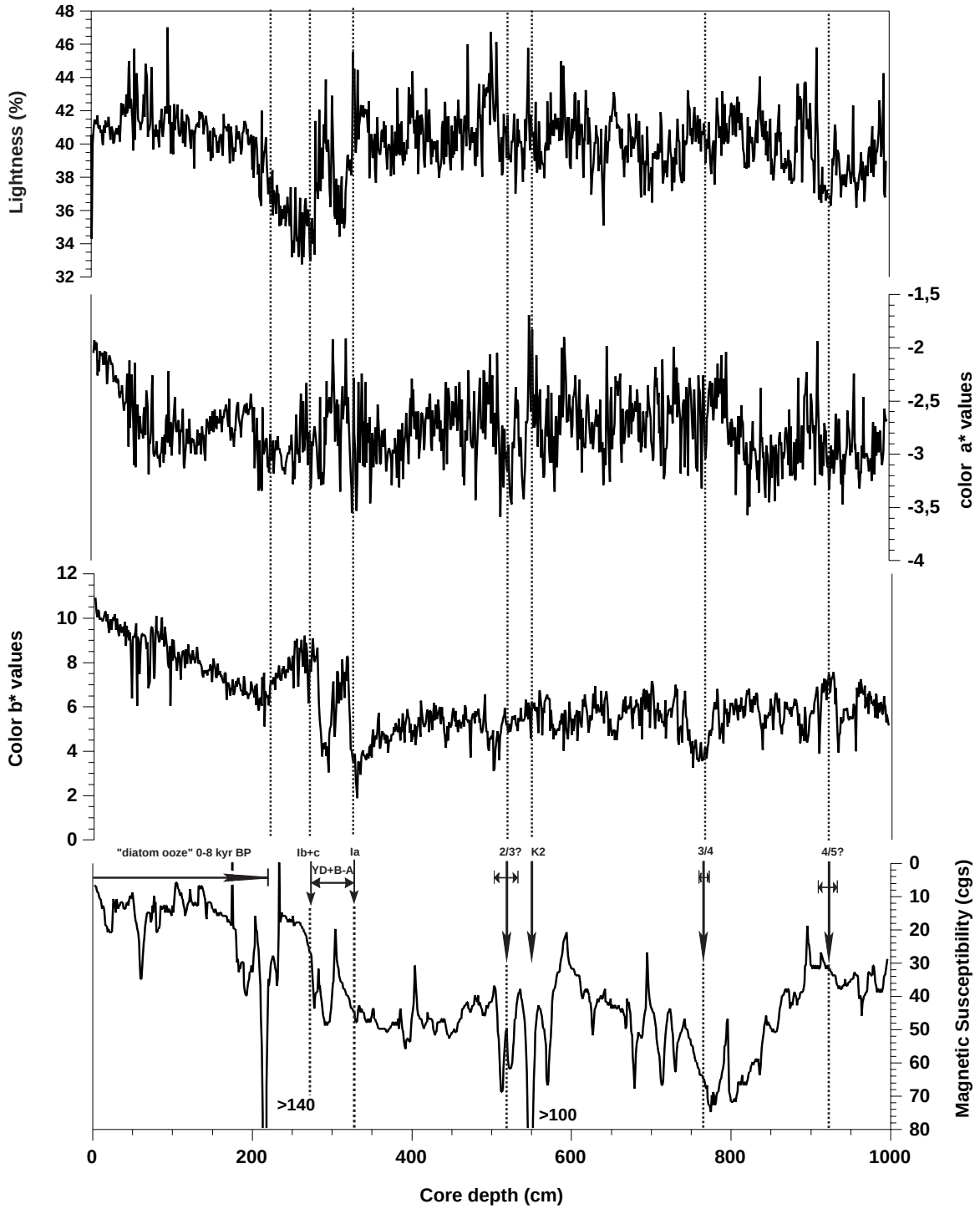

Fig. 8.2: *LV29-72-3, from top to bottom, Lightness of color reflectance spectra, Color spectrum of red-green chroma, Color Spectrum of yellow-blue chroma and magnetic susceptibility.*

LV29-72-3

In this core, typical late Holocene diatomaceous ooze (deposited during the last 6-8 kyr, according to Gorbarenko et al., 2002) extends down to 229 cm as indicated by decreasing lightness and – more pronounced – color b* values as well as smear slide analysis (*Fig. 8.2*). We place the last deglaciation/Termination Ib around 275-283 cm, preceded by the Younger Dryas (YD)/ Bølling-Allerød (B-A) interval at 283-322 cm. This interval is characterized by coarser grain sizes and weaker sorting, respectively, in the terrigenous fraction and reduced diatom content as well. We suppose the B-A warmer period might be separated from the YD event by notably elevated color b* and a* values pointing towards increased abundance of biogenic particles, though this criterion is not as clearly seen in the lithological description yet. Larger dropstones occur at depths of 510 cm and 526 cm, biasing the color and MS signals. Accordingly, we assume that the MIS 2/3 boundary in this core lies within this interval (ca. 505-530 cm), since we identified ash layer K2 (26 kyr BP) at a depth of 550-555 cm.

Slight changes in lithology and the increase in MS values point to the MIS 3/4 transition to be located around 788-91 cm as we observe frequent dropstones and higher sand/silt content between 788 cm and 930 cm, indicating colder climatic conditions. Finally, we dare to place the MIS 4/5 transition at 925-935 cm core depth due to a remarkable decrease in MS values and coincident appearance of diatoms (mostly fragments), though quite rare.

8.3.2 North Sakhalin slope

8.3.2.1 Setting

The study area is located on the northeastern Sakhalin continental slope proximate to the Derugin Basin. The goals of this investigation are the influence of Amur River on the paleoceanography and sedimentation in the Okhotsk Sea within the last 10,000 to 15,000 years. Extremely high sedimentation rates on the Sakhalin slope allow us to get high-resolution records of the climate, surface water conditions, sea-ice cover and varying productivity. Two echosounding profiles and four stations (LV29-78, LV29-79, LV29-81, LV29-82) were conducted in this area.

8.3.2.2 SL-R (LV29-78-2, LV29-79-2, LV29-82-1)

Cores LV29-78-2 and LV29-79-2 were taken on the southern profile from depths of 655 m and 1,102 m respectively. The echosounding data shows parallel reflections of high amplitude at depths of more than 7-8 m (see Chapter 3). Station LV29-82 was set at a depth of 795 m on the northern profile. The echosounding data shows here exposed ancient sediments, but core LV29-82-1 penetrated only sediment of MIS 1 and did not reach older strata.

All these cores showed similar sediment sequences. Diatom ooze or diatomaceous silty clays compose the upper part. Weakly diatomaceous silty clays and clayey silt follow below. The core descriptions (see Appendix 6) and records of the component composition, physical properties (see Appendix 6) allow us to determine the sediment age to be not older than MIS 1. An additional age record may be established by the biogenic opal content. The base of intensive diatom accumulation in the Okhotsk Sea usually corresponds to the 6-8 ka period (Gorbarenko et al., 2002).

8.3.2.3 SL-G (LV29-78-3, LV29-79-3)

Onboard work concentrated on cores LV29-78-3 and LV29-79-3 (*Figs. 8.3* and *8.4*). Both cores show sedimentation patterns very similar to the Russian gravity cores (SL-R). MS are very low in both cores, it is generally assumed that below values of 30 cgs units, pre-

cise analysis is hampered by a low signal/noise ratio. However, neither do we see an increase in MS values nor complete changes in lithology in the lower parts of both cores, thus we strongly believe that they consist entirely of Holocene sediments without covering the last deglaciation. This in turn points to an extremely high sedimentation rate of more than 100 cm/kyr averaged over the complete core length. In LV29-78-3, we may put the basal boundary of the diatom-rich facies at ca. 600-640 cm, based on slight changes in color a*, b* values and a decrease in diatom content.

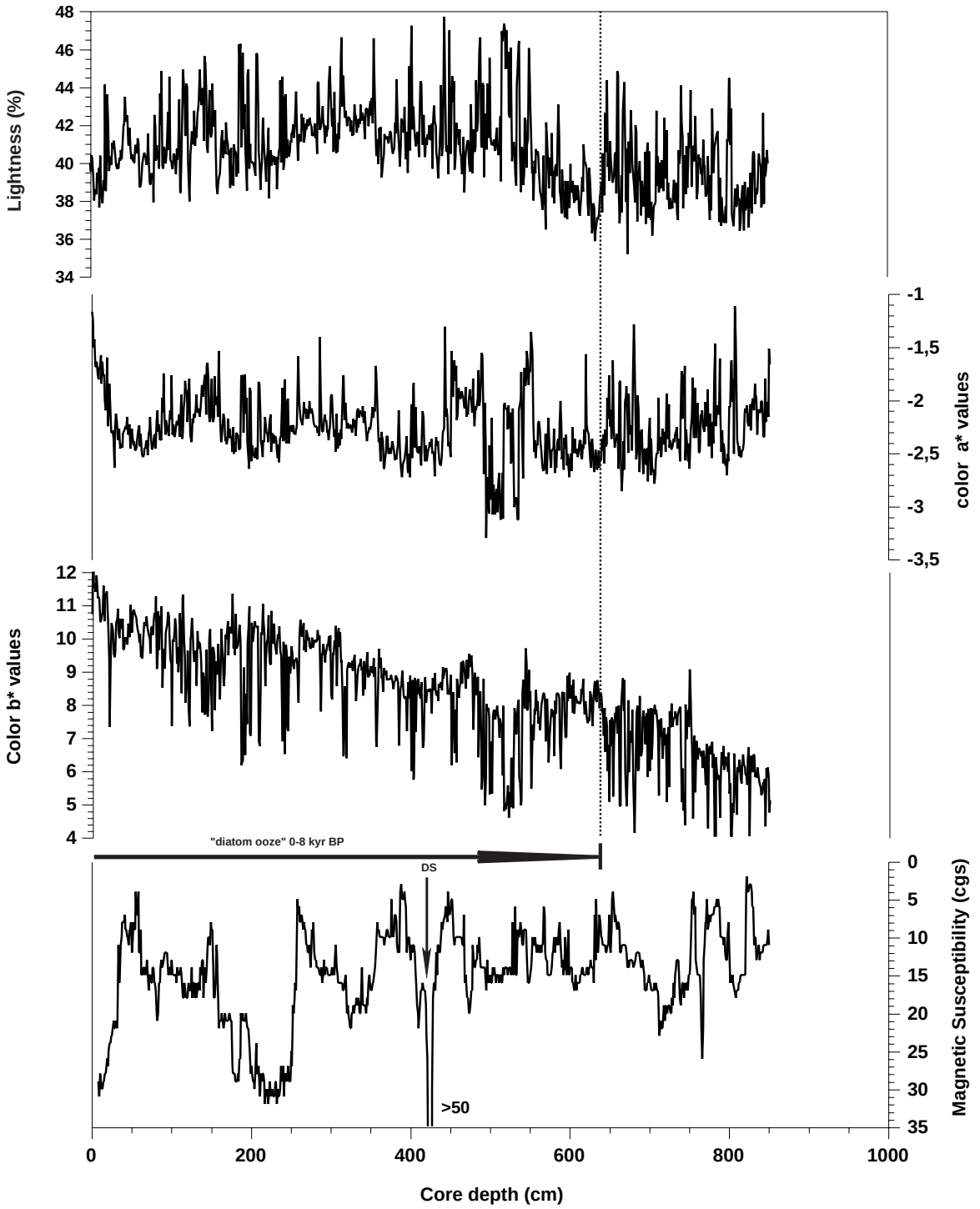

Fig. 8.3: *LV29-78-3, from top to bottom, Lightness of color reflectance spectra, Color spectrum of red-green chroma, Color Spectrum of yellow-blue chroma and magnetic susceptibility.*

At core LV29-79-3 we observe a distinct decrease in diatom abundance around 650 cm, though several intervals with lower diatom abundance occur in the upper part, e.g. around 540 and 570 cm, together with a slight coarsening of the siliciclastic fraction downcore. So far, we did not succeed in reliably correlating MS or color records of the two new cores to our well dated core LV28-4-4 from a more southern position at the Sakhalin continental margin.

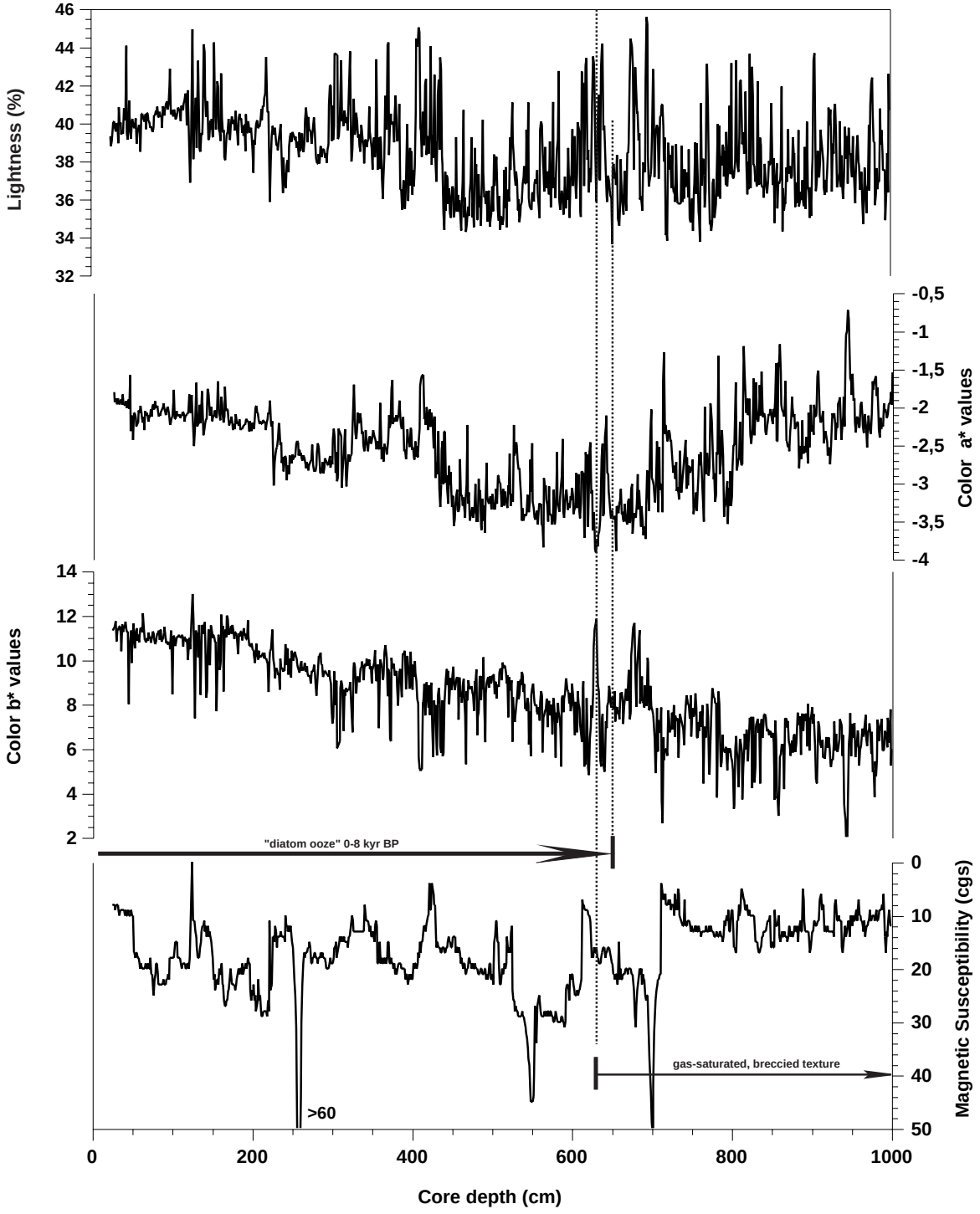

Fig. 8.4: *LV29-79-3, from top to bottom, Lightness of color reflectance spectra, Color spectrum of red-green chroma, Color Spectrum of yellow-blue chroma and magnetic susceptibility.*

However, we put forth the proposition that the occurrence of early diagenetic alterations (see Chapter 8.3.2.3) has appeared rather synchronously at the Sakhalin margin due to a

regional event (degassing, as indicated from seismic profiles and the correlation of the new cores diagenetic alterations and primary lithology). At core LV29-78-3, diagenesis starts at a core depth of 491 cm, at core LV29-79-3 at 631-635 cm and at reference core LV28-4-4 at 427 cm core depth currently resembling an age of ca. 3,700 cal. yrs BP.
Further stratigraphic work will have to be carried out to achieve a precise age model of our new cores and in turn solve the question if diagenetic alterations really represent a regional feature possibly recorded in other sites (Tiedemann et al., 2001).

8.3.2.4 Early diagenetic alterations

Typical textures of gas migration and an H_2S odor were revealed in all cores at depths of more than 400-500 cm. At or below this border an intensive diagenetic mineralization occurs in the form of globule pyrite and microcrystalline carbonate (see *Figs. 8.3 and 8.4*). Lenses and interlayers of dense diagenetic sediment with carbonate cement compose the bases of cores LV29-78-2 and LV29-79-2. Diagenetic layers of low water content and low porosity with globule pyrite cementation were revealed in cores LV29-79-2 and LV29-82-1. Reflector boundaries on the 8 kHz profiles of the studied cores are well correlated with diagenetic changes in the sediment like diagenetic carbonate cement, diagenetic sulfide layer, the top boundary of brecciated sediment.

8.3.3 Kashevarov Bank (LV29-94-2)
8.3.3.1 Setting

The cores at station LV29-94 were recovered from the southern slope of the Kashevarov Bank from a depth of 1,142 m (LV29-94-2, SL-R) and 1,134 m (LV29-94-3, SL-G), respectively. Previous studies indicate that the sedimentation pattern at this location is completely governed by material input from the northern shelf of the Okhotsk Sea while being separated from the Amur River influence by Staretsky Trough. The Kashevarov Bank with a shallow top is exposed to strong tidal currents having large influence on the sedimentary regime in this area.

8.3.3.2 SL-R (LV29-94-2)

The MIS 1 sediment in core LV29-94-2 has a very small thickness (16 cm) and consists of sandy silt with diatoms, likely being reworked (see Appendix 6). The sediment of this core bears a significant proportion of sand through the entire core. Especially large amounts of sand with gravel were observed in horizon 625-750 cm, which may be very preliminary correlated with MIS 4. The strongly reflected boundary in the 8 kHz records at a depth of nearly 9 m is apparently connected with this horizon. In line with the MS records, water content and an ash layer hypothetically identified as K2 (see Appendix 6), the MIS 2/3 transition was set at 360 cm.

8.3.3.3 SL-G (LV29-94-3)

In this core the abundance of diatomaceous sediments drastically decreases in the upper 80 cm pointing towards either a reworking of sediment or a missing upper section of softer sediment. Though at this location, a non-continuous sedimentation regime is very likely, MS records point out the possibility of a rather undisturbed record in the upper part of the core. We presume the YD and the preceding B-Al period to occur at depths of 241-260 cm and 260-286 cm, respectively, the latter mainly based on MS record (*Fig. 8.5*). As well, we put the MIS 2/3 transition at ca. 400-410 cm, due to a significant decrease in MS values. MIS 3/4 boundary is assumed to appear at 638-640 cm, based on remarkable increases in

small dropstones, sand lenses and layers and a general coarsening of the siliciclastic fraction. MIS 4/5 might be set at a depth of ca. 840 cm as MS values decrease to minimum MIS 3 values, though not reaching Holocene minima.

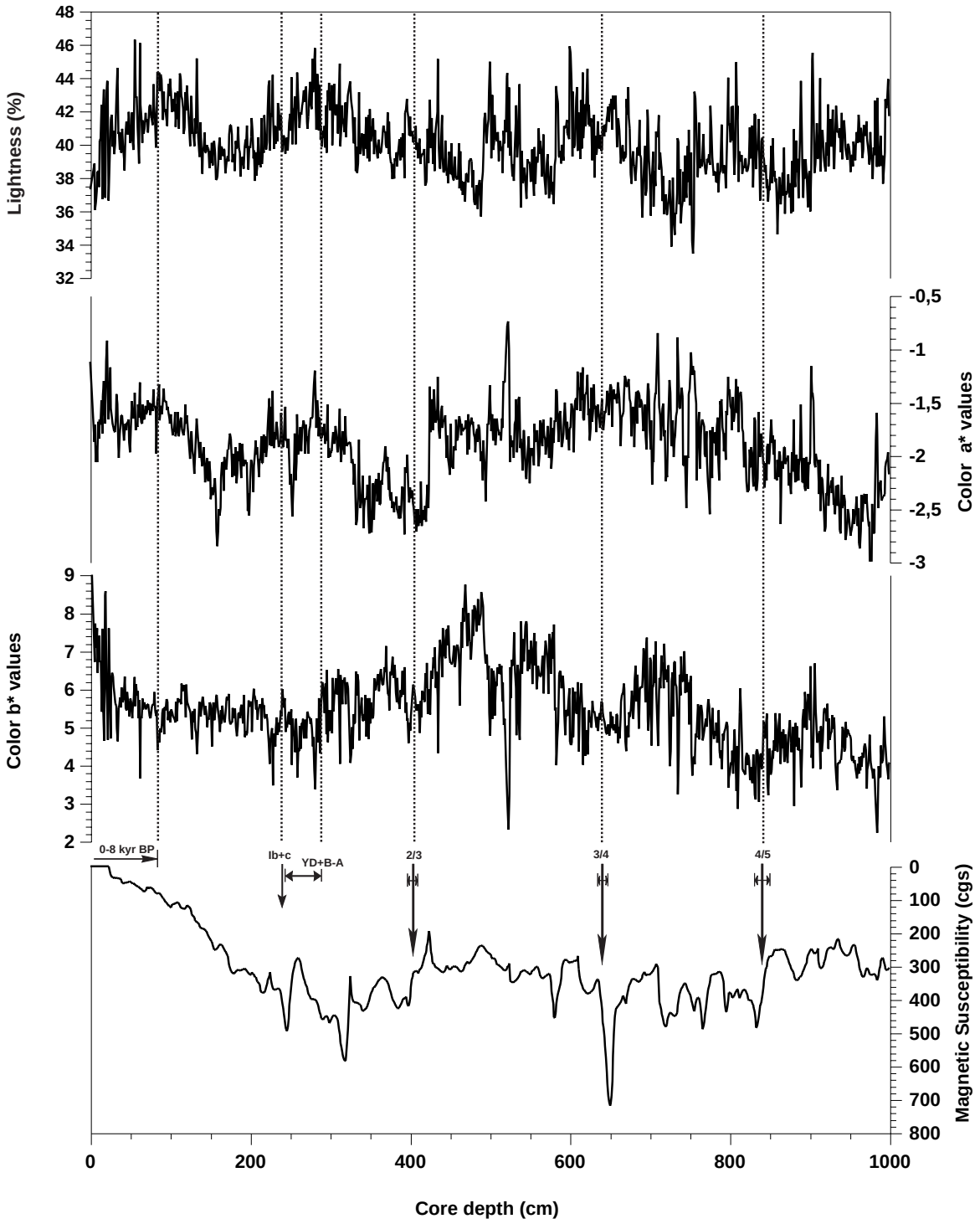

Fig. 8.5: *LV29-94-3, from top to bottom, Lightness of color reflectance spectra, Color spectrum of red-green chroma, Color Spectrum of yellow-blue chroma and magnetic susceptibility.*

8.3.4 Sakhalin Gulf (LV29-89, LV29-91)

8.3.4.1 Setting

Sampling points were chosen subsequent to a preliminary analysis of the 3.5 kHz echosounder data. Practically the entire seafloor of the gulf is covered by sediments of sandy

grain size (Astakhov, 1986; Dudarev et al., 2000). Within the upper part of the sedimentary section (0-15 cm), well sorted medium-fine-grained sands of grayish-green color usually occur. They are related to palimpsest deposits according to the classification of McManus (McManus, 1975).

In the area of station LV29-91, the upper part of the sedimentary layer is composed of marine sediments with a thickness of about 27 cm, consisting of well sorted sands amongst which mixed sandy-gravel-pebble sediments occur. Below 35 cm this lithology is replaced by gravel-pebble deposits, which probably belong to a beach facies.

8.3.4.2 SL-R/ SL-G

Core LV29-89 recovered a typical section of relict inshore-marine and lagoon-estuarine deposits of hypothetically late Pleistocene age. The upper part of the core (5-22 cm) is described as inshore-marine and beach deposits consisting of silty sand, sand with admixture of gravel and pebble; rare shell fragments occur. Below, these deposits are gradually replaced by lenticular-bedded compact sediments of dark gray color with an interchange of thin laminae of silt, clayey silt, sandy silt, and they have a lagoon-estuarine origin. Besides, fragments of wood branches and a large quantity of mica occur in this facies.

8.3.5 Derugin Basin (LV29-103, LV29-104)
8.3.5.1 Recent environments and coring position

The investigation of the southern depression of the Derugin Basin was made for discovering and studying anoxic sediments and environments in different glacial-interglacial periods based on the existence of closed depressions and recent hydrochemistry of bottom waters. They are located within the oxygen minimum layer (OML), and the oxygen content in the water column decreases towards the bottom. The oxygen content of the Okhotsk Sea bottom waters is very low (Bezrukov, 1957; Bruyevich et al., 1960; Freeland et al., 1998). These bottom waters of the deeper part of the Derugin Basin can be interpreted as suboxic due to the absence of oxygen. An anoxic environment can arise from small changes in hydrochemical conditions. The deeper part of the Derugin Basin is one of the possible places for the development of anoxic conditions.
Besides, the investigation goal was to study the Amur River deep paleo-fan during glaciation when the river delta was located on the recent shelf to the north of Schmidt Peninsula. The possible deep-sea fan enriched in fine organic matter sediment and turbidities was recovered earlier in the northern part of the Derugin Basin (stations LV27-3, GE99-30, GE99-31) (Astakhov et al., 2000). In this region, turbid seismic facies were mapped (Lüdmann et al., 2002). Their location indicates the nearest part of the deep fan to the river mouth during glaciation (Astakhov, 1986). Such specific seismic facies were also revealed on the shelf (prograding clinoforms) and slope (lenticular, stratified to wavy) (Lüdmann et al., 2002).
On the outer part of the deep fan outside the turbid facies two coring stations (LV29-103 and LV29-104) were chosen on the basis of preceding echosounding. According to the echosounding data, the bottom of the southern Derugin Basin is rough with many smooth elevations. On the top of one of these elevations ancient sediments are exposed. On the sides of the elevations, older sediments are covered by stratified sediments with several reflectors. The first one can be traced areawide at a depth of 2-4 m. The next reflectors submerge to the central part of the depression from 5-8 to 15-20 m. The deeper part of the depression has a smooth relief and is covered by stratified sediment with horizontal reflectors. It is noteworthy that, according to our data, the depth of the deeper part of the Derugin Basin does not prevail 1,760-1,770 m, although many bathymetric maps show

depths of more than 1,800 m. The 12 kHz echosounder (ELAC) was calibrated by the CTD sound and pressure sensor for water depth. The coring position for station LV29-103 was selected on the slope of a small elevation not far from its top. The reflectors are here close to one another with the first 10 m including 3-4 reflectors. Station LV29-104 is located in the central part of the depression. Here, all reflectors are situated in deeper layers (15-20 m).

8.3.5.2 Sediment peculiarities

All four cores from the Derugin Basin recovered similar sediments about 10 m thick. In the following, core LV29-104-2 from the central deeper part of the southern depression is discussed as an example for the general sedimentary sequence (see Appendix 6). The sedimentary sequence basically consists of two units. The upper one part can be grouped together as sequences of MIS 1 and 2 (Gorbarenko et al., 2002), including a Holocene diatom layer (0-37 cm), a terrigenous, weakly diatomaceous and foraminifera layer of 1 MIS (37-95 cm) with carbonate peaks IA, IB, IC, and Younger Dryas sediments (67-78 cm). These layers are well visible as color changes, which were recorded in the visual description as well as in colormetric data (see Appendix 6). A black and brownish-black layer of oxic sediments is also indicated well in interval 0-13 cm of the color data.
The sediment unit of interval 5-242 cm correlates with the MIS 2 sediments of previously dated cores (Gorbarenko et al., 2002) with regard to component composition and physical sediment properties. These sediments contain a significant amount of IRD and include green diagenetic dense lenses typical for glacial sediments of the northern Okhotsk Sea. In interval 170-200 cm a more intense diagenetic alteration with microcrystalline carbonate cement and an enrichment in pyrite globules occur.
The core part below 242 cm consists of homogeneous silty clay without IRD and a significant portion of marine biogenic matter (rare diatoms). However, it is also enriched with respect to terrestrial plant debris. This layer was possibly formed during short-time periods in the distal part of Amur River at times of intensive suspension input. The homogenous composition is confirmed by the main component distribution and physical properties values (see Appendix 6). According to color spectra this layer is divided into two horizons. The upper olive-green layer (242-710 cm) formed in oxic or suboxic conditions, whereas the black layer (>710 cm) was deposited under anoxic conditions. These layers are mainly distinguished by the composition of diagenetic minerals.
The first unit of the olive-green sediment contains a large amount of globular pyrite (see Appendix 6) and coarse-grained broken carbonate aggregates. The latter consist of large yellow grains and microcrystalline aggregates of white carbonate. Possibly, these represent remains of large crystals of hydrocarbonate (Ikaite) as revealed in similar sediments of core LV27-3 (Nürnberg et al., 1997). The black sediments do not contain any coarse authigenic minerals. The smear slides show large amounts of black amorphous matter (hydrotroilite?). Its color quickly disappears after air contact of the sediment or smear slides. Beside the black color and absence of diagenetic alteration, this sediment is distinguished from the olive-green sediment by shell fragments and less water content.
Core LV29-103-2 displays a similar sequence including MIS 1 sediment (0-149 cm), top sediments of MIS 2 (149-256 cm) and homogeneous olive-gray and black organic-rich silty clay (see Appendix 6) of the Amour's deep-sea fan. It differs from core LV29-104-2 by the appearance of turbidity layers (683-703, 846-857 cm) and interlayers of normal accumulation (936-983 cm). The turbiditic layers were determined from MS records and clastic grains content (see Appendix 6). Diagenetic processes intensively change sediment layers under turbidites. They are enriched in large pyrite aggregates as "globules", "grains" and "sticks" and partly cemented by microcrystalline carbonate.

8.3.5.3 Stratigraphy and origin of black sediments

The age of the top boundary of the deep-sea fan deposits is lithostratigraphically established as MIS 2. The age of the bottom part of the sequence is not determined. Based on the absence of ash layer K2, which was discovered in cores to the north (GE99-36 (Biebow et al., 2000)) and south (GE99-37 (Gorbarenko, pers. com.), it can be supposed that the age of the investigated core is less than 24 ka. Still, other suppositions may be considered, especially for core LV29-103-2 which seems to have penetrated older parts of the fan sequence.
The black sediments are discovered in the Okhotsk Sea for the first time. Today, a number of opinions exists about the depositional environment leading to the formation of anoxic sediments and its ancient analogy – black shales. Apart from anoxic water (Kristensen & Blackburn, 1987; Canfield, 1989; Wortmann et al., 1999), another necessary condition is a massive input of organic matter of possibly terrestrial origin (Habib, 1982) by different ways, specifically by turbidity currents (Dean et al., 1978; Jansa et al., 1979; Dean & Gadner, 1982), or high primary production (Pedersen & Calvert, 1990; Calvert & Pedersen, 1993*).*
Possible sources of organic matter (OM) leading to the formation of black sediments in the Derugin Basin might be massive input of terrestrial OM by debris flow from the paleo-river mouth. The cause for the appearance of anoxia waters has yet not been found out. One of the possible causes is the extraction of oxygen from bottom waters for oxidation of OM at times of low vertical convection. Another cause may be a special geodynamic and fluid activity of the Derugin Basin.

8.3.6 West Kamchatka profile (LV29-106, LV29-108)
8.3.6.1 Setting

The goals of this sediment profile were extended investigations of the influx of northwestern Pacific waters into the Okhotsk Sea and their influence on the regional paleoceanography. Station LV29-106 was set on the continental slope of Kamchatka Peninsula at a water depth of 510-511 m. The cores at station LV29-108 were recovered from depths of 625-627 m close to the older core LV28-44. The sediments of the shallow cores (LV29-106-2 and LV29-106-6) are characterized by coarser grain sizes than those of the deeper ones.
The sediments of this region reveal a significant influx of volcanogenic material from the eastern Kurile Islands and Kamchatka and, consequently, show high MS values.

8.3.6.2 SL-R (LV29-106-2, LV29-108-4)

The description of cores LV29-106-2 and LV29-108-4 and records of the component composition and physical properties (see Appendix 6) allow us to establish the stratigraphy in terms of marine oxygen isotope stages. Ash layer K0 (see Chapter 8.3.9) with an age of 8 ka (Gorbarenko et al., 2002) is clearly expressed in both cores, confirming the position of the MIS 1/2 boundary. The sediment of the cold MIS 2 is characterized by high MS values, dry bulk density and a clastic component content. Regularities of these records allow us to determine the MIS 2/3 boundary in both cores (see Appendix 6).
Sediment with high diatom abundance starts to accumulate in both cores just above ash K0 after 8 kyr. Sediments enriched in diatoms were observed in core LV29-108-4 below ash K0 down to the boundary MIS 1/2. In core LV29-106-2, there diatom contents increase during stage 3 (see Appendix 6). Apparently, the variability in biogenic opal accumulation is a special feature of this region related with the strong influence of Pacific waters (Haug et al., 1995; Gorbarenko, 1996).

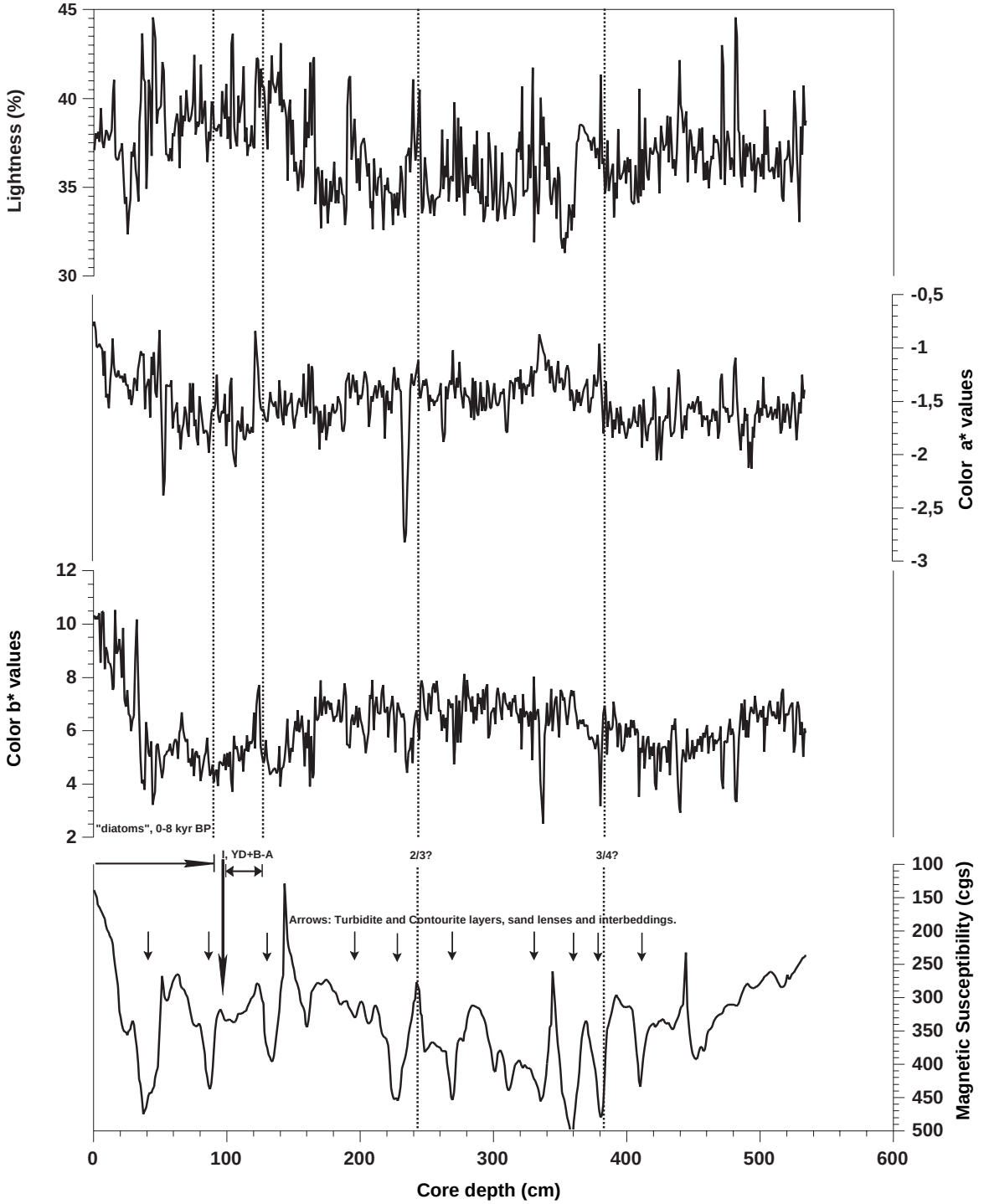

Fig. 8.6: *LV29-106-6, from top to bottom, Lightness of color reflectance spectra, Color spectrum of red-green chroma, Color Spectrum of yellow-blue chroma and magnetic susceptibility.*

8.3.6.3 SL-G (LV29-106-6, LV29-108-5)

At one of the locations, we were able to establish a preliminary age model primarily based upon the records of MS and the lithological changes.
At core LV29-106-6 we obtained a record rather disturbed by frequent intercalation's of sand lenses and layers presently inhibiting us to put forward a precise age model. Prominent layers and lenses enriched in sand and silt, sometimes with graded bedding and signs of eroded paleo-surfaces, occur at core depths 33-43, 90-95, 130-136, 199-208, 225-228, 267-273 cm, etc., a feature also depicted in the records of MS (*Fig. 8.6*). At present, we are

only able to assume that the Holocene diatom-rich layer ends somewhere around 60 and 90 cm (based upon color values) and that the Younger Dryas/Bølling-Allerød might appear close to 100-130 cm, but this assumption is very preliminary. Due to the numerous events of rapid clastic sedimentation in this core indicating frequent turbidites, contourites with sediment erosion and reworking, considerable work has to be undertaken for developing a precise age model.

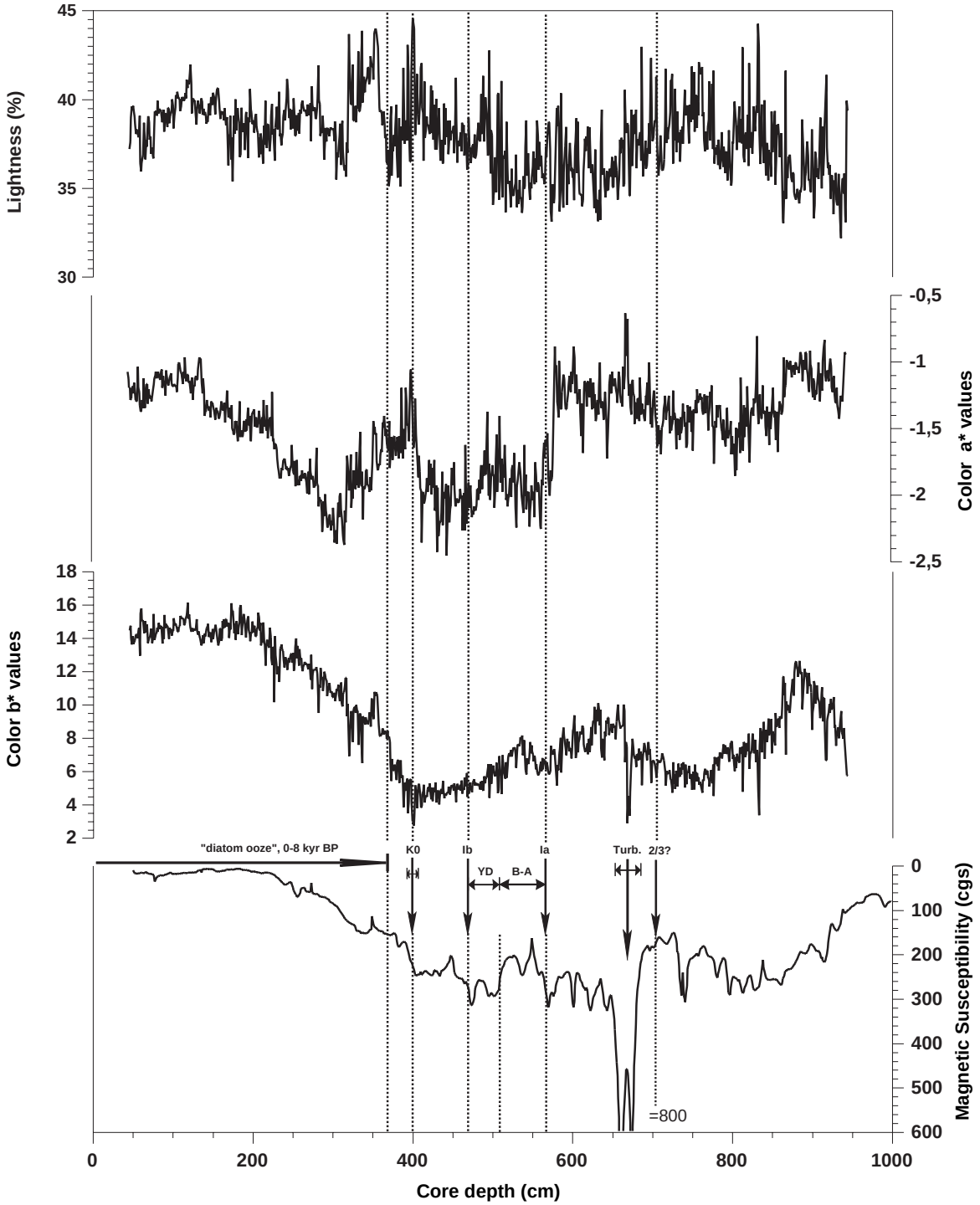

Fig. 8.7: *LV29-108-5, from top to bottom, Lightness of color reflectance spectra, Color spectrum of red-green chroma, Color Spectrum of yellow-blue chroma and magnetic susceptibility.*

Core LV29-108-5 gives a somewhat different picture: according to the MS records and changes in lithology, at LV29-108-5 we attribute the upper ca. 373 cm of the core to late

Holocene diatomaceous ooze with rather abundant foraminifera, representing the last 6,000-8,000 yrs BP (*Fig. 8.7*). We have to admit, though that we already see a slight decrease in diatom content and compaction of sediment from 301-305 cm downcore.
However, in good agreement with our first assumption, ash layer K0 (8,000 cal. yrs BP; Gorbarenko et al., 2002) was deposited in this core shortly below the basal boundary of the diatom-rich facies at 397-405 cm.
A short interval enriched in tiny dropstones and detrital terrigenous grains corresponds to Termination Ib at 470-479 cm, preceded by the YD down till approximately 510 cm. Between 510 and 561 cm, we note a characteristic double peak in the MS record, which we attribute to the warmer Bølling-Allerød interval. The basal boundary of this section consists of an interval with enhanced black streaks and mottles (661-668 cm) and an underlying coarser-grained 2 cm thick layer with sand particles which then would represent Termination Ia. At present, we are unable to present a clear indication for the MIS 2/3 boundary. A lithological change at ca. 610 cm towards sandier material (coarsening downward) to us seems to indicate LGM conditions (~18-24 kyr BP). Unfortunately, both MS values and lithology show the deposition of a ca. 28-30 cm thick incomplete turbidite sequence at 657-686 cm core depth. Preliminary we set the MIS 2/3 transition shortly below the turbidite sequence at ca. 700-705 cm as we already note an increased abundance of diatoms in the sediment. This assumption would also correlate quite well with the age model of the Russian core LV29-108-4 (SL-R), seemingly offset by 70-90 cm towards the top as can be seen from the position of K2, the aforementioned turbidite sequence and another contourite at 734-746 cm (German core, SL-G) and ca. 660-690 cm (Russian core, SL-R).
However, we are aware of the fact that one could also determine a gradual lithological change between 900 and 935 cm as MIS 2/3 boundary. Here, we observe an increased content of diatoms and finer-grained detrital components as well as a clear decrease in MS values pointing towards slightly warmer transitional climatic conditions. Yet, the latter age model would mean the average sedimentation rate to decrease not more than by a factor of two compared to Holocene values, a feature that seems unlikely by comparison with older nearby cores featuring well established age models (e.g. LV28-44 shows a fivefold decrease in Holocene to LGM sedimentation rates).
Further investigation of geochemical parameters (opal content, XRF-scanning) will hopefully help to resolve this question.
There are several turbiditic layers and layers with large content of black sand throughout all cores (*Figs. 8.6 and 8.7*). An influx of coarse material is clearly observed in the MS records and induced peculiarities of the Kamchatka slope accumulation.

8.3.7 Eastern Kurile Basin slope profile (LV29-110, LV29-112, LV29-114)

8.3.7.1 Setting

Coring stations LV29-110, LV29-112 and LV29-114 are located on the northeastern slope of the Kurile Basin in a depth range from 1,218, 1,309 to 1,764 m. These sites are strongly influenced by the proximate North Pacific water inflow into the Okhotsk Sea and should therefore permit to reconstruct the temporal evolution of the deeper Pacific water in comparison to the east Kamchatka profile.

8.3.7.2 SL-R (LV29-110-2, LV29-112-2, LV29-114-2)

The sediment of core LV29-110-2 belongs to MIS 1 according to available records (see Appendix 6). The upper 180 cm contain weakly diatomaceous sandy silt with a basal age close to 6 kyr. Carbonate peaks occur at 140 cm, 280 cm and 340 cm core depth, apparently correlated with carbonate spikes of terminations IC, IB and IA with ages of 5, 9.5 and

12.5 C^{14} kyr (Gorbarenko et al., 2002). An unidentified volcanic ash is located at the core base (345-350 cm). MS record and core description indicate the appearance of two turbidite layers at 231-232 cm and 301-302 cm.
According to physical property records and color spectra, core LV29-112-2 has principally to be filed as of MIS 1-3's age. In agreement with the location of the bottom boundary of terrigenous-diatomaceous sediment at 140 cm, the MIS 1/2 boundary is set at 240 cm depth. A pronounced, so far unidentified volcanic material layer with complex composition was found at a depth of 494-510 cm. In line with our available data, the boundary of MIS 2/3 may be preliminary placed at a depth of 520 cm, just below the volcanic ash. The core description and MS record indicate several sandy layers through the entire core length likely induced by turbidites.
The strong reflector boundary at nearly 5.5 m depth in the 8 kHz echosounder records in profile 34 (*Fig. 3.8,* Chapter 3) definitely correlates with the aforementioned ash layer located at 494-510 cm core depth in LV29-112-2. A less strong boundary at nearly 4 m depth may be correlated with the accumulation of sandy sediment with high MS values in interval 430-460 cm. The weak reflector boundary in the seismic records at nearly 1 m depth likely correlates with the base of diatomaceous sediment (0-140 cm).
Core LV29-114-2 supposably encompasses MIS 1-4. The beginning accumulation of diatomaceous sediment in the upper 175 cm and changes of other parameters allow us to set the MIS 1/2 boundary at a depth of 190 cm. The high MS values, low color b values and absence of diatoms in depth interval 250-300 cm place the MIS 2 base at 330 cm. The boundary MIS 3/4 may be very preliminary put at core depth 560 cm in consistence with color spectra variability. Volcanic ash preliminary identified by mineralogy as K3 was found at the core base (766-767 cm) and accumulated within MIS 4 (Gorbarenko et al., 2002). The high values of MS and presence of several sandy layers in this core, similar to cores LV29-110-2 and LV29-112-2, indicate a strong influence of volcanic activity from the northern Kurile Islands and southern part of Kamchatka, transported into the sea likely by sea ice.

8.3.8 La Perusa Strait (LV29-69, LV29-131)

8.3.8.1 Setting

At this location, the goal was to reconstruct the Soya Current inflow into the Okhotsk Sea and its influence on paleoceanography.
Stations LV29-69 and LV29-131 were set in a rather flat area with a depth range of 800-1,000 m between La Perusa Strait and the western part of the Kurile Basin.

8.3.8.2 SL-R/ SL-G

Cores LV29-131-2 and LV29-131-3 were taken from the top of a smooth hill with a depth of 760-761 m and cores LV29-69-3 (841 m) and LV29-69-5 (652 m) roughly at the same location.
The onboard results of MS, color spectra, dry bulk density, water content and main component composition according to smear slide analysis are plotted in Appendix 6. Generally, the MIS 1 sediments show a high water content and low bulk density and a considerable amount of diatoms according to the smear slides analysis. The sediment of MIS 2 is represented by an increased terrigenous material with high density and slightly increased MS values. The transition from MIS 2 to 1 is clearly indicated by changes in the color spectra. The MIS 2 and 3 sediments have low b values that show a prevalence of blue chroma in the sediment of the cold MIS 2 and intermediate MIS 3. The boundary of MIS 2/3 in core

LV29-131 was determined based on a significant sand admixture in the sediments of the cold stage 2 and a relative decrease in the MS values in stage 3.
The sedimentation rate in core LV29-69 is higher than in core LV29-131, which coincides with the bottom topography and sedimentation regularities. Cores LV29-131 were recovered from an elevated relief comparable with core LV29-69.
The sediments of the early part of MIS 1 have low MS values, which are typical for the Okhotsk Sea sediments (Gorbarenko et al., 2002). The considerable increase in MS values in the late part of MIS 1, which was registered in both cores, was likely induced by the opening of La Perusa Strait and an additional influx of magnetic terrigenous material with the Soya Current. According to the curve of the sea level change during last 18 kyr (Fairbanks, 1989), La Perusa Strait opened approximately 8 kyr ago (the modern depth of the La Perusa Strait equals 53 m). Therefore, considerably warm and saline Soya Current water masses began to flow into the Okhotsk Sea 8-7 kyr ago. The rise in the MS values presumably caused by transport of additional terrigenous material by the Soya Current allows us to interpret the higher MS values during MIS 3 as a possible earlier opening of La Perusa Strait.

8.3.9 Mineralogy of volcanic ash layers

In sediments of cores studied aboard, we discovered frequent pyroclastic material. Tracing tephra as pure layers or lenses is of considerable interest for investigation. Their identification with already known Okhotsk Sea ash layers conduces to carry out a stratigraphic intercore correlation.
Tephra layers in Holocene-Pleistocene sediments of the Okhotsk Sea have already been studied in the past (Gorbarenko et al., 2000; Biebow et al., 2000). On the basis of mineralogical features, chemical composition, stratigraphic position and radiocarbon dating of these layers, their connections with eruptions of Kamchatka or Kurile volcanoes and also areas of distribution were distinguished (Gorbarenko et al., 2000, 2002).
Samples for mineralogical analysis were selected from the most pristine parts of ash layers. However, it was not always possible to completely avoid contamination's by terrigenous particles of the surrounding sediment (due to bioturbation and the small thickness of some ash lenses). From thicker layers, some samples were selected with regard to particle size, color or texture. The results of mineralogical analysis were processed with multivariate statistics (cluster and R-mode factor analyses) (*Figs. 8.8* and *8.9*).
Pyroclastic material was discovered in 12 cores taken within near-Sakhalin and Kurile-Kamchatka areas (*Tab. 8.1*). As can be seen from *Figure 8.8*, stations can be grouped according to our mineralogical study. The analysis of these data, and also their comparison with known Okhotsk Sea ash layers permitted to identify them as tephra marker layers K0, K2 and K3. Some fluctuations in the composition of the main components (even within one ash layer) are related with the differentiation of volcanic particles in density and size during transport and settling on the bottom (Kir'yanov & Solovyeva, 1990; Felitsin & Kir'yanov, 1987) which can be especially seen in thick layers (station LV29-108, horizon 313-316 cm; station LV29-112, horizon 494-510 cm). This regularity was already observed in Okhotsk Sea cores recovered on previous cruises (Gorbarenko et al., 2000; Biebow et al., 2000). On the other hand, samples selected from thin layers or lenses contain admixtures of terrigenous particles. This is well expressed in the r-mode factor analysis (*Fig. 8.9)*. Minerals of terrigenous origin (hornblendes, epidote, garnet, zircon etc.) form associations with stable positive correlative connections. One can see that the main components of volcanoclastics - clinopyroxene and orthopyroxene - are sharply isolated from terrigenous components sharing negative correlation's.

Table 8.1. *Mineralogical composition of ash layers from sediments of the Sea of Okhotsk*

N st.	Horizon, cm		Cpx	Opx	bgHb	bHb	gHb	OHb	Ep	Gar	Zr	Ap	Sph	Chl	Mt	Ol	Act	Bi	Ilm	Mgt	Rf
LV29-53*	174	K_2	18.86	23.14	18.28	0.28	1.14	0.29	10.00	2.00	0.28	0.86	1.14	0.28	0.00	0.00	1.14	4.86	1.71	4.57	11.17
LV29-53*	175-176	K_2	26.97	34.24	5.76	0.00	0.61	0.00	4.85	0.30	0.30	1.21	0.30	0.61	0.00	0.00	0.61	1.82	1.52	9.70	11.21
LV29-53	178-179	K_2	27.13	48.58	2.52	0.32	0.00	0.00	1.89	0.00	0.00	0.63	0.32	0.00	0.31	0.00	0.00	0.95	0.31	5.99	11.04
LV29-56	251-252	K_2	19.94	42.68	7.16	0.93	0.93	0.00	2.49	0.00	0.00	1.87	0.00	0.93	0.00	0.00	0.00	2.49	0.00	8.10	12.46
LV29-63	114-115	K_2	24.76	41.27	0.32	0.00	0.95	0.32	0.95	0.00	0.32	0.63	0.00	0.00	0.00	0.32	0.00	0.63	0.32	17.46	11.75
LV29-70*	381	K_2	11.66	46.36	4.37	0.29	2.62	0.00	3.50	0.00	0.00	0.29	0.00	0.58	0.29	0.58	0.29	3.68	2.92	11.66	10.91
LV29-70*	727-727.6	Spfa-1	14.39	14.11	19.66	0.00	3.00	0.00	9.66	1.61	2.44	3.83	0.78	1.33	0.00	1.89	1.05	4.66	3.83	4.39	13.37
LV29-72*	569	K_2	13.40	36.92	2.81	0.00	0.00	0.00	1.34	0.00	0.00	0.00	0.00	0.00	0.00	0.00	0.75	1.92	2.51	34.28	6.07
LV29-94*	468	K_2	19.66	16.02	18.34	0.37	1.24	0.37	9.36	0.95	0.00	0.95	0.37	0.37	0.00	0.37	0.66	4.72	3.85	5.00	17.40
LV29-100	195	K_2	25.30	36.61	5.65	0.00	0.89	0.30	1.49	0.30	0.30	1.19	0.60	0.00	0.00	0.00	0.00	0.30	0.89	14.58	11.61
LV29-106	54-56	Ko	17.47	29.62	9.87	0.00	0.00	0.00	0.25	0.00	0.00	0.76	0.00	0.00	0.25	0.00	0.25	0.25	5.32	23.80	12.15
LV29-108	313-315	Ko	17.58	30.84	4.32	0.00	0.00	0.29	1.44	0.00	0.00	0.86	0.00	0.00	0.00	0.29	0.00	0.29	6.34	27.67	11.53
LV29-108	315-316	Ko	14.77	23.01	4.83	0.00	0.00	0.28	0.28	0.00	0.00	1.14	0.00	0.00	0.28	0.57	0.00	0.56	6.53	36.93	11.08
LV29-110	350	?	24.36	22.56	3.08	0.26	0.26	1.54	3.59	0.00	0.00	0.51	0.00	0.00	0.00	0.26	0.26	0.26	2.31	31.28	9.49
LV29-112	496.5-499	?	31.31	22.47	8.59	0.25	0.00	2.53	2.27	0.00	0.00	0.76	0.00	0.00	1.01	1.52	0.25	0.76	5.05	14.37	8.84
LV29-112	500.5-505	?	26.36	25.27	8.15	0.00	0.27	0.27	3.53	0.27	0.00	0.00	0.00	0.00	0.27	0.00	0.00	0.82	6.79	14.40	13.59
LV29-112	505-507.5	?	23.91	23.37	10.05	0.00	0.00	0.00	2.99	0.00	0.00	2.17	0.00	0.27	0.27	0.00	0.00	0.54	4.08	16.30	16.03
LV29-112	507.5-510	?	16.80	22.46	8.98	0.20	0.00	0.39	1.56	0.00	0.00	0.78	0.00	0.00	0.00	0.20	0.39	0.40	16.41	25.98	5.47
LV29-114	766	K_3?	18.99	24.33	0.89	0.00	0.00	0.30	0.30	0.00	0.00	2.08	0.00	0.30	0.00	0.00	0.00	0.00	3.26	35.61	13.95

Minerals: Cpx - clinopyroxene, Opx - orthopyroxene, bgHb - brown-green hornblende, bHb - brown hornblende, gHb - green hornblende, OHb - basaltic hornblende, Ep - epidote, Gar - garnet, Zr - zircon, Ap - apatite, Sph - sphene, Chl - chlorite, Mt - metamorphic minerals (andalusite, staurolite, sillimanite etc.), Ol - olivine, Act - actinolite, Bi - biotite, Ilm - ilmenite, Mgt - magnetite, Rf - rock fragments.

Note: * - Asterisk marks samples selected from thin interlayers and lenses; they contain admixture of terrigenous particles. Ko, K_2, K_3, Spfa-1 - indexes of ash layers.

8.3.9.1 Tephra marker layer A

This layer was discovered at stations LV29-106 (54-56 cm) and LV29-108 (313-316 cm). At the first station, the tephra is traced as bioturbated lenses with small thickness. At the second, it gains in thickness and complex composition. The light gray (to white) tephra of silty sand in size (~1 cm in thickness) lies within the lower part of the ash layer. Volcanic glass shows a fluid-vesicular variety, and a large quantity of white pumiceous fragments causes the layer's whitish tone. This tephra is overlapped by a gray interlayer of sandy silt in size and variable thickness (0.6-2.5 cm). The volcanic glass has an analogous variety, but pumiceous fragments occur in smaller quantities. Overlying terrigenous sediments are enriched in very fine ash particles; thus, these sediments have a whitish tone. Volcanic ash consists of fragmentary-vesicular and lamellar glass.

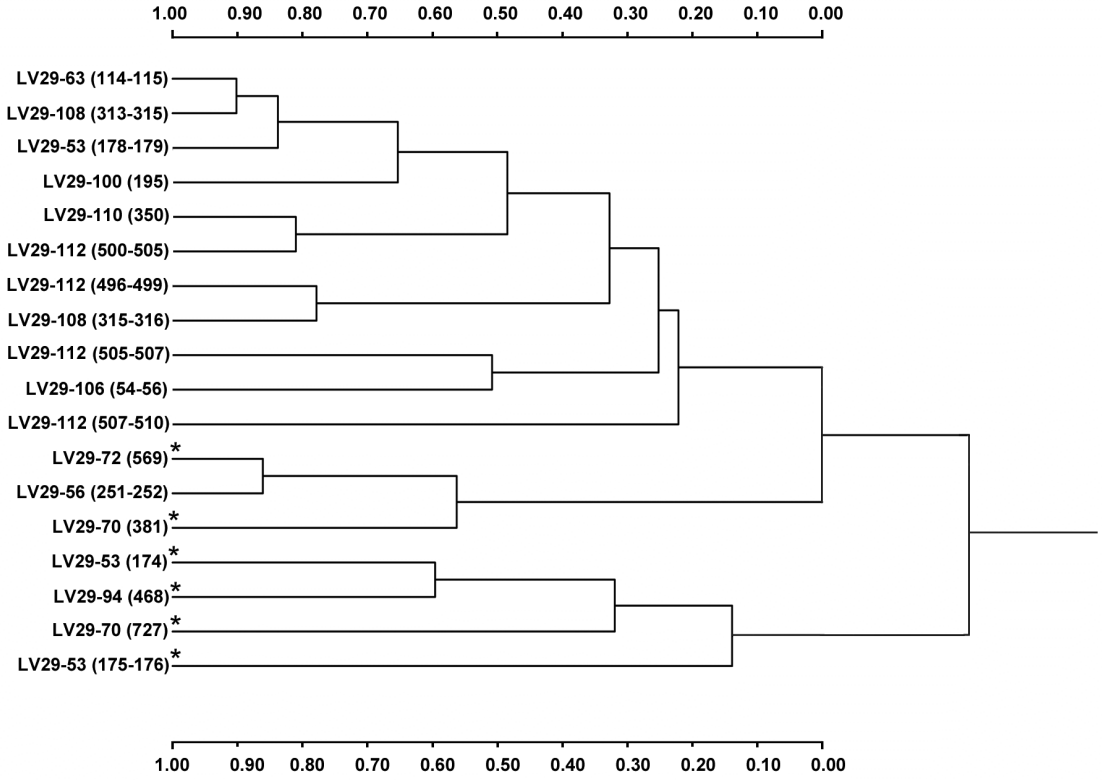

Fig. 8.8: *Cluster graph of the mineralogical composition of different ash layers from sediments of the Okhotsk Sea.*

8.3.9.2 K0 ash layer

The mineral complex of ash layer K0 is characterized by a prevalence of orthopyroxene (23.0-30.8% or 50.6-55.2% after recalculation on transparent minerals) and clinopyroxene (14.8-17.6% or 29.9-31.4%, accordingly). Besides, the high content of dark ore minerals is typical (29.1-43.5%). The distinctive feature of this ash layer is the increased content of brown-green hornblende, often with grains encased in volcanic glass, and also the presence of brown and basaltic hornblendes.
The source of pyroclastics for ash layer K0 is the explosive eruption of Kurile Lake volcano (southern Kamchatka) which happened, according to new radiocarbon data on wood remains, 7618 ±14 years ago (Zaretskaia et al., 2001).

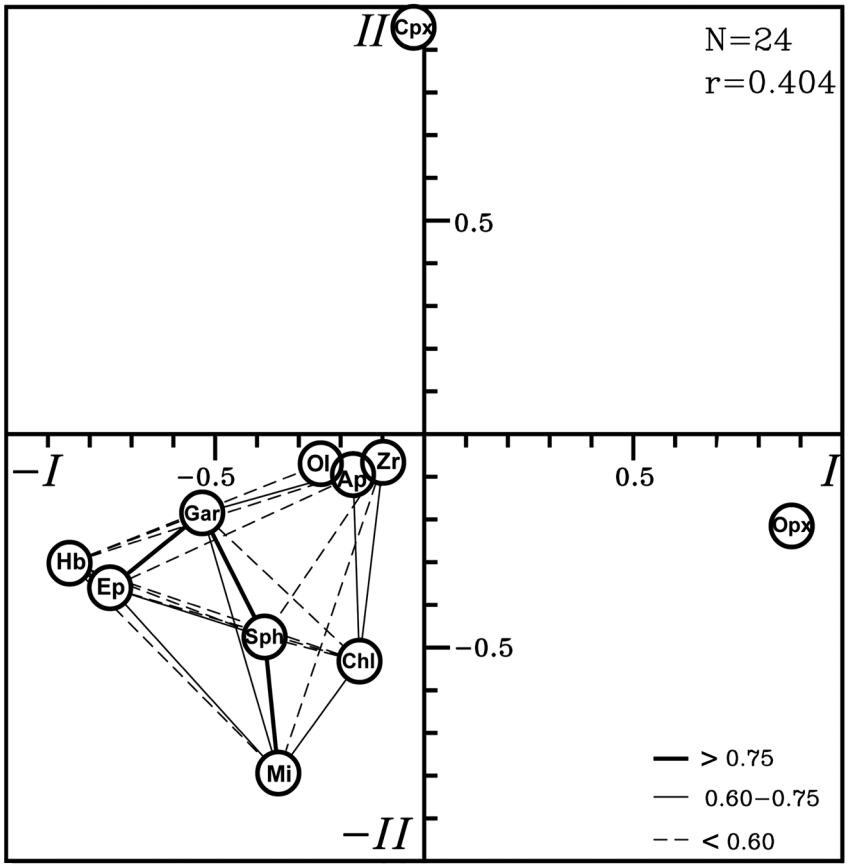

N - quantity of mineralogical analyses (6 analyses from other cruises with identified ash layers as standard are added to the initial data);
r - significant correlation's between minerals; which are shown by lines of different thickness: bold line - strong positive correlation, regular line - moderate correlation, dotted line - weak correlation. Indexes of minerals are given in *Table 8.1*.

Fig. 8.9: *Plot of R-mode factor analysis for heavy minerals from ash layers in sediments of the Okhotsk Sea.*

8.3.9.3 Tephra marker layer K2

This layer is distributed over a wide area in the central part of the Okhotsk Sea (Gorbarenko et al., 2000; Biebow et al., 2000). So far, it has been found in cores LV29-53, LV29-56, LV29-63, LV29-70, LV29-72, LV29-94 and LV29-100. This tephra is a gray ash with pink tone of sandy silt in size, which is one of the main characteristic features of this layer. It occurs as interlayers of 1-2 cm in thickness (stations LV29-53, LV29-56, LV29-63, LV29-100) or as small lenses of 0.5-0.6 cm in diameter (stations LV29-70, LV29-72, LV29-94). The volcanic glass has mainly a fragmentary-vesicular and fluid-fibroid and rarely a fluid-cellular shape. There is a small quantity of light gray (to white) pumiceous fragments. Characteristic for this layer is the prevalence of orthopyroxene in comparison with clinopyroxene (36.6-48.6% and 11.7-27.1%, accordingly). The content of dark ore minerals varies widely (*Tab. 8.1*). *Figure 8.8* shows the scattering of stations containing ash layer K2 in the form of small lenses. It is related with the admixture of terrigenous particles of surrounding sediments (*Tab. 8.1*).
The absence of ash layer K2 within near-Kamchatka areas (stations LV29-106, LV29-108, LV28-44) allows the suggestion that most probably its source is a large explosive eruption of one volcano situated in the northern part of Kurile Island Arc. The stratigraphic position

of this layer in sediment cores (~26,000 years) (Gorbarenko et al., 2002), and also the data of radiocarbon dating on land within sections with similar tephra characteristics (Braitseva et al., 1995; Melekestsev et al., 1997) allow us to consider the most real source of this ash layer to be the largest caldera-forming explosive eruption of volcano Nemo-III situated in northern part of Onekotan Island that happened about 25,000 years ago.

8.3.9.4 Unknown tephra layer – Paramushir Island

Among the other ash layers discovered in the cores, the tephra of station LV29-112 taken near Paramushir Island is of highest interest. A thick ash layer was recovered here at 494-510 cm core depth. Its consists of light gray ash of fine sandy silt in size. Within the layer, thin lenses and interlayers of darker color occur. The quantity of sandy particles decreases from bottom to top, whereas the amount of fine silty particles increases. At 494-505 cm, a high content of light gray pumice of gravel in size was observed.
The investigation of the ash mineral composition shows a differentiation of tephra in both particle density and size. Within the coarse lower part of the layer, the ore minerals content (42.4 %) increases in comparison with the fine-grained upper part. The content of clinopyroxene and orthopyroxene is approximately equal to the small prevalence of orthopyroxene in the lower part of the layer (*Tab. 8.1*). Among coarser ash particles, light gray pumiceous fluid and white volcanic glass prevails, while fluid-vesicular glass occurs in small quantity. On the contrary, the prevalence of colorless fluid-vesicular and lamellar glass is characteristic for fine ash particles; pumiceous glass occurs rarely.
In spite of the close stratigraphic position of the studied layer to ash layer K2, at present it seems impossible to identify it as K2 because of some distinctions. First of all, there is no characteristic pink tone as typical for K2 ash. Besides, the ratio clinopyroxene/orthopyroxene is lower (*Tab. 8.1*), and the content of pumiceous glass is higher than for layer K2. These distinctions in the mineral composition are reflected well in our results from cluster and factor analyses (*Figs. 8.8* and *8.9*).

8.3.9.5 Tephra marker layer K3

This layer may be preliminary distinguished at station LV29-114 at 766-767 cm. It consists of sandy silt with admixture of coarse sand and pumice. Coarse ash particles are represented by gray and dark gray pumiceous fluid fragments, and also by dark brown (almost black) fine-porous fragments. Fine ash particles consist of mainly colorless fragmentary-vesicular and fluid glass.
In the same core and also in core LV29-110 (at 350 cm), small lenses of volcanic ash and large quantities of dispersed pumice were discovered, but it is currently not possible to determine their significant features for a stratigraphic correlation.

8.3.9.6 Unknown tephra layer #2 – Spfa-1?

One more tephra layer differing in composition and morphology from other layers was discovered in the western part of the Okhotsk Sea in core LV29-70 (at 727-727.6 cm). It has a light gray color with glassy lustre. The ash of this layer consists of only colorless volcanic glass of sandy silt in size with a very small admixture of crystalloclastics. This glass is mainly made up of fragmentary lamellar and fragmentary vesicular particles. A low content of heavy minerals is characteristic for this layer. It is similar to the ash layer of station LV28-62 (at 1,108-1,113 cm) (Biebow & Hütten, 1999) and may be compared with ash layer *Spfa-1* of the eruption of volcano Sikotsu (Hokkaido Island) that happened about 40,000 years ago (Machida, 1999).

9. INVESTIGATION OF FORAMINIFERA IN SURFACE SEDIMENTS OF THE OKHOTSK SEA

Natalya Bubenshchikova, Lester Lembke, and Nicole Biebow

9.1 Introduction

Quite a few previous investigations have dealt with the distribution and ecology of benthic foraminifera of the Okhotsk Sea (e.g. Asano, 1958; Saidova, 1961, 1997; Fursenko et al., 1979) covering a wide range of environments from the Amur River estuary to the deep basins extending temporally from modern conditions to glaciated shelves in the past. It has been shown that late Quaternary glacial-interglacial changes in oceanography and productivity of this region are closely coupled to strong variations of benthic foraminiferal assemblages in sediment samples (Saidova, 1961; Fursenko et al., 1979; Belyaeva & Burmistrova, 1997; Gorbarenko, 1991; Barash et al., 2001).
However, the vast majority of studies are hampered by the fact that almost no regional data of living benthic foraminfera is available in connection with their environmental characteristics (Basov & Khusid, 1983). This in turn considerably aggravates any attempt to calibrate existing datasets against oceanographic and ecological boundary conditions like nutrient supply, water depth, ventilation of water masses, current strength, surface sediment composition, etc. As well, little is still known about microhabitat preferences of the majority of benthic foraminiferal taxa in the Okhotsk Sea.
Hence to date, few attempts have succeeded in quantifying physical and chemical changes in bottom water characteristics by using benthic foraminiferal assemblages as proxy datasets.
Modern planktic foraminifera assemblages of the Okhotsk Sea are strongly dominated by the polar species *N. pachyderma sin.* and subpolar species *G. bulloides* both in sediments traps and in Late Quaternary sediments (Shchedrina, 1958; Saidova, 1961; Lipps & Warme, 1966; Alderman, 1996). The rare subpolar species *N. pachyderma dex., G. glutinata, T. quinqueloba, G. uvula, G. scitula* and tropical specimens *N. dutertrei, G. ruber, G. conglobatus, G. quadrilobatus* were found only as minor faunal components.
The aim of the study is to investigate the ecological preferences of living benthic foraminiferal assemblages and to extend their options to serve as paleoceanographic proxies. Concomitant counts of planktic foraminifera shall further elucidate possible interconnections with overlying surface water mass properties.

Within this main objective the tasks are considered as following:

Russian Group:
1. to determine abundance, diversity, taxonomic composition of living and dead benthic foraminifera from a set of sediment surface samples (0-1 cm) from different sites (shallow, intermediate, deep-water environments);
2. to determine the microhabitat preferences of the dominant benthic species from living assemblages in the upper surface sediments (0-8 cm);
3. to assess the preservation potential of benthics for Quaternary paleoceanographic reconstruction's from comparing living and related dead assemblages;
4. to investigate planktic foraminiferal distribution in surface sediments (0-1 cm) and to determine factors controlling the changes in faunal distributions;

German Group:
5. to distinguish responses of different selected species to oceanographic changes by comparison to stable isotope analyses and sediment geochemistry (TC/TOC, opal, chlorine's, etc.);

6. to calibrate the imposed dataset from benthic communities against stable isotope data from bottom water samples taken simultaneously;
7. to evaluate response of benthic communities to subtle oceanographic changes during the last 15,000 years caused by variations in the riverine discharge of Amur River;
8. to calculate SST-proxydata from planktic foraminifera (MAT, Mg-Ca);
9. numerical approximation of T/S characteristics from combined foraminiferal geochemical data for OSIW (σ_θ =26.7-26.9) on a transect along the Sakhalin continental margin.

Finally, we plan to jointly relate the observed living benthic assemblages to present and past environmental conditions (nutrient supply, water depth and chemistry, oxygen content, current strength, surface sediment composition).

9.2 Materials and methods

We collected undisturbed surface sediments from multicorer tubes. The upper 8-10 cm of the sediment were cut in slices of 1cm thickness and stored in dyed Ethanol (min. 70%, with added Rose Bengal: 2g/l) solution immediately after MUC retrieval according to modified methods described e.g. in Lutze & Altenbach (1991). To obtain a sufficient amount of material for the array of investigations, we took three parallel sample series from each station, whenever possible. A total of 457 single samples was collected during the cruise, out of which we chose a set of 11 samples from intermediate water depths for preliminary analysis (see *Tab. 9.1*, and *Figs. 9.1-9.3* for locations of samples).

Tab. 9.1: *Samples for preliminary analysis.*

Station No.	Sample depth (cm)	Water depth (m)
LV29-69-1	0-1	881
LV29-78-1	0-1	640
LV29-84-1	0-1	720
LV29-108-3	0-1	625
LV29-110-1	0-1	1218
LV29-110-1	1-2	1218
LV29-110-1	2-3	1218
LV29-110-1	3-4	1218
LV29-110-1	4-5	1218
LV29-110-1	5-6	1218
LV29-110-1	7-8	1218

Samples were wet sieved over 63 μm mesh size and dried at about 70°C. Foraminifera were counted in the fraction >100μm in splits estimated to contain at least 300 specimens of planktic, 300 living (Rose Bengal-stained) and 300 dead benthic foraminifera (Appendix 7). Samples containing little foraminifera were analyzed without splitting. Planktic foraminifera were identified following the taxonomy of Hemleben et al. (1989). Benthic foraminifera were classified according to the taxonomic works of Loeblich & Tappan (1953), Saidova (1961, 1975), Feyling-Hanssen et al., (1971), Fursenko et al. (1979), Scott et al., 2000 etc., see Appendix 7 for species references and full names. For abundance analyses counts of foraminifera were calculated to 1 cm^3 surface.
We restricted our study aboard to calcareous benthic foraminifera assemblages, as we noticed that agglutinated foraminifera disintegrated easily after death which typically resulted in very low downcore abundance's of tests. In our samples, the ratio of calcareous to agglutinated foraminifera increases sharply from 77% in 0-1 cm to 91% in 1-2 cm and to 96-99% in deeper

samples of MUC LV29-110-1 (*Fig. 9.6*). A rather good preservation of foraminiferal carbonate tests is expected in the chosen samples due to the low carbonate ion concentration (CO_3) of 0.038-0.044 mmol/kg and the high saturation degree of calcite of 0.66-0.72 (Chapter 5). Thus, variations in foraminiferal assemblage compositions can be mainly attributed to ecological environmental parameters and not to preferential dissolution of specific taxa. At our sites, the present sedimentation rates are estimated to range from 30 cm/kyr at "Obzhirov flare" via 50 cm/kyr on the Kamchatka margin to more than 100 cm/kyr at the Sakhalin margin (Chapter 8). Thus, the uppermost centimeter of the sediment approximately represents an approximate time frame of the past 0-500 years, considering the maximal bioturbation depth to range around 15 cm (own observations at MUC tubes).

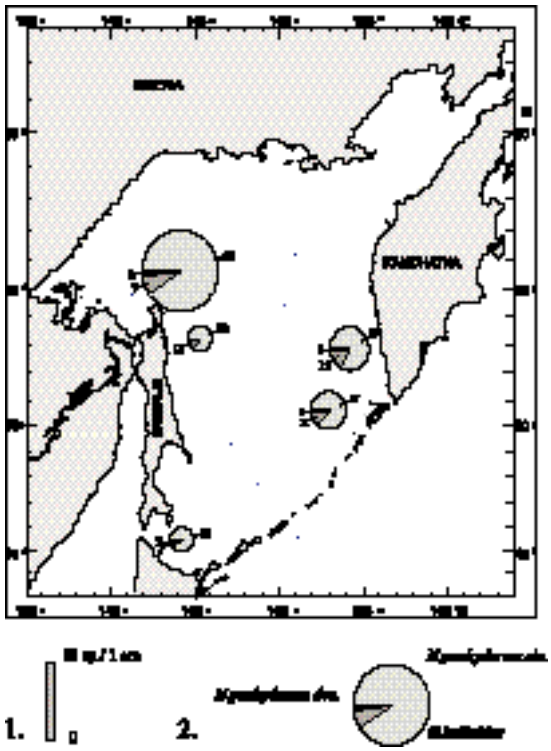

Fig. 9.1: *Distribution of planktonic foraminifera in the surface sediments (0-1cm) of the Okhotsk Sea: 1 - abundance (specimen per 1cm^3); 2 - species composition.*

9.3 Results and Discussion

9.3.1 Planktic foraminifera

The planktic assemblages are characterized by the predominance of two species, *N. pachyderma sin.* and *G. bulloides* (*Figs. 9.1* and *9.7*, Appendix 7). The total maximal abundance of 18 spec./cm^3 occurs in the surface sediments (0-1cm) at site LV29-84-1 ("Obzhirov flare") (*Fig. 9.1*). A species-specific maximum of *G. bulloides* (15%) was found in LV29-108-3 at the southwestern Kamchatka slope (*Fig. 9.1*), suggesting an influence of a relatively warmer surface water inflow of Northwest Pacific origin through Kruzenshtern Strait.

On the downcore profile of LV29-110-1 (eastern slope of the Kurile Basin), the maximum of planktic foraminiferal abundance of 21-28 spec./cm^3 occurs between 3-6 cm (*Fig. 9.7*, Appendix 7). It coincides with an increase of *G. bulloides* up to 20 % and, thus, can be interpreted as an increase of planktic foraminifera productivity and surface water temperature in response to the influence of Northwest Pacific waters.

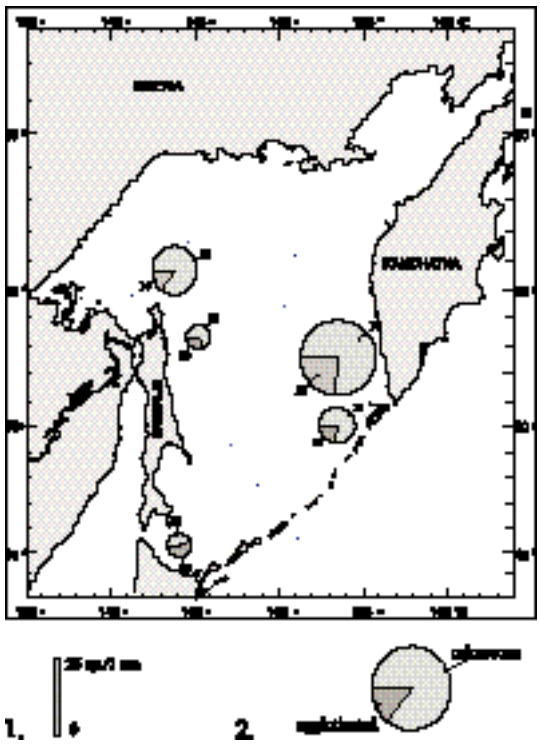

Fig. 9.2: *Distribution of living benthic foraminifera in the surface sediments (0-1 cm) of the Okhotsk Sea. 1 - calcareous and agglutinated abundance (specimen per 1 cm³), 2 - ratio of calcareous and agglutinated foraminifera.*

9.3.2 Benthic foraminifera in surface sediments (0-1 cm)

Totally 66 species and groups of related species are identified in the samples, 33 species in total were counted as living (Appendix 7). *Figures 9.2* and *9.3* summarize living and dead assemblage abundance's and compositions.

The total abundance of living (calcareous and agglutinated) benthic foraminifera increases from 1.7-1.8 to 5.8 spec./cm^3 along a Sakhalin S–N transect (*Fig. 9.2*). In addition, the percentage of agglutinated foraminifera diminishes, which can be regarded both as higher benthic productivity and better carbonate preservation (*Fig. 9.2*). We observed a maximal abundance of living benthic foraminifera of 25 spec./cm^3 at LV29-108-3 (*Fig. 9.2*) on the southwestern Kamchatka slope. This maximum can be related to the absence of seasonal sea-ice cover in this area of the sea and high primary surface productivity of the western Kamchatka shelf and slope areas (Arzhanova & Zubarevich, 1997). Strong upwelling of cold, nutrient-rich water induced by inflow of North Pacific waters has been reported by Sapozhnikov et al. (1999) for the western Kamchatka shelf and continental slope. Similarly to the Kamchatka region, the Sakhalin epicontinental areas exhibit high primary surface productivity as well (Arzhanova & Zubarevich, 1997; Sapozhnikov, 1999) and, thus, high benthic foraminifera productivity should be expected. However, the preliminary results presented in this report do not show high living benthic abundance's at the Sakhalin slope.

The absolute values of living benthics of 1.7-25 spec./cm^3 in the surface sediments (0-1 cm) are rather low. Maxima of living benthics are very likely to occur at deeper sediment levels corresponding to mostly infaunal living species (*Fig. 9.3*). This assumption is justified by our analysis of profile LV28-110-1, where the maximum of living benthics is found at 2-5 cm (*Figs. 9.5* and *9.6*).

The absolute abundance's of the counted living benthic foraminifera are rather low, but the assemblage compositions are typical for high-productivity areas (*Fig. 9.3*). The living species *Uvigerina akitaensis* is one of the major components in almost all of the analyzed samples

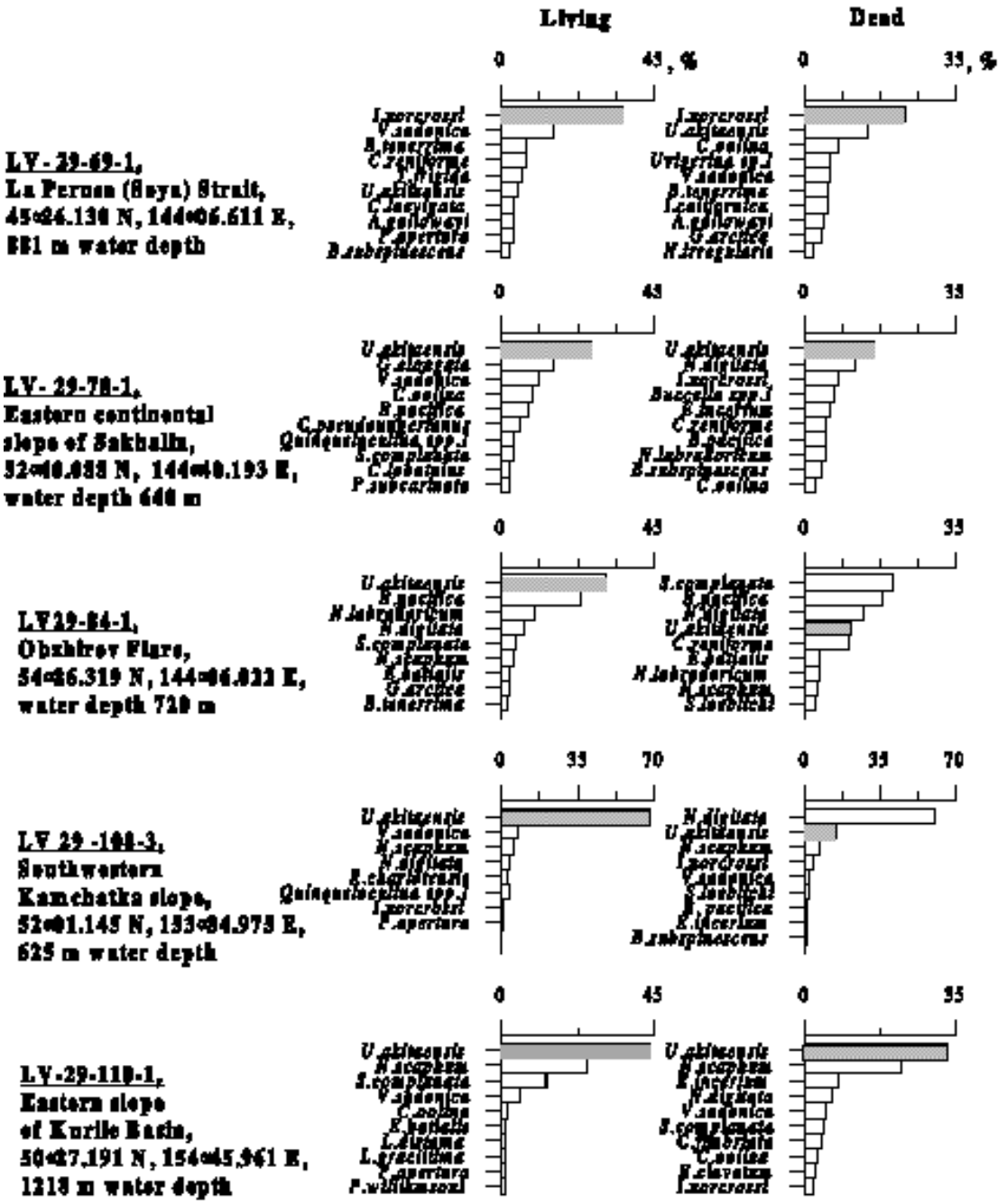

Fig. 9.3: *Rank diagrams (%) for benthic foraminiferal samples from surface sediments (0-1 cm), showing the ten most abundant species in a sample. Grey bars correspond to the dominant living species.*

(*Fig. 9.3*). We suppose the species *U. akitaensis* Asano to be distinct but morphologically close to the species *U. peregrina* Cushman according to original descriptions (Cushman, 1923; Asano, 1950) and investigation of Jung (1988). However, recent taxonomical work (Scott et al., 2000) determined *U. akitaensis* as synonym to *U. peregrina*. The species *Uvigerina genera* is globally abundant in regions of high surface productivity and, hence, of increased flux of organic matter (Loubere, et al., 1995; Mackensen et al., 1995). Thus, *U. akitaensis* is used as a principal proxy indicator of surface productivity in the Sea of Okhotsk. Other dominant living species of surface assemblages (*Fig. 9.3*, Appendix 7) belong to taxa *Nonion, Nonionella, Chilostomellina, Chilostomella, Bolivina, Globobulimina* and *Pullenia* – infaunal genera inhabiting continental slope areas with increased flux of organic matter (Sen Gupta & Machain-Castillo, 1993; Bernhard et al.,1997; Jannink et al., 1998).

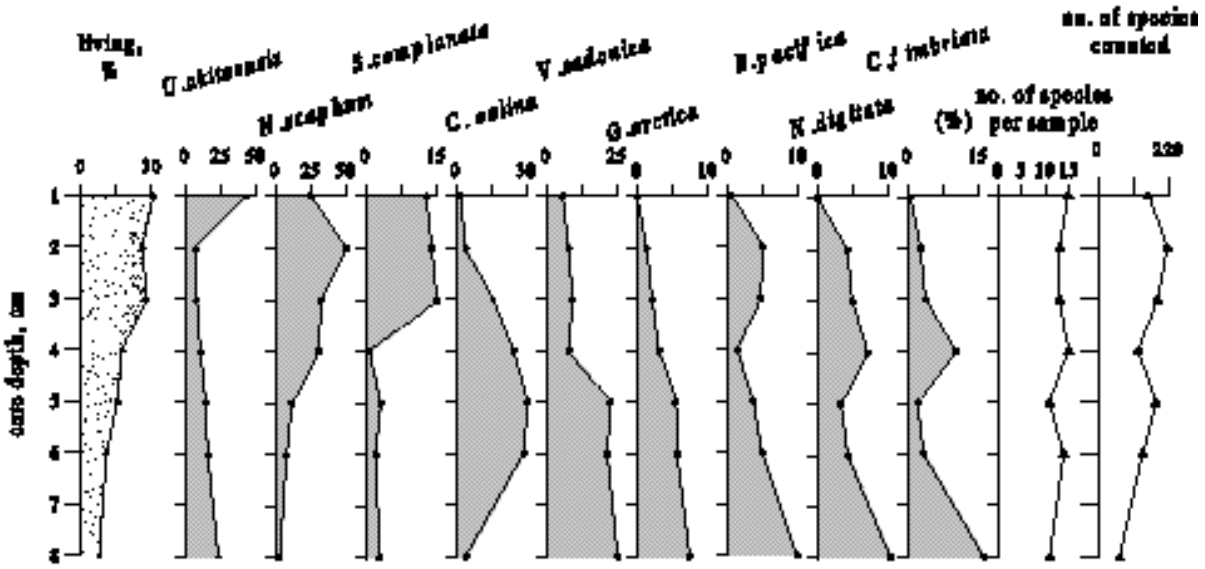

Fig. 9.4: *Percentages of major taxa of living benthic foraminifera in core LV-29-110-1.*

Living benthic foraminiferal assemblages characterizing relatively high, moderate and low primary productivity of the overlying surface waters are discriminated based on the percentage of the dominant species and on the presence of common taxa. The relatively low productivity assemblage is characterized by the dominance of *I. norcrossi* (up to 40 %) and the presence of *V. sadonica, B. tenerrima, C. reniforme, B. frigida* and *U. akitaensis* (Appendix 7, *Fig. 9.3*; revealed in LV29-69-1, La Perusa Strait). The lowest portion of calcareous foraminifera (*Fig. 9.2*) and low total abundance of living foraminifera point towards a relatively low surface productivity in this part of the Okhotsk Sea.

The main feature of the moderate-productivity assemblage is a high content of *U. akitaensis* (25-40%). Other dominant species of this assemblage are *V. sadonica, N. scaphum, B. pacifica, S. complanata, G. elongata* (*Fig. 9.3*). On the southwestern Kamchatka slope, the high productivity group is strongly dominated by *U. akitaensis* with up to 70% of living fauna (*Fig. 9.3*). Thus, both the species composition and the abundance of living benthics (*Figs. 9.2* and *9.3*) from the Kamchatka slope sample show the highest benthic foraminiferal productivity as compared to analyzed data from other parts of the Okhotsk Sea.

The observed maxima of foraminiferal abundance correlate with Okhotsk Sea Intermediate Water (OSIW) properties (app. 600-1,200 m water depth, □□ 26.8–27.4; Aramaki et al., 2001, Wong et al., 1998), as well. While bottom water temperature and salinity variations are insignificant for all the samples under study, oxygen concentrations show pronounced differences (2.07ml/l at LV29-108-3 and 1.16 ml/l at LV29-69-1; Chapter 4). Different values of oxygenation correlate quite well with the observed minimal and maximal living benthic foraminifera productivity at stations LV29-108-3 and LV29-69-1. Thus, our preliminary analysis shows that both surface productivity and hydrological conditions are likely vital for ongoing studies of living benthic foraminifera in the Okhotsk Sea.

The species composition of living and dead benthic foraminiferal assemblages differs little at stations LV29-69-1, -78-1, -108-1 (*Fig. 9.3*) reflecting low carbonate dissolution and bioturbation effect on the fauna. However, we found pronounced differences between living and dead assemblages at stations LV-29-84 and LV-29-110 at "Obzhirov flare" and the southwestern Kamchatka slope. These results cannot be explained by poor carbonate preservation, because high occurrences of translucent and easily degraded foraminiferal shells of *N. digitata, S. complanata* and *B. pacifica* were found in the dead assemblages (*Fig. 9.3*). The high percentage of living *U. akitaensis* is probably attributed to a recent seasonal increase in benthic productivity.

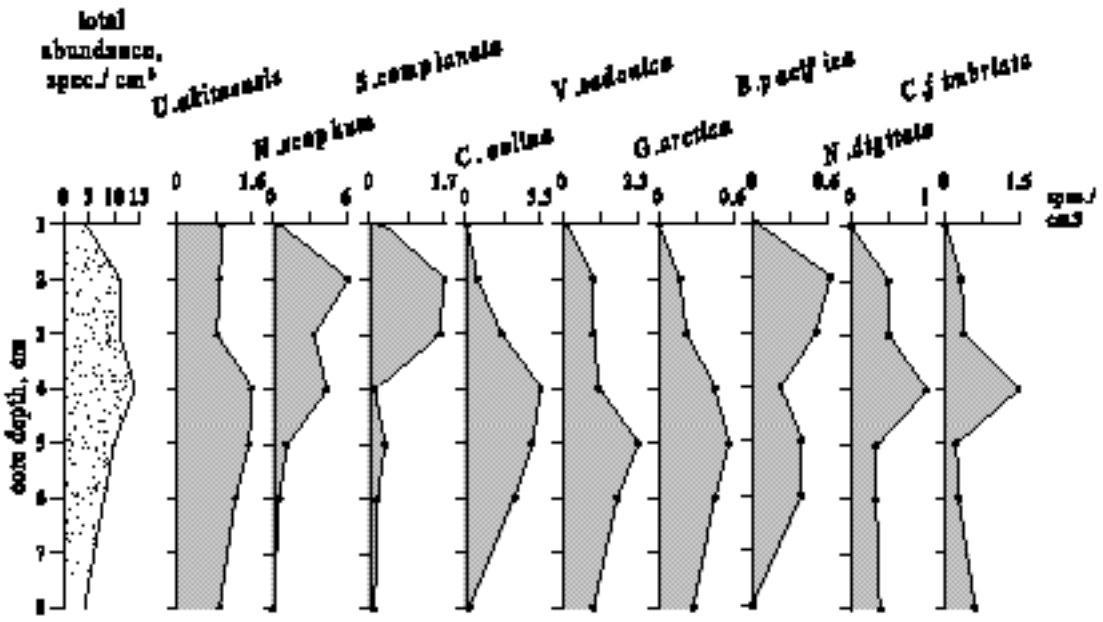

Fig. 9.5: *Abundance's (spec./cm³) of major taxa of living benthic foraminifera in core LV-29-110-1.*

9.3.3 Vertical distribution of benthic foraminifera in subsurface sediments (0-8 cm)

The species *N. scaphum, C. oolina, S. complanata, V. sadonica* and *U. akitaensis* are the major components of living benthic foraminifera assemblages of MUC LV29-110-1 as it is seen from relative concentrations (%) and abundance's (spec./cm³) (*Figs. 9.4* and *9.5*). Rare *P. apertura, C. lobatulus, C. pseudoungerianus*, some species of *Elphidium* and *Lagena* genera are also found as living (Appendix 7). The species diversity of living benthic foraminifera amounts to 11–15 species/cm-interval. The abundance of living foraminifera reaches 10–14 spec./cm³ at 2–5 cm (*Fig. 9.4*, Appendix 7) and decreases down to 4 spec./cm³ at 8 cm.

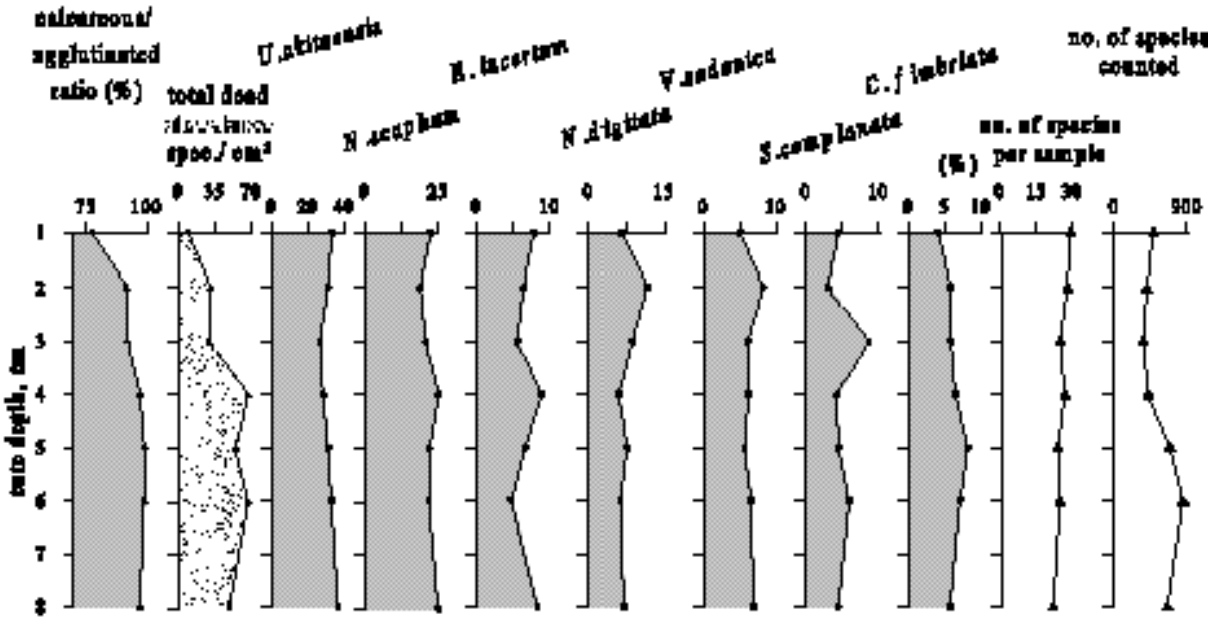

Fig. 9.6: *Percentages of major taxa of dead benthic foraminifera in core LV-29-110-1.*

The downcore variation in relative concentrations (%) and abundance's (spec./cm³) of living benthic foraminifera (species representing >5 % of the assemblage in at least one interval) allows a preliminary subdivision of the species into the following microhabitat categories:

shallow infauna 0-3 cm (*U. akitaensis, N. scaphum, S. complanata*), intermediate infauna 3-6 cm (*C. oolina, B. pacifica*) and deep infauna >6 cm (*V. sadonica, G. auriculata, N. digitata, C. fimbriata*). The dominating species *U. peregrina* has a maximum of 50% in the upper 0-2 cm decreasing down to 25% at 7-8 cm core depth. It remains dominant in all intervals and thus cannot be ascribed to a single microhabitat category.

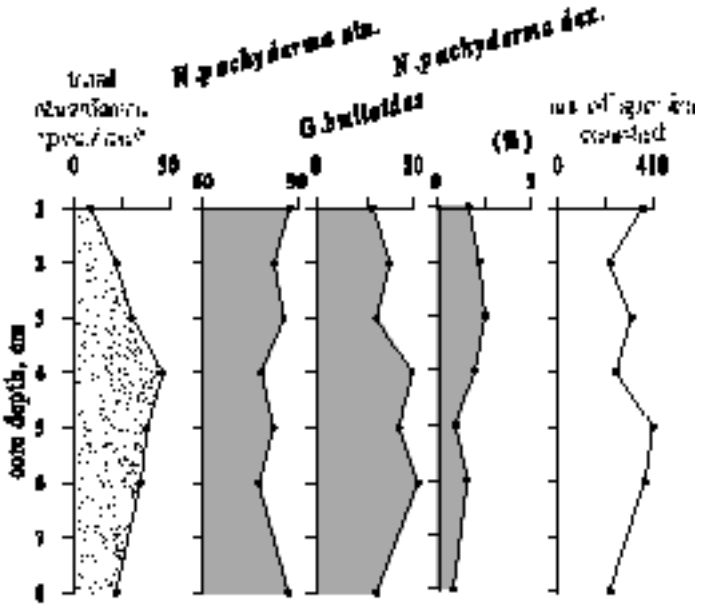

Fig. 9.7: *Percentages of planktonic foraminifera in core LV-29-110-1.*

Dead and living benthics assemblages of LV29-110-1 show a very similar species composition (*Figs. 9.4 - 9.6*). Relatively weak differences of these assemblages can be likely related to processes of bioturbation and dissolution of some calcareous foraminifera. The effect of dissolution is seen from the increase of concentrations of the dissolution-resistant species *U. akitaensis* and *E. incertum* and the decrease of the more fragile *C. oolina* and *G. auriculata* in dead benthic assemblages (*Figs. 9.4 - 9.6*). Little downcore variations in relative concentrations of the dead species through the section (*Fig. 9.6*) are likely resulted from bioturbation. The poor preservation of agglutinated foraminifera in this section is likely caused by taphonomical processes.

9.4 Conclusions

1. The preliminary analysis shows that both surface productivity and bottom water features are important for further studies of benthic foraminifera in the Okhotsk Sea;
2. The total abundance of living benthic foraminifera, the percentage of calcareous benthics and dominance of the species *U. akitaensis* show the highest benthic foraminifera productivity on the western Kamchatka slope as compared to analyzed data from other parts of the Okhotsk Sea;
3. Pronounced differences between living and dead assemblages from "Obzhirov flare" and the southwestern Kamchatka slope probably reflect a recent increase in benthic foraminiferal productivity;
4. Relatively high (*U. akitaensis* up to 70% of total living fauna), moderate (*U. akitaensis* 25-40%) and low productivity groups (*I. norcrossi* up to 40%) of living benthic foraminiferal assemblages are distinguished;
5. Dominant benthic foraminifera occurring in the LV29-110-1 profile are subdivided into three microhabitat categories: shallow infauna (*U. akitaensis, N. scaphum, S.*

complanata), intermediate infauna (*C. oolina, B. pacifica*) and deep infauna *(V. sadonica, G. auriculata, C. fimbriata, N. digitata*).

10. MAIN MORPHOLOGICAL FEATURES OF THE SUBMARINE KURILE BACK-ARC VOLCANOES

Boris Baranov, Andrey Koptev, and Anatoly Salyuk

10.1 Introduction

Bathymetric investigations conducted during Leg 2 of LV29 concentrated on the mapping of the submarine volcanoes chosen for dredging. The shipboard single-beam echosounder ELAC was used for this purpose. This echosounder operated also on all tracks run during the second leg.

3 volcanoes, namely volcanoes 6.4, 6.5, and 7.12 (according to Avdeiko et al., 1992), and Loskutov seamount were mapped in the rear arc zone of the Kurile Island Arc. The first three volcanoes are located inside the Browton and Iturup transverse zones; Loskutov seamount is an isolated volcano located in a distance of ca. 55 nm from the Kurile Island Arc.
Due to lack of time, we did not have the possibility to regularly survey each volcano except for Loskutov seamount where tracks were run in NS and WE direction with a space between them of 0.5-1 nm. But in any case, the obtained data provides information which will be useful for the understanding and classification the volcanoes` main morphological features. Taking into account that the survey of the volcanoes was carried out for dredging purpose, the description of the studied volcanoes and the maps are presented in the Chapter 11 and only summarized preliminary conclusions are given below.

10.2 Methods

During LV29 digital records were made by the ELAC 12 kHz echosounder parallel to the investigation of hydroacoustic anomalies and flare imaging. Depending on the depth range, the period of registration was 1-6 s. A sound velocity of 1,500 m/s was applied. A total of about 500,000 seafloor records were made in the first leg. Using the GPS coordinates and real time of depth measurements, a depth file was generated including date, coordinates and depth. The total size of this ASCII file amounts to about 27 MB. The depth records can be calibrated by a comparison with the bottom depth at corresponding CTD stations, where the seafloor can be determined very accurately for regions with steep relief by calculating the depth from CTD pressure measurements at the moment of bottom contact. The length of the wire between the bottom sensor and the sea floor was 8 m. Furthermore, these calibrated profiles will be used to calibrate data previously obtained mainly from manually digitized analog records of standard shipboard echosounder and multibeam echosounder surveys of cruise GE99 and Leg 1 of LV29.

The central echosounding beam of 12° by 12° was recorded on the LAZ72 Echograph and the depth was digitally displayed on the STG721 Surveying Digitizer.

The ELAC deep-sea echosounding system consists of the following operating elements:
- Echograph LAZ72
- Display selector DSG 4
- Surveying Digitizer STG 721
- Transducer selector SCK 80
- Listening Adapter HV 14

10.3 Preliminary conclusions

1. Different kinds of volcanoes occur in the rear arc zone of the Kurile Island Arc. Some of them have a classic shape like volcano 6.4, others represent volcanic ridges consisting of many volcanic cones accreted to each other (Browton and Hydrographer Ridges, Loskutov seamount). Certainly, the latest are connected with weak zones represented by continuous faults. As the strike of these ridges consistently changes from the NW (Browton Ridge) via WNW (Hydrographer Ridge) to the WE (Loskutov seamount), we can suggest the same change in the ridge-controlling faults.
2. A field of parasitic cones was observed west of volcano 6.4 (Browton transverse zone). The thick sediment layers indicate young eruption processes.
3. One of the submarine volcano (Loskutov seamount) shows an evident imprint of the Kurile Basin tectonics. It consists of three dextral en-echelon chains of volcanic cones striking in WE direction. In contrast, the Kurile back-arc volcanic chains are mainly orientated in NW-SE, SW-NE and NS directions (Avdeiko et al., 1992). The strike and alignment of Loskutov seamount differ from that of the volcanic chains located on the slope and near the Kurile Island Arc and therefore could be connected with the tectonic of the Kurile Basin itself.

11. PETROLOGY AND VOLCANOLOGY

Reinhard Werner, Igor Tararin, Yevgeny Lelikov, and Boris Baranov

11.1 Introduction

Petrological sampling on cruises within the scope of KOMEX I (LV27, LV28, GE99; Nürnberg et al., 1997; Biebow & Hütten, 1999; Biebow et al., 2000) aimed mainly to extend our northern, central (Bussol Strait) and southern transects across the Kurile Island Arc as far as possible into the Kurile Basin in order to study interaction and dependencies between crustal and mantle sources, petrogenetic processes as well as the type and amount of volatiles in the eruptive products in different plate tectonic environments (e.g., rear arc/back-arc vs. volcanic front). These studies are continued and extended within KOMEX II by focussing on profiles across and along the active continental margin of Kamchatka and on detailed investigations of selected island volcanoes of the Kurile Island Arc. Extensive sampling of Geophysicist seamount in the northeastern part of the Kurile Basin on the above mentioned KOMEX I cruises and subsequent lab analyses of the dredged rocks also provided new informations on the structure and geodynamic evolution of the Kurile Basin (e.g., Baranov et al., 2002; Werner et al., subm.). Therefore, the major goal of the volcanological, petrological, and geochemical studies of seamounts in the Okhotsk Sea within KOMEX II is to make further contributions - in cooperation with other KOMEX II working groups - to a model for the geodynamic evolution of marginal basins by reconstruction of volcanic, magmatic and tectonic processes in the Kurile Basin. These objectives should be achieved by:

(1) reconstruction of the paleo-environment of the volcanoes at the time of their activity (e.g., subaerial vs. shallow water vs. deep water) with volcanological methods,
(2) age dating of the volcanoes, and
(3) characterization of tectonic setting of the volcanoes (situated on continental or oceanic crust; mid-ocean-ridge vs. back-arc vs. arc signatures; etc.) with petrological and geochemical methods.

Accordingly, the planned dredge sites on RV *Akademik Lavrentyev* cruise LV29 did not primarily focus on submarine arc volcanoes but on volcanic structures in the Kurile Basin being probably not directly related to the Kurile Island Arc as, for example, the western foothills of Browton Ridge in the central Kurile Basin, Hydrographer Ridge west of Iturup Island, and Loskutov seamount in the southern Kurile Basin. These structures had been discovered on former Russian cruises but had not been mapped in detail, and the sampling of basement rocks failed since the volcanoes seem to be largely covered by marine sediment, ice-rafted debris (dropstones) and/or encrustation's. Despite these difficulties we decided to focus on these volcanoes on cruise LV29 since we expected very interesting new results in case of successful sampling. To achieve the best possible results, approximately half of the time designated for petrological sampling was spent for detailed bathymetric and, at some places, additional seismic surveys. The hydroacoustic and seismic data gained on these surveys did not only enable us to select the most promising sites for dredge hauls, but also provided additional new informations on these volcanoes (see below).

Apart from the Kurile Basin volcanoes, the dredging schedule on cruise LV29 included several structures in the Derugin Basin. The objectives of these dredging operations were:

- Sampling of basement rocks at the northern slope of the Derugin Basin (southern part of the Kashevarov Bank) in order to get information on the basement structure of this area. According to seismic reflection data and echosounding surveys, basement outcrops occur there on a steep slope of a prominent tilted block. Gnibidenko (1985) proposed that this tectonic block is composed of deformed geosynclinal rocks intruded by granodiorites being Upper Cretaceous to Lower Paleogene in age.

- Sampling of tabular calcite and barite-calcite precipitates at the "Barite Mounds" in the northeastern part of the Derugin Basin (see also Chapter 10, Part I of this Report). OFOS (Ocean Floor Observation System) records showed big clamfields consisting of thousands of shells in this area. These shells are considered to be a reliable indicator for active gas seepage.
- Sampling of (sedimentary?) rocks at a small hill (so-called "Lola Hills") close to the "Barite Mounds" in order to gain information on the composition and origin of this structure.

11.2 Methods

Sampling of volcanic, sedimentary and plutonic rocks in the Kurile and Derugin Basins was carried out using rectangular chain bag dredges and a cylindrical ton dredge. Chain bag dredges are similar to large buckets with a chain bag attached to their bottom and steel teeth at their openings, which are dragged along the ocean floor by the ship or the ship's winch.
General station areas were chosen on the basis of bathymetric data, seismic reflection profiles or OFOS data gained on former cruises. The final selection of dredge sites was critically dependent on detailed echosounding surveys carried out at most station areas prior to dredging (e.g., *Fig. 11.1 – 11.4*). The final positioning of the ship over the dredge sites was done using GPS and the bathymetric data gained on the surveys, and allowing for weather and drift conditions. Dredge tracks at the seamounts were usually located - depending on the morphology of the structures - on steep slopes or at small cones on the flanks or tops of the seamounts. This was done (1) to avoid areas of thick sediment cover and (2) to receive rocks as young and accordingly as fresh as possible.
Taking into account the widespread ice-rafted debris in the Okhotsk Sea, detailed analysis of the obtained rocks was carried out to identify bedrock fragments. The criteria used for distinction include but are not restricted to (1) shape of the fragments (angular vs. well-rounded), (2) existence of fresh surfaces formed by tearing away from the bedrock outcrops, and (3) homogeneity of the dredged material.

11.3 Results

Altogether 18 dredge hauls at 4 sites in the Derugin Basin and 4 seamounts in the Kurile Basin on cruise LV29 recovered a wide variety of volcanic, plutonic and sedimentary rocks.

11.3.1 Derugin Basin

The first dredge haul in the Derugin Basin was carried out on its northern slope where – according to seismic reflection surveys – prominent tectonic blocks of the acoustic basement were revealed. The dredge track at the northwestern slope of a tectonic block rose up to 600-700 m above the seafloor of the Derugin Basin and yielded 80-100 kg of rocks comprising some boulders (up to 50 cm) of granodiorites, fragments of rhyodacite and quartz with sulfide mineralization, dropstones (pebbles and fragments of plutonic, volcanic, sedimentary and metamorphic rocks) and Fe-Mn-oxide crusts up to 1 cm thick. Many pebbles are encrusted with ferromanganese minerals.

Granodiorites: Medium-grained light gray rocks composed of plagioclase, quartz, K-feldspar, biotite and hornblende containing sub-rounded fine-grained diorite enclaves up to 3-5 cm in diameter. In terms of mineral assemblages, these rocks are very similar to Upper Cretaceous granodiorites of diorite-granite units being widespread on the Kashevarov Bank, on the Okhotsk Rise and on the Institute of Oceanology and Academy of Sciences Rises.

Rhyodacite: Dark gray sparsely porphyritic or rare aphyric rock with predominant plagioclase phenocrysts. Analogical rhyodacite with K-Ar age of 93.4 Ma associated with dacite, andesite and dolerite were sampled near this dredge site (Emel'yanova, 2001). These volcanic rocks have geochemical peculiarities of high-Al calc-alkaline series that allow to compare them with the Upper Cretaceous volcanic rocks from the Okhotsky-Tchukotsky volcanic belt (Bely, 1978).

The second target in the Derugin Basin was a rise in its northern part – the so-called "Barite Mounds" (Biebow et al., 2000). Detail studies of this rise yielded a wide distribution of various types of carbonate and barite mineralization (Astakhova, 1987; Derkachev et al., 1999, 2002; Biebow et al., 2000). For example, calcite-barite tabular bodies, calcite and barite concretions, barite spherulites and crusts were revealed in Holocene-Pleistocene sediments. At the upper part of the "Barite Mounds" outcrops of pure travertine-like barite chimneys up to 3-10 m high were also discovered (Biebow & Hütten, 1999). On cruise LV29 additional investigations of the eastern part of the "Barite Mounds" were conducted by OFOS surveys, dredging and core sampling. Two dredge hauls at the "Barite Mounds" (stations LV29-98 and -99) recovered various sedimentary rocks, dropstones, barite crusts and specific benthic fauna associated with seeping processes. The barite mineralization is described in Chapter 10, Part I of this Report.
A dredge haul on the slope of a hill ("Lola Hills") of unclear origin (possible diapir) located west of the "Barite Mounds" (station LV29-101) yielded only a small amount of unlithified sediments in the sediment traps of the dredge suggesting that this structure is covered by marine sediments. Therefore, dredging was ceased at this site.

11.3.2 Browton Ridge (Kurile Basin/ rear arc zone of the Kurile Island Arc)

The submarine Browton Ridge is located on the traverse of the Bussol Strait in the central part of the Kurile Island Arc and belongs to the Browton transverse zone (Avdeiko et al., 1992) which comprises the ridge and four discrete conical volcanoes located northeast of the ridge. Browton Ridge extends about 80 km from the arc northwest into the Kurile Basin and consists of several large volcanoes (like Vavilov Massif) and many smaller volcanic edifices. Its base is located at 3,000-3,200 m below sea level (b.s.l.). The conical volcanic edifices on the volcanic (?) basement of Browton Ridge have a sharp top, steep upper slopes (20°-30°) and rise up to ca. 2,500 m over the ocean floor of the Kurile Basin. The highest rise of the ridge is represented by the small volcanic island Browton.
Recent geological and geophysical surveys of this region provide the geologic, tectonic and petrologic framework for the investigations on cruise LV29. The origin and evolution of Browton Ridge, however, are up to now fairly unknown and probably cannot be explained only by the island arc volcanism of the Kurile Islands. Dredging on former cruises at the submarine volcanoes of Browton Ridge yielded a wide range of rocks (basalt, basaltic andesite, dacite, tuff, tuffaceous sandstone and siltstone, granite, granodiorites, diorite, gialospongia, manganese crust etc.), but many of them are believed to be ice-rafted dropstones (Avdeiko et al., 1992). In particular, the structure and composition of the northwestern part of the ridge is still unclear. Therefore, bathymetric survey and subsequent dredging operations on cruise LV29 focussed on the area of volcano 6.5 (according to the catalog of Avdeiko et al., 1992) at the northwestern Browton Ridge. Notwithstanding that the survey tracks were not closely spaced, it is evident that this part of the ridge consists of many volcanic cones and edifices accreted to each other. Four separated edifices including volcano 6.5 can be distinguished on the profile running along this part of the ridge. Their bases are located at similar depths of 3,000-3,100 m b.s.l., but the tops submerge from ca. 1,900 m b.s.l. in the southeast up to ca. 2,600 m b.s.l. to the northwest. The subsidence occurs not progressive but intermittent with the location of the tops at depths of 1,900, 2,300 and 2,600 m b.s.l., correspondingly. The most southeastern and highest cone (unlisted in the catalog of

Avdeiko et al., 1992) was selected for dredging because of its steep flanks and many small cones and, therefore, was mapped in more detail (*Fig. 11.1*).

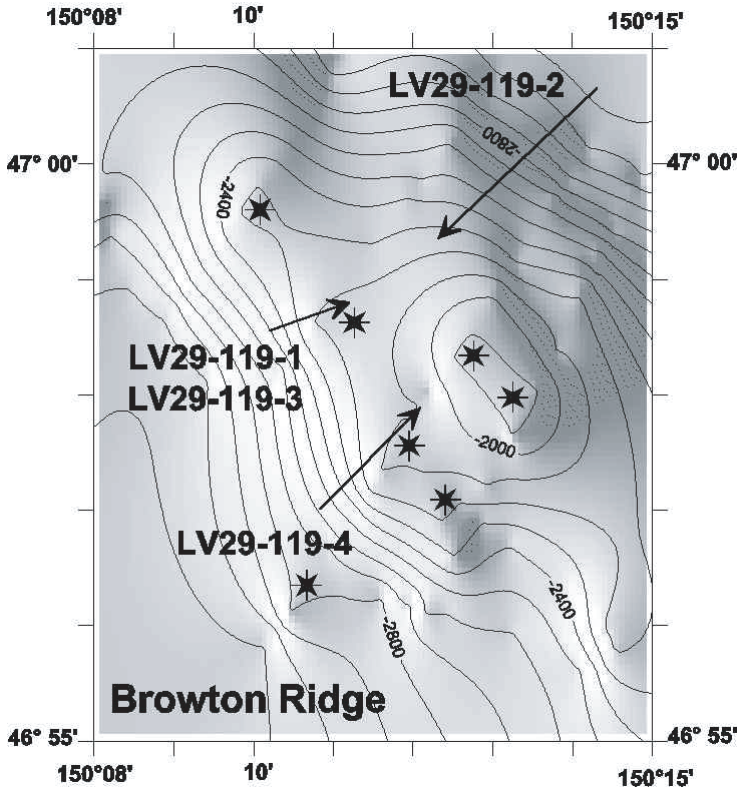

Fig. 11.1*: Bathymetric map of the northwestern Browton Ridge volcano. This volcano as the ridge itself consists of many cones (stars) accreted to each other. Numbered solid arrows mark the dredge tracks and station number. Contour interval is 100 m.*

Four dredge hauls were carried out at this volcano: LV29-119-1, -119-3 and -119-4 from the southwestern slope and LV29-119-2 from its northeastern slope (*Fig. 11.1*). Dredge haul LV29-119-1 (2,600-2,200 m b.s.l.) did not recover rock samples, because the chain bag of the dredge opened during dredging, but a few manganese fragments (<1 cm) were found in the sediment traps of the dredge. Dredge haul LV29-119-2 (3,000-2,400 m b.s.l.) yielded about 30 kg of boulders and fragments of ice-rafted debris.

Dredge haul LV29-119-3 (2,600-2,200 m b.s.l.) recovered about 50 kg rocks comprising predominantly blocks and fragments of tuffaceous diatomite's and tuffaceous sandstone's, gialospongia and dropstones (pebbles, fragments and boulders of volcanic and plutonic rocks). Most fragments of the stratified tuffaceous sedimentary rocks contain numerous small fragments and pebbles of altered volcanic rocks and are coated and impregnated by ferromanganese material. Their shape, the fresh surfaces and homogeneity indicate an in situ origin of these sedimentary rocks at Browton Ridge.

Dredge haul LV29-119-4 (2,700-2,400 m b.s.l.) yielded about 250 kg rocks comprising dropstones, numerous blocks and fragments of yellow-greenish slightly lithified tuffaceous diatomite's and tuffaceous sandstone's, gray-greenish highly lithified tuffaceous sandstone's and diatomite's, boulders (up to 50-80 cm) of black volcanogenic conglomerato-breccia with tuffaceous matrix, blocks of gialospongia impregnated by manganese, and a fragment (up to 25 cm) of comparatively fresh, sparsely porphyric vesicular olivine-plagioclase basalt (probably dropstone?).

Additionally, one dredge haul (LV29-122) was carried out on the submarine volcano 6.4 (according to the catalog of Avdeiko et al., 1992) located ca. 47 km northeast of Browton

Island and ca. 50 km northwest of Simushir Island. This seamount has a very regular, conical volcanic edifice with a sharp top and steep upper slopes (up to 25º-30º), and rises up to ca. 1,800 m above the Kurile Basin floor. Its base is equal to 20 km in diameter; the total volume of the edifice is ca. 280 km^3 (Avdeiko et al., 1992). The volcano is characterized by a slightly negative magnetic anomaly with maximum values under the northeastern slope (-20 nT) and minimum values (-110 nT) under the southwestern slope (Avdeiko et al., 1992). Dredging on former cruises yielded fragments, blocks and boulders of plutonic, volcanic and sedimentary rocks (e.g., layered gravel, breccias, altered basalt, andesite, dacite, diorite, porphyric granite and granodiorites) being most likely ice-rafted debris (Avdeiko et al., 1992).
The bathymetric survey on cruise LV29 proved that this seamount is a classic volcanic edifice being slightly elongated in NW-SE direction (*Fig. 11.2*). Bends of the contour lines may indicate parasitic cones on the flanks of the volcano. Furthermore, a field of small volcanic cones was detected on a bathymetric profile extending westward from the base of the volcano. One dredge haul (LV29-122, 2,700-2,200 m b.s.l.) on the northeastern slope of volcano 6.4 (*Fig. 11.2*) recovered about 30 kg rocks comprising predominantly blocks and fragments of tuffaceous diatomite's and tuffaceous sandstone's impregnated by manganese, gialospongia and dropstones (pebbles, fragments and boulders of volcanic and plutonic rocks).

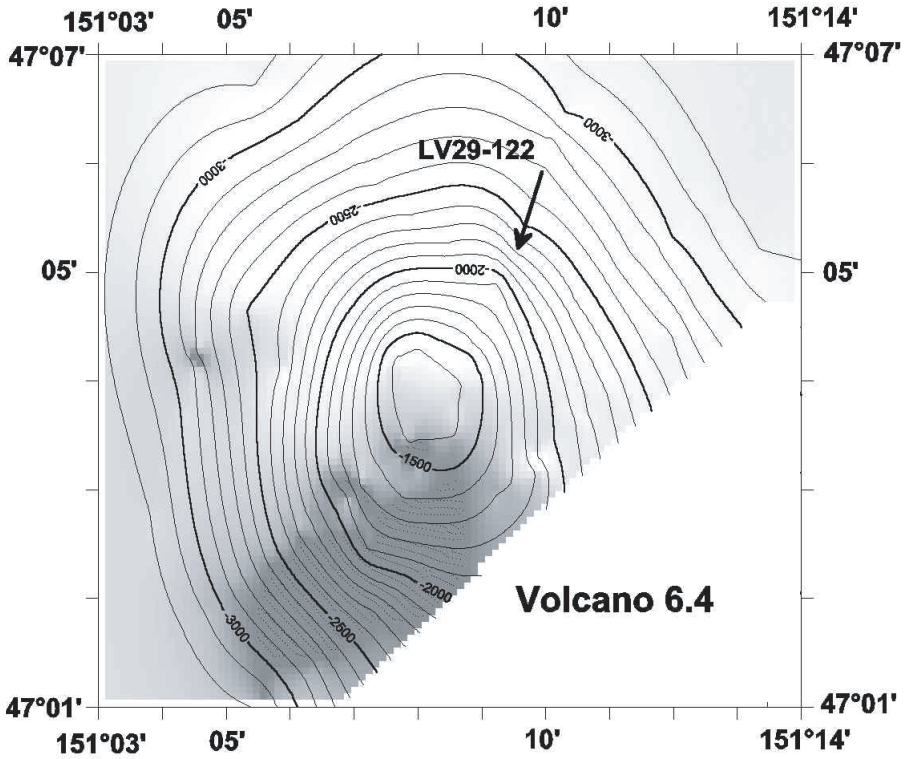

***Fig. 11.2**: Bathymetric map of volcano 6.4. This volcano has a very regular shape and uplifts above the flat Kurile Basin floor up to ca. 1,800 m. Arrow marks the dredge track. Contour interval is 100 m.*

In summary, the dredged material yielded at Browton Ridge and volcano 6.4 indicates that the slopes of these structures are most likely completely covered by slightly to highly lithified diatomaceous sedimentary rocks, manganese crusts, (fossil) colonies of gialospongia impregnated by manganese, and dropstones ranging in composition from basalt to granodiorites. The diatomaceous sedimentary rocks represent probably the sedimentary bedrock's of Browton Ridge. Land-based studies of these rocks may provide information on the (minimum) age of the ridge (Miocene-Pliocene?).

11.3.3 Submarine volcanoes of the North-Iturup transverse zone (Hydrographer Ridge)

Hydrographer Ridge, located in the North-Iturup transverse zone of the Kurile Island Arc, is a ca. 20 km long, WNW-ESE-trending ridge structure elevating up to ca. 1,600 m above the floor of the Kurile Basin. According to Avdeiko et al. (1992), the ridge represents a chain of three volcanoes (7.12, 7.13, 7.14). Dredging on former cruises yielded a wide variety of rocks, among them basalts and basaltic andesites, yet these have been considered to be most likely dropstones. The bathymetric and seismic survey conducted on cruise LV29 revealed significant differences in the morphology of the western and eastern part of the ridge. The eastern part (volcano 7.14) shows a cross section of a typical stratovolcano with a flat top probably tilting towards the Kurile Basin, whereas the western Hydrographer Ridge (volcano 7.12) has an asymmetric profile with a steeper southern slope.

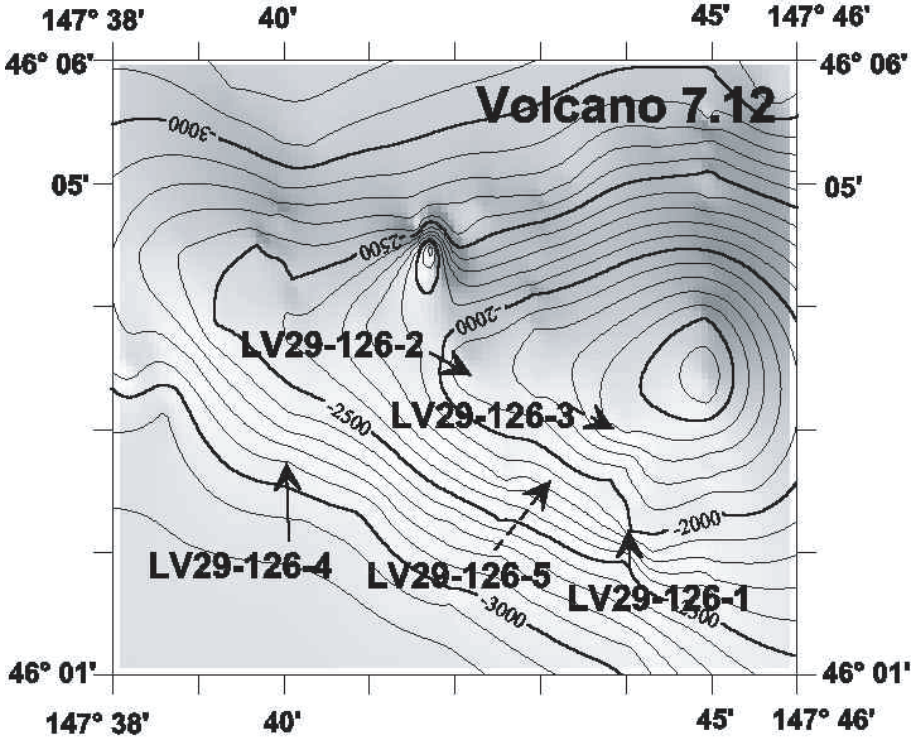

Fig. 11.3*: Bathymetric map of the western Hydrographer Ridge (volcano 7.12). This part of the ridge has an asymmetric cross section. Numbered solid arrows mark the dredge tracks and station number, dashed where the dredge was empty or only ice-rafted material was recovered. Contour interval is 100 m.*

Five dredge hauls were carried out at volcano 7.12 subsequent to the hydroacoustic and seismic survey: LV29-126-1, -126-4 and 126-5 from the lower southern slope to the top and LV29-126-2 and -126-3 at the small cones on the crest of the ridge (*Fig. 11.3*). Dredge hauls LV29-126-3 and -126-5 yielded only numerous fragments of gialospongia and dropstones ranging in composition from granodiorites to basalt. Dredge haul LV29-126-2 recovered besides dropstones a small (ca. 5 cm in size) fragment of orthopyroxene-clinopyroxene-plagioclase basaltic andesite which possibly represents the bedrock of this site.
Dredge haul LV29-126-1 (ca. 2,500-2,000 m b.s.l.) on the southern slope of volcano 7.12, however, yielded ca. 100 kg of angular fragments of homogeneous pillow-like basaltic lava, ranging from a few centimeters to ca. 30 x 30 cm in size. The homogeneity, angular shape and rough surfaces of the dredged rocks strongly indicate that they are fragments of a (pillow)-lava flow once formed by an eruption of volcano 7.12, i.e. they represent in situ rocks. The lava fragments are highly porphyric (up to 5-10 vol.%), frequently vesicular

basalts or basaltic andesites with rounded to oval-shaped vesicles being commonly 1-3 mm in diameter. Major phenocrysts are plagioclase, clinopyroxene, olivine, amphibole, and Fe-Ti-oxides; orthopyroxene occurs minor. The groundmass is characterized by a microlitic texture and consists of glass with numerous plagioclase microlites and varying amounts of clinopyroxene, amphibole and Fe-Ti-oxides. The phenocrysts and the groundmass of these rocks are fresh or show only minor alteration.
Dredge haul LV29-126-4 recovered numerous fragments (ca. 8-10 kg) of slightly lithified diatomaceous sedimentary rocks, gialospongia, and a block (ca. 25 x 30 cm in size) of porphyric, vesicular olivine-orthopyroxene-clinopyroxene-plagioclase basalt. The material yielded by this dredge shows some evidence for an in situ origin as homogeneity (sedimentary rocks), angular form, and rough, "broken" surfaces (sedimentary rocks, basaltic block). The basaltic block is only minor affected by alteration with the exception of the olivine phenocrysts which are partially replaced by secondary minerals. The noteworthy feature of this lava is common glomerophyric clusters of gabbro (cpx+plag) and wehrlite (ol+cpx±plag), which are considered to be enclaves of cumulated rocks.

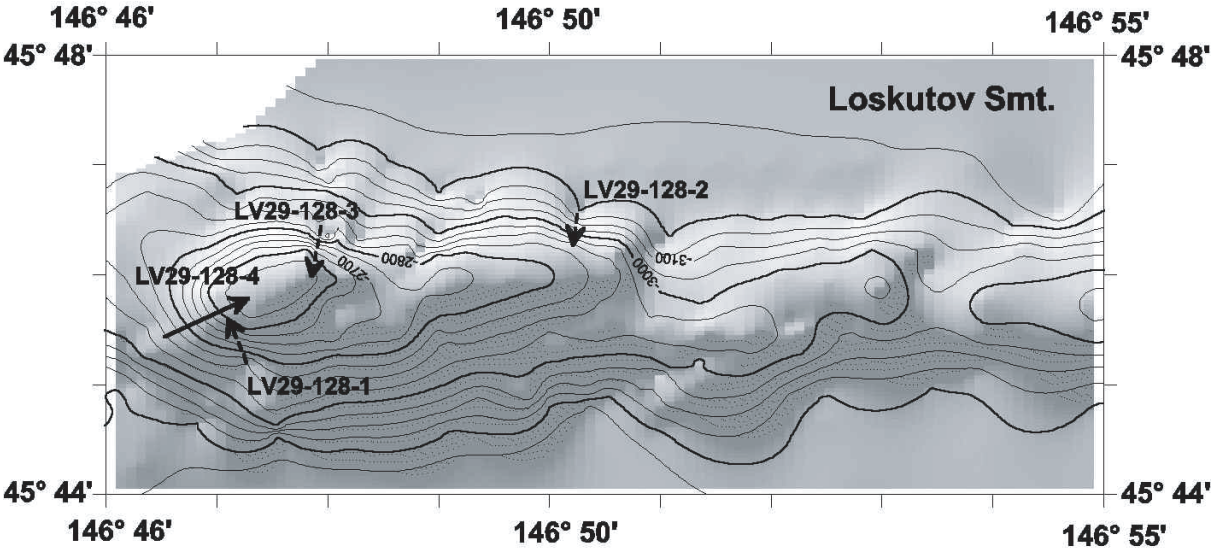

Fig. 11.4: *Bathymetric map of the deepest volcano (Loskutov seamount) dredged on cruise LV29. This volcano consists of many volcanic cones and shows a dextral en-echelon pattern. Numbered solid arrows mark the dredge tracks and station number, dashed where the dredge was empty or only ice-rafted material was recovered. Contour interval is 25 m.*

11.3.4 Loskutov submarine volcano

Loskutov seamount is located ca. 100 km northwest of the Kurile Island Arc in the Kurile Basin. The seamount does not show any visible relationship with the arc, and its origin and evolution is still unknown. It has a ridge-like structure which is outlined by the 3,500 m contour line and extends ca. 20 km in W-E direction (*Fig. 11.4*). The bathymetric survey on cruise LV29 proved that this ridge consists of several volcanic cones (similar to Browton Ridge). The highest cone is located in the western part and elevates up to 2,510 m b.s.l. The cones align in three chains that show a dextral en-echelon pattern.
Altogether 4 dredge hauls were carried out on the southern slope (LV29-128-1), the northern base (LV29-128-2), and in the top area of the western cone (LV29-128-3, -4) of Loskutov seamount (*Fig. 11.4*). None of these dredge hauls recovered in situ volcanic (or plutonic) rocks. Dredging at sites LV29-128-1, -2, and -3 yielded only a couple of dropstones and small amounts of unlithified (marine) sediments. However, paleoceanological studies of slightly

lithified sedimentary rocks recovered at site LV29-128-4 may possibly provide informations on the (minimum) age and evolution of Loskutov seamount.

12. REFLECTION SEISMICS

Boris Karp, Boris Baranov, Viktor Karnaukh, and Vladimir Prokudin

12.1 Method and instruments

The applied seismic reflection system consists of one air gun, a single-channel streamer, a digital data acquisition system and air gun trigger unit. The Pulse-6^{TM} air gun pressurized nominally at 130 bar was towed in a distance of ca. 10 m behind the ship and triggered every 10-11 sec with pulses generated by a master clock. The streamer has an active section with a length of 25 m and two inactive sections (ahead and behind of the active section) with a length of 25 m each, leading to a total length of the streamer of 75 m. The towing depth of the streamer was 6 m, and the offset was 150 m.
The operational characteristics of the single-channel seismic reflection system are summarized in *Table 12.1*.

Table 12.1: *Operational characteristics of the single-channel reflection system.*

Source	
Type	Pulse-6^{TM} air gun
Volume	3.5 or 2.5 liters
Pressure	130 bar nominal
Firing interval	10-11 sec
Source depth	5 m
Streamer	
Streamer depth	6 m
Active section offset	175 m
Length of active section	25 m
Total length of streamer	75 m
Recording	
Recording length	3-4 sec
Sampling frequency	1000 Hz
Bandpass analog filter	20-400 Hz

The analog seismic signals are digitized via a PC-based commercial sound card (Sound Blaster 16, Vibra) and written onto the harddisk of a Pentium-PC. A backup copy was made on CD. A single-channel digital acquisition system permits real-time data monitoring (quality control) on screen. The GPS unit is connected to the serial port of the PC. Recording and adjustment of the dynamic range of the seismic signals are controlled on the PC monitor by software developed for this purpose.

Specification of the single-channel data acquisition system:

- data format: SEG-Y files, 16 bit
- sampling rate: 1 or 2 ms
- length of trace: 4…6 sec
- software: acquisition, filtering, viewing, printing, testing

12.2 Results

Reflection seismic profiling was carried out during cruise LV29 of RV *Akademik Lavrentyev* continuing and extending the study area of the SAKURA expedition in the central part of the Kurile Basin and on Browton and Hydrographer Ridges to the north (*Fig. 12.1*). In addition,

seismic profiling was carried out parallel to the sediment echosounder SES-2000DS profiles excluding the profiles in the Sakhalin Gulf and in the enter of La Perusa Strait (see Appendix 8). This report includes the preliminary interpretation of seismic profiles in the central part of the Kurile Basin.

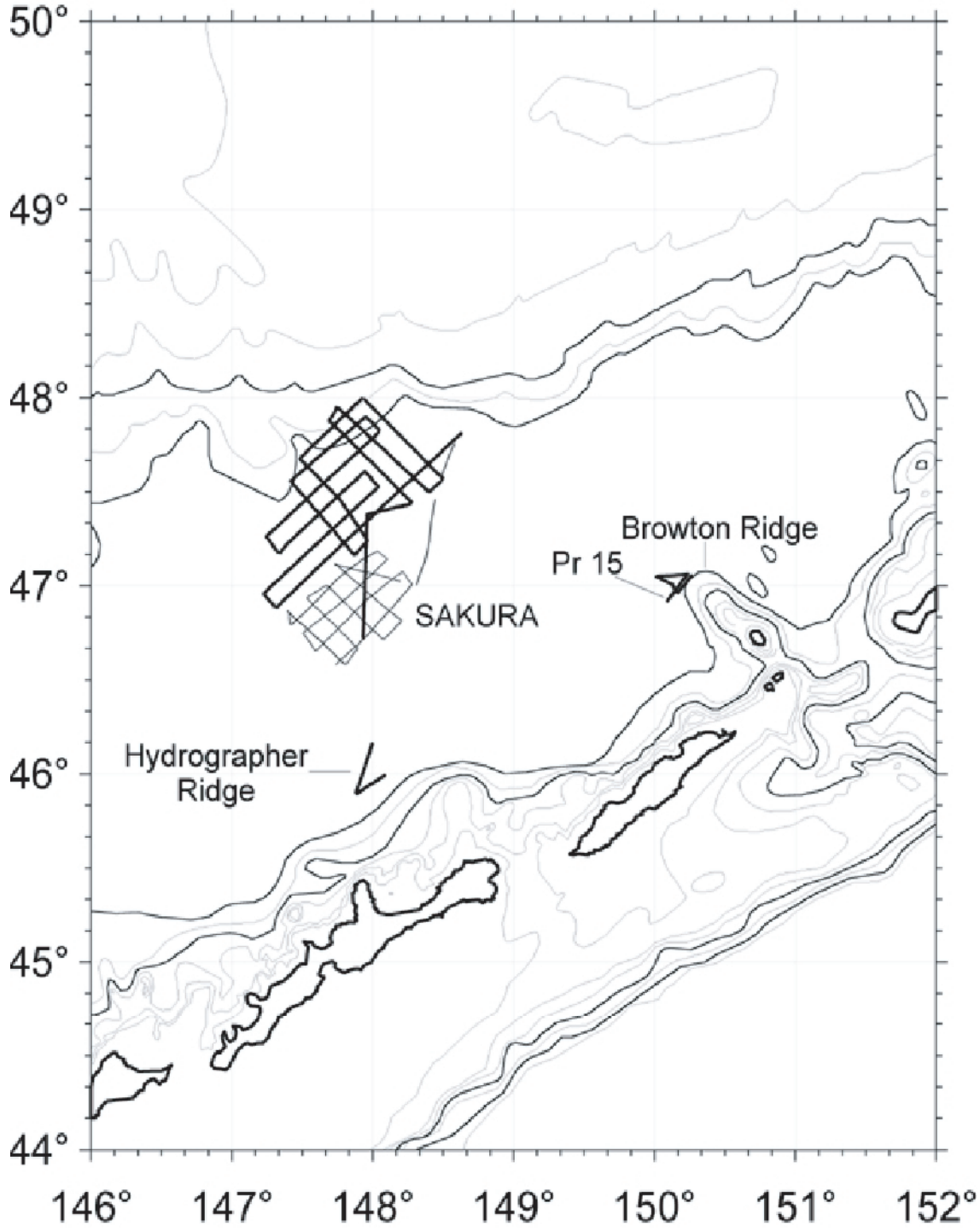

Fig. 12.1: *Seismic profiles of the present expedition and of the SAKURA cruise in the central Kurile Basin. Marked are the present expedition lines.*

The acoustic basement can be seen on most parts of the profiles. It is clearly expressed up to a depth of 6.0 s TWT below the sea surface and appears as a weak reflector at greater depth. The acoustic basement is represented by an envelope of diffraction hyperbolas. The chaotic internal reflections of the basement probably indicate a volcanic (basaltic) composition of the

basement. A map of the distribution of basement depths compiled from the SAKURA and the present expedition data is shown in *Figure 12.2*. The main structural element of the SAKURA area is Sakura Ridge (Biebow et al., 2000). It is clear from *Figure 12.2* that Sakura Ridge extends to the north. Its crest is displaced to the east at approximately 47°23'N.

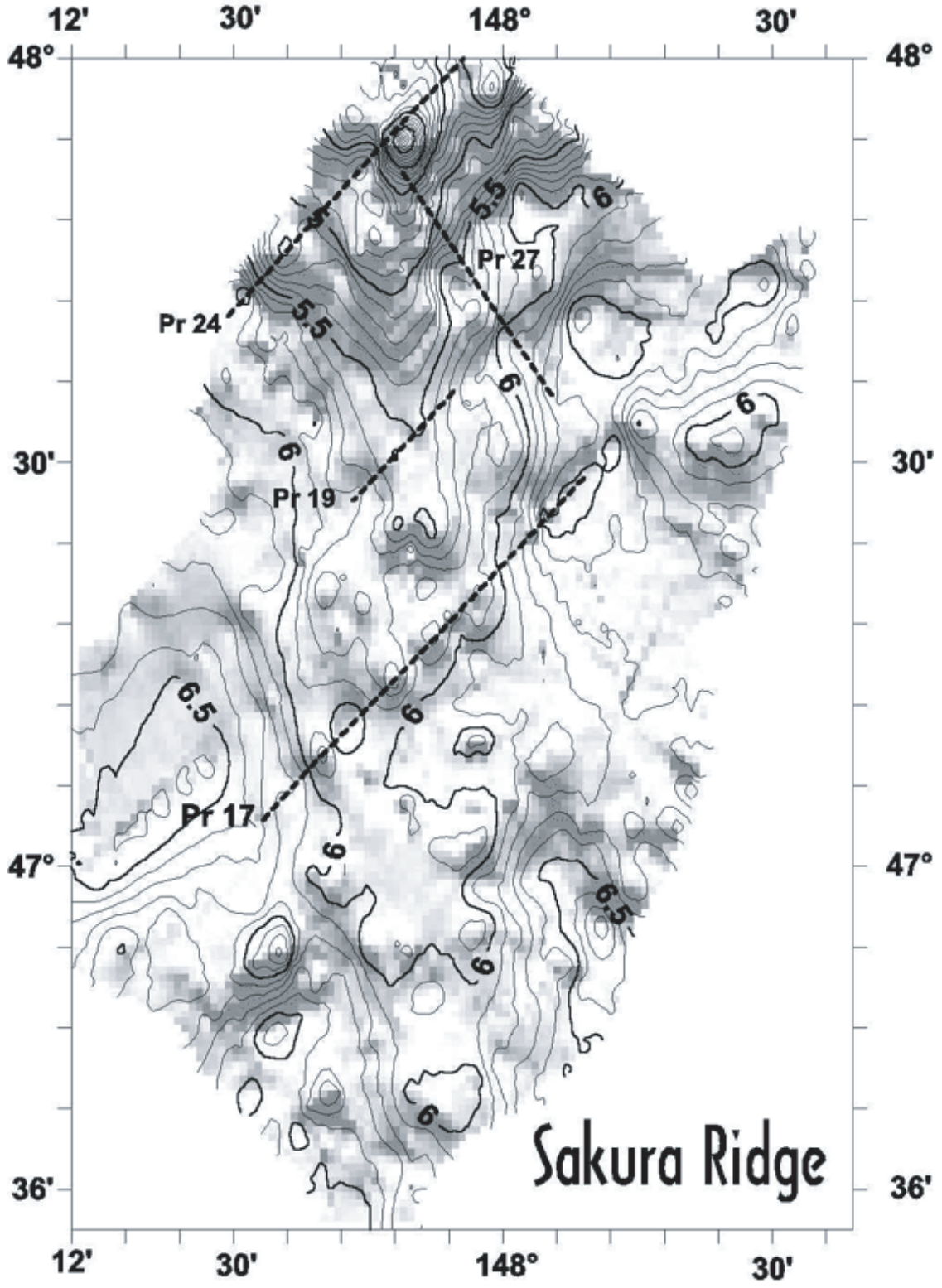

Fig. 12.2: *Basement morphology of Sakura Ridge. This ridge has very pronounced wedge-shape outlines suggesting propagated rift. Contour interval is 0.1 s. Dashed lines mark location of the seismic profiles shown in Fig. 12.4 — 12.8.*

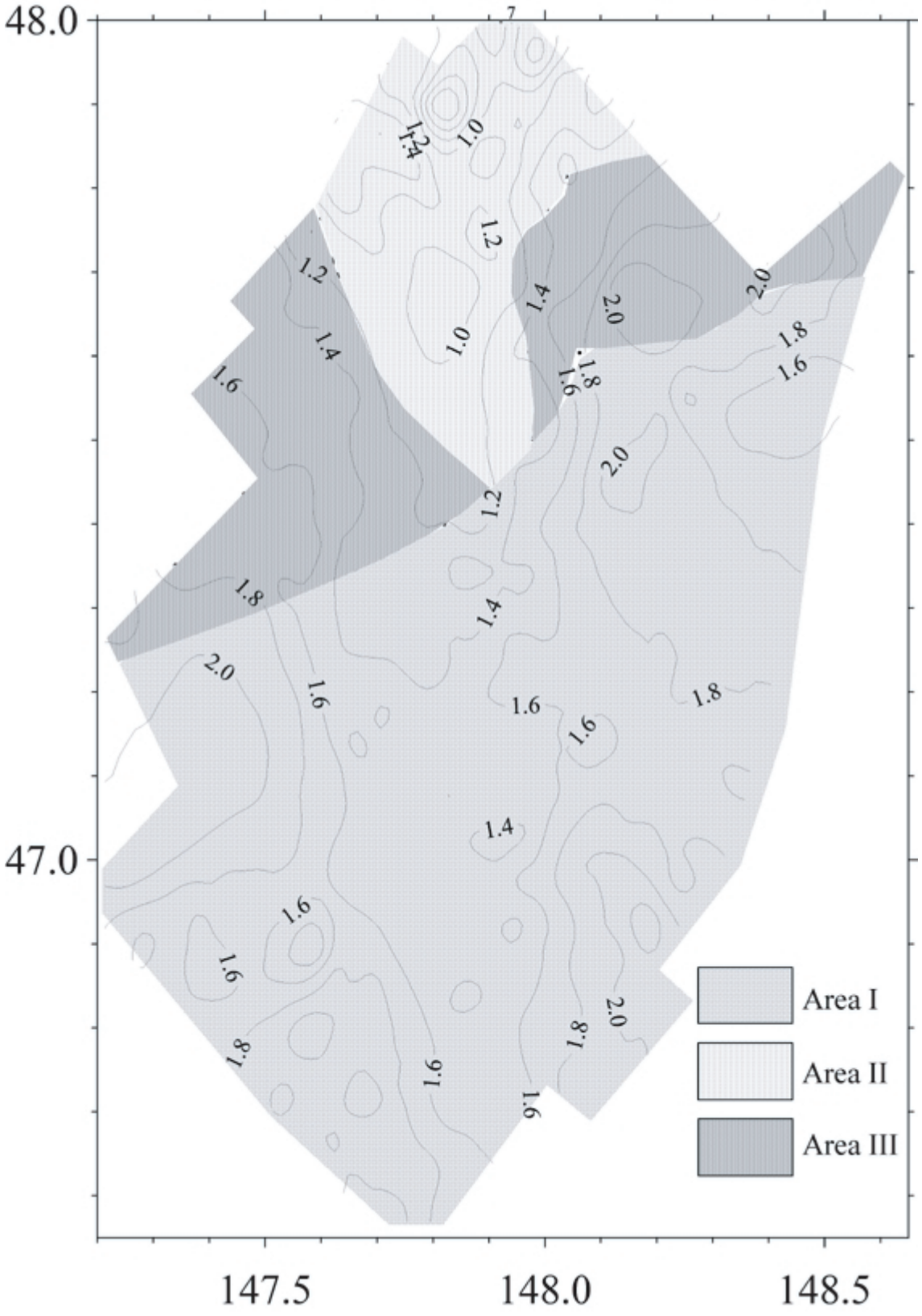

Fig. 12.3: *Map of location of areas with different seismo-stratigraphic characteristics. 1 = area I, 2 = area II, 3 = area III. Thin continuous lines mark thickness of sedimentary layer in sec. Contour interval is 0.2 s.*

The ridge is bounded by an acoustic basement high striking in SW-NE direction in the north. The sediment thickness above the ridge does not exceed 1.6 s. However, it reaches 2.0 s (*Fig.*

12.3) in the basement depressions that are located to the southwest and to the northeast of the ridge.

The investigated part of the Kurile Basin can be divided into three areas, each having its own distinct seismo-stratigraphic characteristics (*Fig. 12.3*). The first (area I) is located in the south. Its sedimentary section comprises two seismic units: an upper, well stratified unit and a lower, semi-transparent unit (*Fig. 12.4*). The thickness of the upper unit is nearly constant at 0.8 – 1.0 s. Fluctuations in the total thickness of the sedimentary layer are largely a result of variations in the thickness of the semi-transparent unit. The well stratified unit consists of a series of subparallel, subhorizontal reflectors. In contrast, the semi-transparent unit comprises only occasional, low-amplitude, continuous reflectors that drape the acoustic basement. The boundary between these two units is marked by a high-amplitude, low-frequency reflector. The well stratified unit may be subdivided into two sequences (A1 and A2, *Fig. 12.4*) that differ in the thickness of the intercalated transparent layers and layers with discontinuous reflectors of low amplitude.

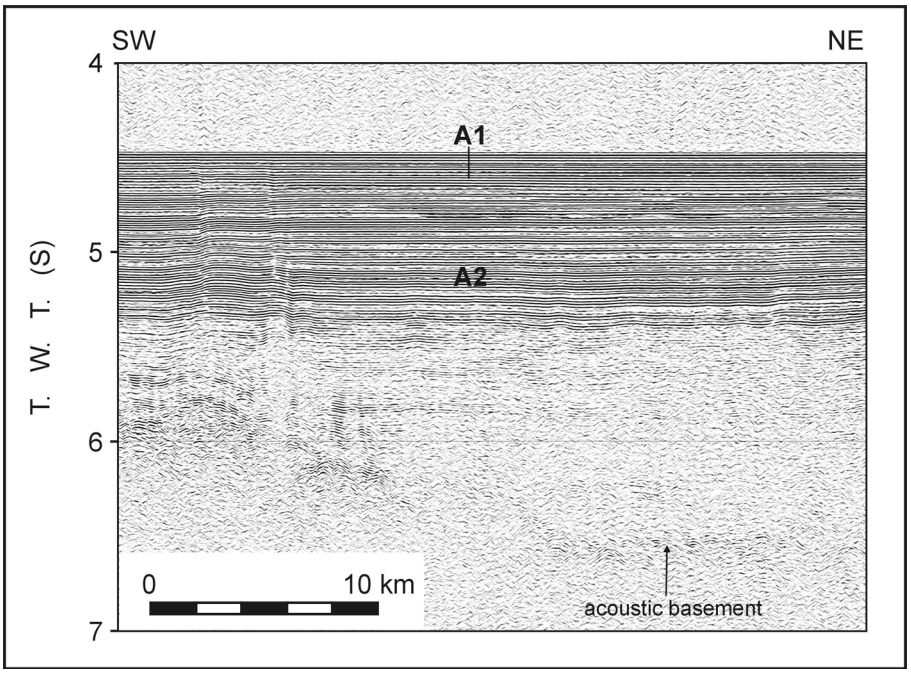

Fig. 12.4: *Part of seismic profile 17 showing the seismic section in area I. Location of profile is shown in Fig. 12.2.*

Area II occupies the ridge and its slopes. The sedimentary section of area II, where the ridge is buried by sediments and does practically not manifest in the seafloor (profiles 19 and 20), comprises seven seismic units: four well stratified sequences and three semi-transparent sequences (profile 19, *Fig. 12.5*). The upper two well stratified sequences consist of subparallel seismic reflections. The upper of them is characterized by continuous reflectors of high amplitude. The reflectors have a curve upward configuration. The lower sequence comprises subparallel continuous reflectors of medium amplitude and a curve downward configuration. These sequences are bounded by an unconformity. All semi-transparent sequences have only occasional, low-amplitude, discontinuous reflectors. The lower two well stratified sequences drape underlying semi-transparent sequences. The sedimentary section of area II where the ridge manifests in topography is characterized by the presence of four well stratified sequences on the top and upper slope of the ridge (profile 27, *Fig. 12.6*). A semi-transparent sequence is subjacent to these sequences. The well stratified sequences are separated by three unconformities that show erosion truncation in places. On the middle and lower slopes three upper well stratified sequences are truncated by the seafloor. The semi-

transparent unit separates the lower well stratified sequence and the upper well stratified sequence. The external configuration of the semi-transparent unit is mound-like (downlap of the reflectors). On the middle slope buried sediment waves occur. There are scarps and displaced masses (slides) on the ridge lower slope.

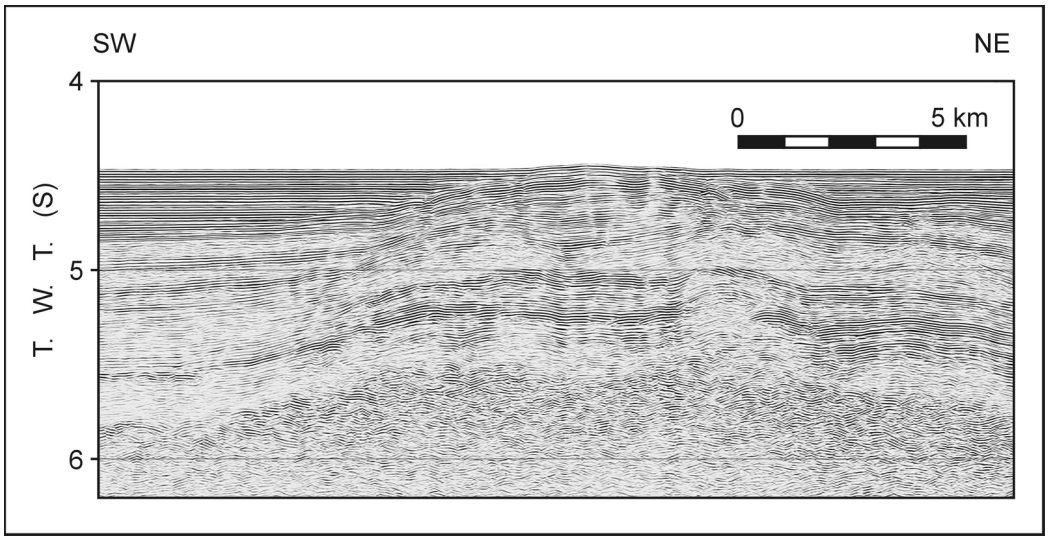

Fig. 12.5: *Part of seismic profile 19 showing the seismic section of the ridge buried by sediments (area II). Location of profile is shown in Fig. 12.2.*

Area III differs from area I by the fact that several (2-3) semi-transparent layers thicken considerably in the interior of the upper well stratified unit and that a prominent well stratified layer appears within the lower semi-transparent unit. The boundary between area II and area III coincides with the ridge's lower slope buried by sediments. In general, area I grades area III and the boundary between them is not clear.

12.3 Discussion

12.3.1 Sediment processes

The sedimentary section of the Kurile Basin consists of an upper stratified and a lower semi-transparent sequence. The boundary between them is marked by a high-amplitude reflector (Gnibidenko et al., 1995). The same sedimentary section is observed in area I. In addition, the upper sedimentary column directly above Sakura Ridge is repeatedly interrupted by vertical regions of acoustic turbidity in which diffraction hyperbolas dominate. Typical are also the accompanying apparent deformations and interruptions of the flat-lying horizons. These regions are probably fissure zones. Sediment processes change abruptly in the northern part of Sakura Ridge (area II). The lower semi-transparent sequence displays an apparent drape of the basement highs of the ridge. In contrast, the upper well stratified sequence onlaps the ridge's proper sedimentary layers. These relationships between sedimentary section and ridge basement indicate that the Kurile Basin sediments accumulated here during an inactive period of the basin's development.

The depositional history of the ridge after semi-transparent sequence accumulation includes at least three periods. Turbidites and interbedded hemipelagits overlay the semi-transparent sequence. The deposits appear as well stratified units on the seismic section. The thickness of the unit decreases from north to south amounting to 0.3 – 0.4 s in the north (profile 24) and 0.1 – 0.15 s in the south (profile 19). This unit extends to area III as the prominent well stratified layer within the lower semi-transparent unit. The reduction of the thickness of the

well stratified unit from north to south suggests that a source of turbidites was located on the northern Kurile Basin slope. The top of the unit is an erosional discontinuity. Simultaneously with erosional processes, the ridge slope became more instable. The instability resulted in mass movements causing erosion at the top and the middle of the slope as well as debris flows at the base of the slope. These debris flows extend to the basin (probably as turbidity currents) and create semi-transparent layers in area III. This process was repeated at least two times during the depositional history of the ridge. At present, the processes of mass wasting prevail in the northern part of the ridge. The topographic Sakura Ridge is a sediment ridge except for its northern termination.

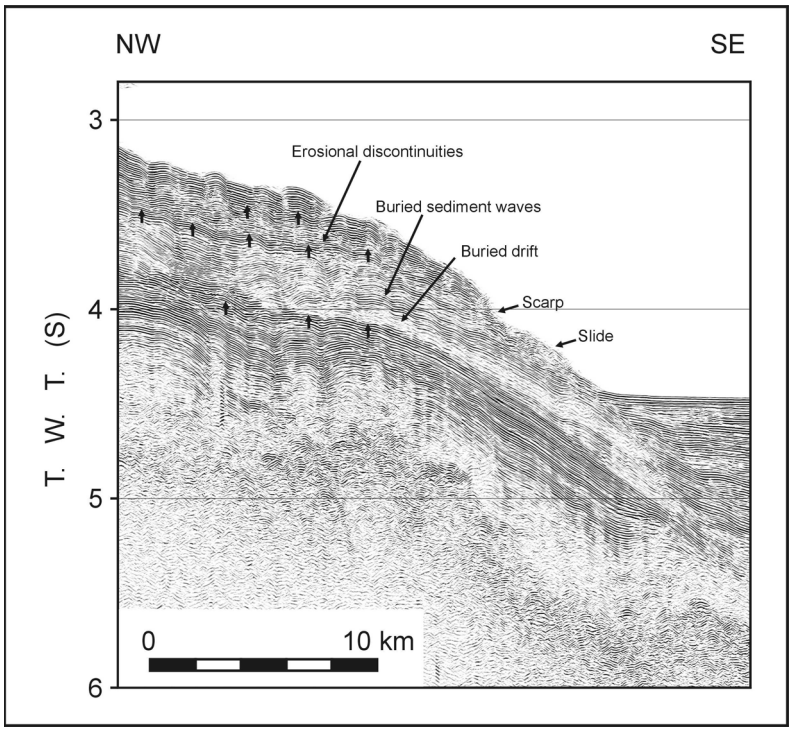

Fig. 12.6: *Part of seismic profile 27 showing the seismic section of the northern termination of the ridge (area II). Location of profile is shown in Fig. 12.2.*

12.3.2 Tectonic structure of Sakura Ridge

12.3.2.1 Previous studies

The seismic survey in the central part of the Kurile Basin was carried out to study the nature of a specific basement rise, which separates two subbasins with a depth to the basement of up to 7 km.

For the first time this basement rise in the central part of the basin was investigated during the Pacific expedition “Souzmorgeo” in 1976. The expedition showed that the rise has a complicated structure and consists of isometric basement highs. The depressions between them form fan-like, undulating systems that resemble river valleys. Over the top of the swell, the basement lies at a depth of about 5 km; in the depressions to the southwest and the northeast, it was found at depths of 8 and 7 km, respectively (Zhuravlev, 1982). The origin of the rise remained unknown. It was only much later that they were supposed to represent shear/lateral fault zones that defined an opening direction orthogonally to the general strike of the Kurile Basin (Gnibidenko et al., 1995).

For the second time, the rise was investigated during the SAKURA expedition in 1999 (Biebow et al., 2000). The data obtained showed that this rise (named Sakura Ridge) has a clear rift imprint. The morphology of its axial high suggests that it corresponds to a spreading axis. This axis (a spreading ridge) strikes N-S, i.e. in correspondence to the general strike of

the Kurile Basin. Although this data is insufficient for a reliable identification of the spreading axis, it provides clear evidence for a SW-NE spreading direction, implying that the Kurile Basin opened along its general strike as a pull-apart basin (Baranov et al., 2002). During the SAKURA expedition we mapped only one segment of it and the question how far the ridge continues to the north and south remained open. Obvious is only that it becomes wider to the north, and it was suggested that the ridge is apparently bounded near the northern slope of the Kurile Basin by a strike-slip or transform fault. On cruise LV29 the mapping of the ridge was therefore continued to the north.

12.3.2.2 Recent study

Six seismic profiles crossing the ridge axis were obtained (*Fig. 12.1*); the ridge shows symmetry on each of them. On the most southern cross-section it consists of a central dome and two adjacent blocks (*Fig. 12.7*). These outwardly tilted blocks are bounded by inward-facing fault scarps. The ridge is getting higher to the north and the central dome becomes more massive. Two symmetrical heights appearing on its top can be interpreted as small volcanic edifices.

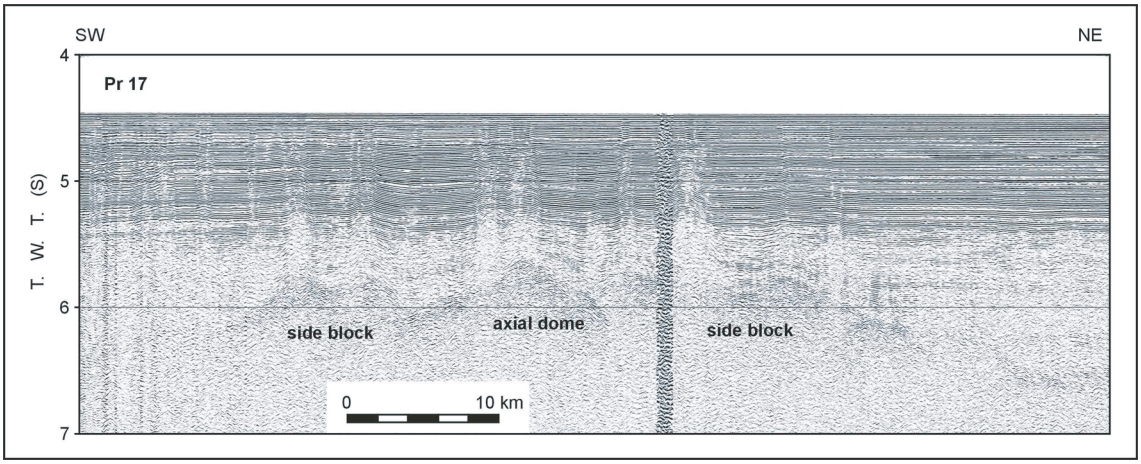

Fig. 12.7: *Part of seismic profile 17 showing the symmetry of Sakura Ridge where on both sides of central dome two blocks are located. Location of the profile is shown in Fig. 12.2.*

At the latitude of ca. 47°30’ the ridge starts to appear at the seafloor as a small gentle swell. Our investigations do not support the suggestion (Gnibidenko et al., 1995) that this swell continues to the south across the whole Kurile Basin. At an approximate latitude of 47°45’ N the ridge goes onto the northern slope of the Kurile Basin or, to be more exact, forms this part of the northern slope. The high mount occupies the central part of the ridge in the northernmost cross-section (*Fig. 12.8*). It has rounded outlines and its altitude equals ca. 1 km. This gives us the opportunity to suggest that this mount is an axial volcano. The NW-SE profile running across this structure shows that its top outcrops on the seafloor. The sedimentary layer covering the ridge on the northern slope is strongly deformed. The character of the deformations is very complex, but some of them are very similar to a wipe-out structure and maybe indicate gas emanations. As seen from *Figure 12.2*, Sakura Ridge tends to be wider and higher to the north as was found before. Therefore, the ridge has wedge-shaped outlines with an acute angle directed to the north. The ridge axis strikes in N-S direction; a very pronounced dextral shift is visible in the central part of the investigation area. This shift is connected with the strike-slip (transform) fault that appears on the axis as a steep SW-WE-striking scarp.

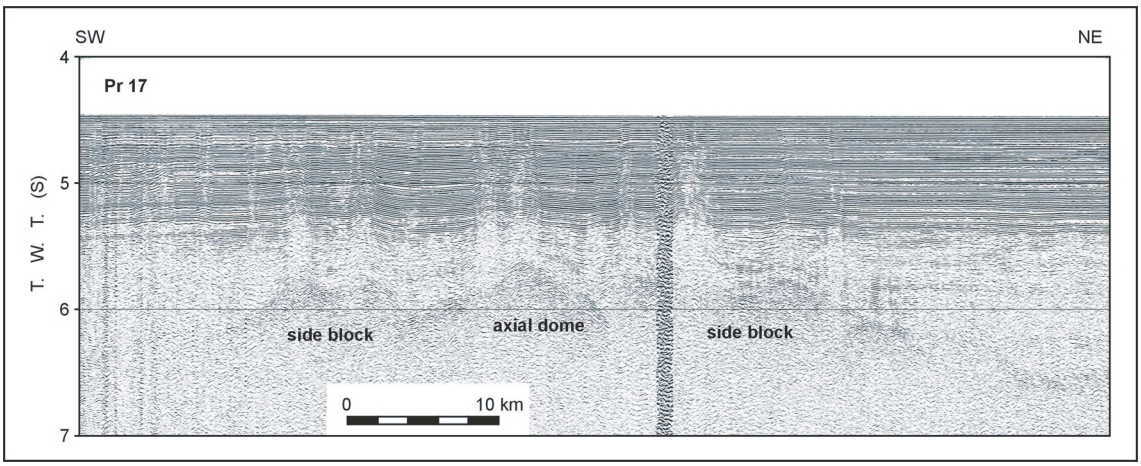

Fig. 12.8: *Large axial volcano located on the northern boundary of the study area as seen on seismic profile 24. Sakura Ridge forms here the northern slope of the Kurile Basin. Location of the profile is shown in Fig. 12.2.*

12.3.2.3 Preliminary conclusions

1. The seismic data allows us to interpret Sakura Ridge as a single structure extending at least up to the middle northern slope of the Kurile Basin (depth ca. 2,300 m). As seen on profiles, the axial zone of this structure represents a high, the dimensions of which increase to the north. Therefore, the axial zone looks like a volcanic dome on the southern cross-sections and on the northern one like a large volcanic edifice (the diameter is about 5 nm and the altitude is approximately 1 km). At least one pair of the blocks bounded by inward-facing fault scarps exists on both sides of the axial zone. This shows a symmetric pattern typical for spreading zones. The symmetry is observed for the small heights on the top of the axial zone, as well. Based on this structural data we can confirm the spreading nature of Sakura Ridge suggested after the SAKURA expedition.
2. There is a change in the morphology of the axial zone with a dimension of ca. 10 nm along the strike of the ridge that suggests the existence of some kind of discontinuities connected with transform faults, the length of magmatic cells and so on. One of such changes occurs in the central part of the ridge where its axis is dextrally shifted indicating on a transform fault.
3. Sakura Ridge has wedge-shaped outlines typical for propagated rifts. From the fact that it propagated from north to south, we can suggest by parity of reasoning with the Japan Sea (Tamaki, 1995) the existence of a large dextral strike-slip zone on the northern slope of the Kurile Basin.
4. There are lots of propagated rifts and spreading ridges, which pass through the ocean basin to the continental margin and further to the continent. Sakura Ridge probably extends from the continental margin to the basin, and in this case the structure of the northern slope of the Kurile Basin is very ambiguous.

13. REFERENCES

Agatova, A.I., Dafner, E.V., Sapozhnikov, V.V. et al., 1996. The trends of distribution of dissolved and particulate organic matter in the Okhotsk Sea. Okeanologiya (Oceanology), 36 (6), 856-864 (in Russian).

Alderman, S.E., 1996. Planktonic foraminifera in the Sea of Okhotsk: population and stable isotope analyses from a sediment trap. Unpublished MS thesis. Massachusettes Institute of Technology. Woods Hole Oceanographic Institution, 88 pp.

Aramaki, T., Watanabe, S., Kuji, T. & Wakatsuchi, M., 2001. The Okhotsk-Pacific seawater exchange in the viewpoint of vertical profiles of radiocarbon around the Bussol' Strait. Geophysical Research Letters, 28, 3971-3974.

Arzhanova, N.V. & Zubarevich, V.L., 1997. The chemical basis of the bioproductivity in the Sea of Okhotsk. Complex studies of ecosistem of the sea of Okhotsk. Moscow: VNIRO Publishing, 86-92 (in Russian).

Asano, K., 1958. The foraminifera from the adjacent seas of Japan, collected by S.S.Soyomary, 1922-1930, Part 4. Buliminidae. Tohoku University, Science Reports, 2nd series (Geology), 28, 1-26.

Asano, K., 1950. Part 2: Buliminidae. In: Stach, I.W. (ed.). Illustrated catalogue of Japanese Teritary smaller foraminifera. Tokio: Hosokawa Printing Co., 14.

Astakhov, A.S., 1986. Late Quaternary sedimentation on the Okhotsk Sea shelf. Vladivostok: Dalnauka, 140 pp. (in Russian).

Astakhov, A., Gorbarenko, S., Tiedemann, R., Wallmann, K. & Volokhin, Yu.G., 2000. Variation of the heavy metals deposition in the Derugin Basin (the Sea of Okhotsk) for the last 25 000 years: evidence of paleoceanological events or fluid venting intensity? Third Workshop on Russian-German Cooperation in the Okhotsk Sea - KOMEX. Program & Abstracts. Moscow, 8-9.

Astakhova, N.V., Lipkina, M.I. & Mel'nichenko, Yu.I., 1987. Hydrothermal barite mineralization in the Derugin Basin of the Okhotsk Sea. Doklady Akademii Nauk SSSR (Talks of the Academy of Science of the USSR), 295 (1), 212-215 (in Russian).

Avdeiko, G.P., Antonov, A.Yu., Volynetz, O.N., Rashidov, V.A., Tsvetkov, A.A., Bondarenko, V.I., Gladkov, N.G., Markov, I.A. & Palueva, A.A., 1992. Submarine volcanism and zonality of the Kurile Island Arc. Moscow: Nauka, 528 pp. (in Russian).

Baranov, B., Werner, R., Hoernle, K., Tsoy, I., Bogaard, P.v.d. & Tararin, I., 2002a. Volcanological, geochemical, paleo-oceanological and geophysical evidence for compressionally-induced high subsidence rates in the Kurile Basin (Okhotsk Sea). Tectonophysics, 350, 63-97.

Baranov, B.V., Wong, H.K., Dozorova, K.A., Karp, B.Ya., Lüdmann, T. & Karnaukh, V., 2002b. Opening geometry of the Kurile Basin (Okhotsk Sea) as inferred from structural data. The Island Arc, August, 2002.

Barash, M.S., Bubenshchikova, N.V., Kazarina, G.Kh., Khusid, T.A., 2001. Paleoceanographic studies in the central part of the Okhotsk sea during the last 200 Kyr (on the basis of micropaleontological data). Okeanologiya (Oceanology), 41 (2), 755-767 (in Russian, English translation).

Basov, I.A., Khusid, T.A., 1983. The living benthic foraminifera and their biomass in sediment of the Okhotsk Sea. Biologiya morya (Biology of the sea), 6, 31-43 (in Russian).

Bely, V.F., 1978. Formations and tectonics of the Okhotsky-Tchukotsky volcanic belt. Moscow: Nauka, 212 pp. (in Russian).

Belyaeva, N.V. & Burmistrova, I.I., 1997. Paleohydrology of Sea of Okhotsk during the last 60 ka. Okeanologiya (Oceanology), 3, 377-385 (in Russian, English translation).

Ben-Yaakov, S., 1973. PH buffering of pore water of recent anoxic marine sediments. Limnol. Oceanogr., 18, 86-94.

Bernhard, J.M., Sen Gupta, B.K. & Borne, P.F., 1997. Benthic foraminiferal proxy to estimate dysoxic bottom-water oxygen concentrations: Santa Barbara Basin, US Pacific continental margin. Journal of foraminiferal Research, 27, p. 301-310.

Bezrukov, P.L., 1957. Bottom sediments of the Okhotsk Sea. Trudy Instituta okeanologii (Proceedings of the Institute of Oceanology), 22, 3-68 (in Russian).

Biebow, N. & Hütten, E. (eds.), 1999. Cruise Reports: KOMEX I and II: RV Professor Gagarinsky cruise 22, RV Akademik M.A. Lavrentyev cruise 28. GEOMAR Report, 82, 188 pp.

Biebow, N., Lüdmann, T., Karp, B. & Kulinich R., 2000. Cruise Reports: KOMEX V and VI: RV Professor Gagarinsky cruise 26, MV Marshal Gelovany cruise 1. GEOMAR Report, 88, 296 pp.

Braitseva, O.A., Melekestsev, I.V., Ponomareva, V.V et al., 1995. Ages of calderas, large explosive craters and active volcanoes in the Kurile-Kamchatka region, Russia. Bull. volcanol., 57, 383-402.

Broecker, W.S., Spencer, D.W., & Craig, H., 1982. Hydrographic data, 1973-1974. In: GEOSECS Pacific Expedition. Natl. Sci. Found, Washington, D.C., 3, 137 pp.

Bruyevich, S.V., 1944. Determination alkalinity of small volumes of sea water by direct titration. In: Instruction of chemical investigation of sea water. Moscow-Leningrad: Glavsevmorput, 83 pp. (in Russian).

Bruyevich, S.V., 1956. Chemistry of the sediments of the Okhotsk Sea. Trudy Instituta okeanologii Akademii Nauk SSSR (Proceedings of the Institute of Oceanology of the Academy of Science of the USSR), 17, 41-132 (in Russian).

Bruyevich, S.V., Bogoyavlensky, A.N. & Mokievskaya, V.V., 1960. Hydrochemical characteristic of the Okhotsk Sea. Trudy Instituta okeanologii Akademii Nauk SSSR (Proceedings of the Institute of Oceanology of the Academy of Science of the USSR), 62, 125-198 (in Russian).

Bruyevich, S.V., Bogoyavlensky, A.N. & Mokievskaya, V.V., 1960. Hydrochemistry of Okhotsk Sea. Trudy Instituta okeanologii AN SSSR (Proceedings of the Institute of Oceanology of the Academy of Science of the USSR), 42 (in Russian).

Bychkov, A.S., Rogachev, K.A., Tishchenko, P.Ya., Pavlova, G.Yu. & Salyuk, A.N., 1996. Hydrochemistry of the Okhotsk Sea: reflection of mesoscale physical processes. Proceedings of the 11th Intern. Symp. on Okhotsk Sea, Mombetsu, Japan, 324-330.

Calvert, S.E. & Pedersen, T.F., 1993. Geochemistry of recent oxic and anoxic marine sediments: implications of the geological record. Mar. Geol, 113, 67-88.

Canfild, D.E., 1989. Sulfate reduction and oxic respiretion in marine sediments: Implication for the organic carbon preservation in euxinic environments. Deep Sea Res. Part A, 36, 121-138.

Cushman, J.A., 1923. The foraminifera of the Atlantic ocean: Part 4 - Lagenidae: U.S. Nat.Mus. Bull., Washington, D.C., U.S.A, 1923, 104, 166.

Dean, W.E. & Gardner, J.V., 1982. Origin and geochemistry of redox cycles of Jurassic to Eocene ago, Cape Verde Basin (DSDP Site 367) continental margin of northwest Africa. In: Nature and Origin of Cretaceous Carbon-rich Facies. Academic, San Diego, Calif., 55-78.

Dean, W.E., Gardner, J.V., Jansa, L.F., Cerek, P. & Seibold E., 1978. Cyclic sedimentation along the continental margin of Northwest Africa. Initial Rep. Deep Sea Drill. Proj., 41, 965-986.

Derkachev, A.N., Bohrmann, G. & Greinert, J., 1999. Mineralogical and morphological types of authigenic precipitates from Derugin Basin sediments. Second Workshop on Russian-German Cooperation in the Okhotsk Sea – Kurile Island Arc System KOMEX. Program and Abstracts, Kiel, 31-32.

Derkachev, A.N., Tararin, I.A., Lelikov, E.P., Mozherovsky, A.V., Greinert, J. & Barinov, N.N., 2002. Manifestation of low-temperature hydrothermal activity in the backarc basin,

Okhotsk Sea (Kurile deep-sea basin). Tikhookeanskaya geologiya (Pacific geology), 21 (3), 14-26 (in Russian).

Dudarev, O.V., Botsul, A.I., Anikiev, V.V. et al., 2000. Modern sedimentation within Amur River estuary. Pacific oceanology, 19 (3), 30-43 (in Russian).

Emel'yanova, T.A., Kornev, O.S., Lelikov, E.P. et al., 2001. Composition and radioisotopic age of volcanic rocks from the floor of Okhotsk Sea. Vladivostok, POI RAS, 44 pp. (in Russian).

Emery, D. & Myers, K.J., 1996. Sequence Stratigraphy. Oxford: Blackwell Science Ltd., 297 pp.

Fairbanks, R.G., 1989. A 17,000 years glacio-eustatic sea level record: influence of glacial melting rates on the Younger Dryas event and deep-ocean circulation. Nature, 342, 637-642.

Felitsin, S.B. & Kir'yanov, V.Yu., 1987. Area variation of tephra composition from some volcanic eruptions on the basis of gross silicate analysis data. Volcanology and seismology, 1, 3-14 (in Russian).

Feyling-Hanssen, R.W., Jorgensen, J.A., Knudsen, K.L. & Andersen, A-L.L., 1971. Late Quaternary foraminifera from Vendsyssel, Denmark and sandnes, Norway. Bull. Geol. Soc. Denm., 21, (2-3), Copenhagen, 317 p.

Freeland, H.J., Bychkov, A.S., Whitney, F., Taylor, C., Wong, C.S. & Yurasov, G.I., 1998. WOCE section P1W in the Sea of Okhotsk. 1. Oceanographic description. J. of Geoph. Res. 1998, 103 (C8), 15613-15623.

Fursenko, A.V., Troitskaya, T.S., Levtchuk, L.K., et al., 1979. Foraminifery dal`nevostochnykh moryey SSSR (Foraminifera of the Far East seas of the USSR). Novosibirsk: Nauka, 287 pp. + 54 pls. (in Russian).

Gnibidenko, G.S., 1985. The Okhotsk Sea - Kurile Island ridge and Kurile-Kamchatka trench. In: Nairn, A.E.M., Stehli, F.G. & Uyeda, S. The Ocean Basin and Margins, Vol. 7A, Plenum Press, 377-418.

Gnibidenko, G.S., Hilde, T.W.C., Gretskaya, E.V. & Andreev, A.A., 1995. Kurile (South Okhotsk) Backarc Basin. In: Taylor, B. (ed.). Backarc Basins: Tectonics and Magmatism, New York: Plenum Press, 1995, 421-448.

Gorbarenko, S.A., 1991. The Stratigraphy of the Upper Quaternary sediments in the central part of the Sea of Okhotsk and its paleooceanography according to data obtained by the $\delta^{18}O$ and other methods. Okeanologiya (Oceanology), 6, 761-765 (in Russian, English translation).

Gorbarenko S.A., 1996. Stable isotope and lithologic evidence of Late Glacial and Holocene oceanography of the Northwestern Pacific and its marginal seas. Quaternary Research, 46, 230-250.

Gorbarenko, S.A., Chekhovskaya, M.P. & Southon, J.R., 1998. Detailed environmental changes of the Sea of Okhotsk Central part during the last glaciation-Holocene. Oceanology, 38 (2), 277-280 (translated from Okeanologiya, 38 (2), 305-308).

Gorbarenko, S.A., Derkachev, A.N., Astakhov, A.S., Southon, J.R., Nuernberg, D. & Shapovalov-Chuprynin, V.V., 2000. Lithostratigraphy and tephrochronology of the Upper Quaternary deposits in the Sea of Okhotsk. Tikhookeanskaya geologiya (Pacific geology), 19, 58-72 (in Russian).

Gorbarenko, SA., Nürnberg, D., Derkachev, A.N., Astakhov, AS., Souton, J.R & Kaiser, A., 2002. Magnetostratigraphy and tephrochronology of the Upper Quaternary sediments in the Okhotsk Sea: implication of terrigenous, volcanogenic and biogenic matter supply. Marine Geology, 183 (1-4), 107-129.

Habib, D., 1982. Sedimentary supply origin of Cretaceous black shales. In: Schlander, S.O. & Cita, M.B. (eds.). Nature and Origin of Cretaceous Carbon-rich Facies. Academic, San Diego, Calif., 113-127.

Haug, G.H., Maslin, M.A., Sarnthein, M., Stax, R. & Tiedemann, R., 1995. Evolution of northwestern Pacific sedimentation patterns since 6 MA (site 882) In: Rea, D.K., Basov, I.A., Scholl, D.W. & Allan, J. F. (eds.). Proceeding of the Ocean Drilling Program, Scientific Results Vol. 145, 293-314.

Hemleben, C., Splinder, M. & Anderson, O.R., 1988. Modern Planktonic Foraminifera. New York: Springer-Verlag Ed., 327 pp.

Holler, P., 1995. Arbeitsmethoden der marinen Geowissenschaften, Stuttgart: Enke.

Jannink, N.T., Van der Zwaan, G.J. & Zachariasse, W.J., 1998. Living (Rose Bengal stained) foraminifera from an upwelling environment: the continental margin south of Karachi, Arabian sea. Deep-Sea Res. I ,145, 1483-1513.

Jansa, L.F., Enos, P., Tucholke, B.E., Gradstein, F.M. & Sheridan, R.E., 1979. Mesozoic-Cenozoic sedimentary formations of the North Atlantic Basin; western North Atlantic. In: Deep drilling results in the Atlantic ocean: Continental margins and Paleoenvironments. Maurice Ewing Ser., 3, AGU, Washington, D.C., 1-57.

Johnson, K.M., King, A.E. & Sieburth, J.M., 1985. Coulometric TCO_2 analysis for marine studies: an introduction. Mar. Chem., 16, 61-82.

Jung, K.K., 1988. Morphology and taxonomy of Late Cenozoic uvigerine foraminifera from Japan: Tohoku University, Science Reports, 2nd series (Geology) 59, 99-175.

Kir'yanov, V.Yu. & Solovyeva, N.A., 1990. The changes of volcanic ash matter composition as a result of gravitational eolian differentiation. Volcanology and seismology, 4, 10-19 (in Russian).

Kristensen, E. & Blackburn, T.H., 1987. The fate of organic carbon and nitrogen in experimental marine sediment system: Influence of bioturbation and anoxia. J. Mar. Res., 45, 231-257.

Lipps, J.Y. & Warme, J.E., 1966. Planktonic foraminiferal biofacies in the Okhotsk Sea. Contrib. Cush. Found. Foram. Research, XVII, Part 4, 125-134.

Loeblich, A.R., Tappan, H., 1953. Studies of Arctic Foraminifera: Smithsonian Miscellaneous Collections, 121 (7), 151 p.

Loubere, P., Meyers, P. & Gary, A., 1995. Benthic foraminiferal microhabitat selection, carbon isotope values, and association with larger animals: a test with Uvigerina peregrina. Journal of Foraminiferal Research, 25 (1), 83-95.

Lüdmann, T., Baranov, B. & Karp, B. (eds.), 2002. Cruise Reports: KOMEX VII. RV Professor Gagarinsky Cruise 32, SERENADE. Seismo-stratigraphic research of northern Sakhalin and in Derugin Basin. GEOMAR Report, 105, Kiel, 42 pp.

Lutze, G. & Altenbach, A., 1991. Technik und Signifikanz der Lebendfärbung benthischer Foraminiferen mit Bengalrot, Geol. Jb, A128, 251-265.

Machida, H., 1999. The stratigraphy, chronology and distribution of distal marker-tephras in and around Japan. Global and Planet. Change, 71-94.

Mackensen, A., Schmiedel, G., Harloff, J. & Giesse, M., 1995. Deep-sea foraminifera in the South Atlantic Ocean: Ecology and assemblages generation. Micropaleontology, 41 (4), 342-358.

McManus, D.A., 1975. Modern versus relict sediment on the continental shelf. Geol. Soc. Amer. Bull., 86 (8), 1154-1160.

Melekestsev, I.V., Volynes, O.N. & Antonov, A.Yu., 1997. Nemo III caldera, Onekotan Island, Northern Kuriles: structure, C^{14} dating, time history of the caldera-generating eruption and the evolution of juvenile products. Volcanology and seismology, 1, 32-51 (in Russian).

Moroshkin, K.V., 1966. Water masses of the Okhotsk Sea. Moscow: Nauka, 66 pp. (in Russian).

Nürnberg, D., Baranov, B.V. & Karp, B.Ya. (eds.), 1997. RV Akademik M.A. Lavrentyev cruise 27 – Cruise Report GREGORY, GEOMAR Report, 60, 69 pp.

Obzhirov, A.I., 1993. Gas and geochemical fields of the benthic layer of seas and oceans. Moscow: Nauka, 131 pp. (in Russian).

Payton, C.E., 1977. Seismic Stratigraphy – Application to Hydrocarbon Exploration. AAPG, Memoir 26, 516 pp.

Pedersen, T.F. & Calvert, S.E., 1990. Anoxia vs. Productivity: what controls the formation of organic-carbon-rich sediments and sedimentary rocks. AAPG Bull., 74, 454-466.

Powers, M.C., 1982. Comparison chart for estimating roundness and sphericity. AGI data sheet 18, American Geological Institute.

Sachs, I.S., Suyehiro, K., Acton, G.D. & Shipboard Scientific Party**,** 2., 2000. Explanatory Notes, In: Proceedings of the Ocean Drilling Programme, Initial reports, 186.

Saidova, Kh.M., 1961. Ecology of foraminifera and paleogeography of the USSR Far Eastern Seas and the northwestern Pacific. Moscow: Nauka, 221 pp. (in Russian).

Saidova, Kh.M., 1975. Benthic foraminifera of the Pacific ocean. Academy of Science of the USSR, P.P. Shirshov Instintute of Oceanology, Moscow, part I-III, 631 pp. (in Russian).

Saidova, Kh.M., 1997. Deep-sea foraminiferal communities of the Bering and Okhotsk seas. Okeanologiya (Oceanology), 1, 105-112 (in Russian, English translation).

Salyuk, A.N., Winckler, G., Sosnin, V.A., 2001. Renewal of the bottom waters in the Okhotsk Sea. In: Danchenkov, M.A. (ed.). Oceanography of the Japan Sea. Proceeding of CREAMS 2000 Intern. Symp. Vladivostok: Dalnauka, 226-229 (in Russian).

Sapozhnikov, V.V., Gruzevich, A.K., Arzhanova, N.V., Naletova, I.A., Zubarevich, V.L. & Sapozhnikov, M.,V., 1999. Principal features of the spatial distribution of organic and inorganic nutrient compounds in the Sea of Okhotsk. Okeanologiya (Oceanology), 39 (2), 198-204 (in Russian, English translation).

Sen Gupta, B.K. & Machain-Castillo, M.L., 1993. Benthic foraminifera in oxygen-poor habitats. Mar. Micropaleontology 20, 183-201.

Scott, D.B., Takayanagi, Y., Hasegawa, S., Saito, T., 2000. Illustration and reevaluation of affinities of Neogene foraminifera described from Japan: Paleontologia Electronica 3 (2), 41 pp., 1.06 MB; http://palaeo-electronica.org/2000-2/foram/issue2_00.htm.

Shchedrina, Z.G., 1958. Foraminiferal fauna off Southern Sakhalin and Kurile Islands. Issled. Dalnev. Moryey SSSR (Investigations of the Far Eastern seas of the USSR), 5 (1), 5-41 (in Russian).

Shepard, F.S., 1954. Nomenclature based on Sand-Silt-Clay ratios. Journ. Sed. Petrol., 24, 151-158.

Tamaki, K., 1995. Opening Tectonics of the Japan Sea. In: Taylor, B. (ed.). Backarc Basins: Tectonics and Magmatism. New York: Plenum Press, 1995, 407-420.

Tiedemann, R. et al., 2001. Abschlussbericht zum KOMEX-Teilprojekt 5: Stratigraphie, CO_2-Kreislauf, Paläo-Ozeanologie und Produktivität im Ochotskischen Meer. In: Suess, E. et al. (eds.). KOMEX - Abschlussbericht zum BMBF-Vorhaben 03G0535A. Kiel, Heidelberg, Bremerhaven, Hamburg, Mai 2001.

Tishchenko, P.Ya., Pavlova, G.Yu., Salyuk, A.N. & Bychkov, A.S., 1998. Carbonate system and dissolved oxygen in the Japan Sea. Estimation of biological and thermal terms. Okeanologiya (Oceanology), 38 (5), 678-684 (in Russian).

Tishchenko, P.Ya., Wong, C.S., Pavlova, G.Yu., Johnson, W.K., Kang, D.-J. & Kim, K.-R., 2001. pH measurements of sea water by means of cell without liquid junction. Okeanologiya (Oceanology), 41 (6), 849-859 (in Russian).

Tsunogai, S., Niskimura, M. & Nakaya, S., 1968. Complexometric titration of calcium in the presence of larger amounts of magnesium. Talanta, 15, 385-390.

Werner, R., Tararin, I.A., Hoernle, K. & Lelikov, E.P., submitted. Petrology and geochemistry of submarine volcanism from the northeastern part of the Kurile Basin: Evidence for interaction of basic magma with continental crust. Gondwana Research (Special Issue).

Wong, C.S., Matear, R.J., Freeland, H.J., Whitney, F.A. & Bychkov, A.S., 1998. WOCE line P1W in the Sea of Okhotsk 2. CFCs and the formation rate of intermediate water, J. Geophys. Res., 103, 15625-15642.

Wortmann, U.G., Hesse, R. & Zacher, W., 1999. Major element analysis of cyclic black shales: Paleoceanographic implications for the Early Cretaceous deep western Tethys. Paleoceanography, 14 (4), 525-541.

Zaretskaia, N.E., Ponomareva, V.V., Sulerzhitsky, L.D. et al., 2001. Radiocarbon dating of the Kurile Lake caldera eruption (South Kamchatka, Russia). Geochronometriya (Geochronometry), 20, 95-102.

Zhuravlev, A.V., 1982. Geological structure and development of the South Okhotsk (Kurile) Basin. In: Tuezov, I.K. (ed.). Structure and Composition of the Sedimentary Cover of the Northwestern Pacific. Vladivostok: Far East Scientific Center, 23-33 (in Russian).

GEOMAR REPORTS

1 GEOMAR FORSCHUNGSZENTRUM FÜR MARINE GEOWISSENSCHFTEN DER CHRISTIAN-ALBRECHTS-UNIVERSITÄT ZU KIEL. BERICHT FÜR DIE JAHRE 1987 UND 1988. 1989. 71 + 6 pp. In German

2 GEOMAR FORSCHUNGSZENTRUM FÜR MARINE GEOWISSENSCHAFTEN DER CHRISTIAN-ALBRECHTS-UNIVERSITÄT ZU KIEL. JAHRESBERICHT/ANNUAL REPORT 1989. 1990. 96 pp. In German and English

3 GEOMAR FORSCHUNGSZENTRUM FÜR MARINE GEOWISSENSCHAFTEN DER CHRISTIAN-ALBRECHTS-UNIVERSITÄT ZU KIEL. JAHRESBERICHT/ANNUAL REPORT 1990. 1991. 212 pp. In German and English

4 ROBERT F. SPIELHAGEN
DIE EISDRIFT IN DER FRAMSTRASSE WÄHREND DER LETZTEN 200.000 JAHRE. 1991. 133 pp.
In German with English summary

5 THOMAS C. W. WOLF
PALÄO-OZEANOGRAPHISCH-KLIMATISCHE ENTWICKLUNG DES NÖRDLICHEN NORDATLANTIKS SEIT DEM SPÄTEN NEOGEN (ODP LEGS 105 UND 104, DSDP LEG 81). 1991. 92 pp. In German with English summary

6 SEISMIC STUDIES OF LATERALLY HETEROGENOUS STRUCTURES – INTERPRETATION AND MODELLING OF SEISMIC DATA. Ed. by ERNST R. FLUEH
Commission on Controlled Source Seismology (CCSS), Proceedings of the 8th Workshop Meeting, held at Kiel – Fellhorst (Germany), August 27-31, 1990. 1991. 359 pp. In English

7 JENS MATTHIESSEN
DINOFLAGELLATEN-ZYSTEN IM SPÄQUARTÄR DES EUROPÄISCHEN NORDMEERES: PALÖKOLOGIE UND PALÄO-OZEANOGRAPHIE. 1991. 104 pp. In German with English summary. Out of print

8 DIRK NÜRNGERG
HAUPT- UND SPURENELEMENTE IN FORAMINIFERENGEHÄUSEN – HINWEISE AUF KLIMATISCHE UND OZEANOGRAPHISCHE ÄNDERUNGEN IM NÖRDLICHEN NORDATLANTIK WÄHREND DES SPÄTQUARTÄRS.
1991. 117 pp. In German with English summary. Out of print

9 KLAS S. LACKSCHEWITZ
SEDIMENTATIONSPROZESSE AM AKTIVEN MITTELOZEANISCHEN KOLBEINSEY RÜCKEN (NÖRDLICH VON ISLAND). 1991. 133 pp. In German with English summary. Out of print

10 UWE PAGELS
SEDIMENTOLOGISCHE UNTERSUCHUNGEN UND BESTIMMUNG DER KARBONATLÖSUNG IN SPÄTQUARTÄREN SEDIMENTEN DES ÖSTLICHEN ARKTISCHEN OZEANS. 1991. 106 pp.
In German with English summary

11 FS POSEIDON. EXPEDITION 175 (9.10.-1.11.1990)
175/1:OSTGRÖNLÄNDISCHER KONTINENTALRAND (65°N)
175/2: SEDIMENTATION AM KOLBEINSEYRÜCKEN (NÖRDLICH VON ISLAND).
Hrsg. von J. MIENERT und H.-J. WALLRABE-ADAMS. 1992. 56 pp. + app. In German with some English chapters

12 GEOMAR FORSCHUNGSZENTRUM FÜR MARINE GEOWISSENSCHAFTEN DER CHRISTIAN-ALBRECHTS-UNIVERSITÄT ZU KIEL. JAHRESBERICHT/ANNUAL REPORT 1991. 1992. 152 pp. In German and English.
Out of print

13 SABINE E. I. KÖHLER
SPÄTQUARTÄRE PALÄO-OZEANOGRAPHISCHE ENTWICKLUNG DES NORDPOLARMEERES UND EUROPÄISCHEN NORDMEERES ANHAND VON SAUERSTOFF- UND KOHLENSTOFF-ISOTOPENVERHÄLTNISSEN DER PLANKTISCHEN FORAMINIFERE *Neogloboquadrina pachyderma* (sin.).
1992. 104 pp. In German with English summary

14 FS SONNE. FAHRTBERICHT SO78 PERUVENT: BALBOA, PANAMA - BALBOA, PANAMA, 28.2.1992-16.4.1992
Hrsg. von ERWIN SUESS. 1992. 120 pp. In German with some English chapters. Out of print

15 FOURTH INTERNATIONAL CONFERENCE ON PALEOCEANOGRAPHY (ICP IV): SHORT- AND LONG-TERM GLOBAL CHANGE: RECORDS AND MODELLING. 21-25 SEPTEMBER 1992, KIEL/GERMANY.
PROGRAM & ABSTRACTS. 1992. 351 pp. In English

16 MICHAELA KUBISCH
DIE EISDRIFT IM ARKTISCHEN OZEAN WÄHREND DER LETZTEN 250.000 JAHRE. 1992. 100 pp.
In German with English summary

17 PERSISCHER GOLF: UMWELTGEFÄHRDUNG, SCHADENSERKENNUNG, SCHADENSBEWERTUNG AM BEISPIEL DES MEERRESBODENS; ERKENNEN EINER ÖKOSYSTEMVERÄNDERUNG NACH ÖLEINTRÄGEN.
Schlußbericht zu den beiden BMFT-Forschungsvorhaben 03F0055 A + B. 1993. 108 pp. In German with English summary

18 TEKTONISCHE ENTWÄSSERUNG AN KONVERGENTEN PLATTENRÄNDERN / DEWATERING AT CONTINENTAL MARGINS. Hrsg. von/ed. by ERWIN SUESS. 1993. 196 + 32 + 68 + 16 + 22 + 38 + 4 + 19 pp.
Some chapters in English, some in German

19 THOMAS DICKMANN
DAS KONZEPT DER POLARISATIONSMETHODE UND SEINE ANWENDUNGEN AUF DAS SEIMISCHE VEKTORWELLENFELD IM WEITWINKELBEREICH. 1993. 121 pp. In German with English summary

20 GEOMAR FORSCHUNGSZENTRUM FÜR MARINE GEOWISSENSCHAFTEN DER CHRISTIAN-ALBRECHTS-UNIVERSITÄT ZU KIEL. JAHRESBERICHT/ANNUAL REPORT 1992. 1993. 139 pp. In German and English

21 KAI UWE SCHMIDT
PALYNOMORPHE IM NEOGENEN NORDATLANTIK - HINWEISE ZUR PALÄO-OZEANOGRAPHIE UND PALÄOKLIMATOLOGIE. 1993. 104 + 7 + 41 pp. In German with English summary

22 UWE JÜRGEN GRÜTZMACHER
DIE VERÄNDERUNGEN DER PALÄOGEOGRAPHISCHEN VERBREITUNG VON *Bolboforma* - EIN BEITRAG ZUR REKONSTRUKTION UND DEFINITION VON WASSERMASSEN IM TERTÄR. 1993. 104 pp.
In German with English summary

23 RV PROFESSOR LOGACHEV. Research Cruise 09 (August 30 - September 17, 1993): SEDIMENT DISTRIBUTION ON THE REYKJANES RIDGE NEAR 59°N. Ed. by H.-J. WALLRABE-ADAMS & K.S. LACKSCHEWITZ. 1993. 66 + 30 pp.
In English

24 ANDREAS DETTMER
DIATOMEEN-TAPHOZÖNOSEN ALS ANZEIGER PALÄO-OZEANOGRAPHISCHER ENTWICKLUNGEN IM PLIOZÄNEN UND QUARTÄREN NORDATLANTIK. 1993. 113 + 10 + 25 pp. In German with English summary

25 GEOMAR FORSCHUNGSZENTRUM FÜR MARINE GEOWISSENSCHAFTEN DER CHRISTIAN-ALBRECHTS-UNIVERSITÄT ZU KIEL. JAHRESBERICHT/ANNUAL REPORT 1993. 1994. 69 pp. In German and English

26 JÖRG BIALAS
SEISMISCHE MESSUNGEN UND WEITERE GEOPHYSIKALISCHE UNTERSUCHUNGEN AM SÜD-SHETLAND TRENCH UND IN DER BRANSFIELD STRASSE - ANTARKTISCHE HALBINSEL. 1994. 113 pp.
In German with English summary

27 JANET MARGARET SUMNER
THE TRANSPORT AND DEPOSITIONAL MECHANISM OF HIGH GRADE MIXED-MAGMA IGNIMBRITE TL, GRAN CANARIA: THE MORPHOLOGY OF A LAVA-LIKE FLOW. 1994. 224 pp. In English with German summary. Out of print

28 GEOMAR LITHOTHEK. Ed. by JÜRGEN MIENERT. 1994. 12 pp + app. In English. Out of print

29 FS SONNE. FAHRTBERICHT SO 97 KODIAK-VENT: KODIAK - DUTCH HARBOR - TOKYO - SINGAPUR, 27.7.-19.9.1994. Hrsg. von ERWIN SUESS. 1994. Some chapters in English, some in German. Out of print

30 CRUISE REPORTS:
RV LIVONIA CRUISE 92, KIEL-KIEL, 21.8.-17.9.1992: GLORIA STUDIES OF THE EAST GREENLAND CONTINENTAL MARGIN BETWEEN 70°AND 80°N
RV POSEIDON PO200/10, LISBON-BREST-BREMERHAVEN, 7.-23.8.1993: EUROPEAN NORTH ATLANTIC MARGIN: SEDIMENT PATHWAYS, PROCESSES AND FLUXES
RV AKADEMIK ALEKSANDR KARPINSKIY, KIEL-TROMSÖ, 5.-25.7.1994: GAS HYDRATES ON THE NORTHERN EUROPEAN CONTINENTAL MARGIN
Edited by JÜRGEN MIENERT. 1994. 186 pp.
In English; report of RV AKADEMIK ALEKSANDR KARPINSKIY cruise in English and Russian

31 MARTIN WEINELT
BECKENENTWICKLUNG DES NÖRDLICHEN WIKING-GRABENS IM KÄNOZOIKUM - VERSENKUNGSGESCHICHTE, SEQUENZSTRATIGRAPHIE, SEDIMENTZUSAMMENSETZUNG. 1994. 85 pp.
In German with English summary

32 GEORG A. HEISS
CORAL REEFS IN THE RED SEA: GROWTH, PRODUCTION AND STABLE ISOTOPES. 1994. 141 pp.
In English with German summary

33 JENS A. HÖLEMANN
AKKUMULATION VON AUTOCHTHONEM UND ALLOCHTHONEM ORGANISCHEM MATERIAL IN DEN KÄNOZOISCHEN SEDIMENTEN DER NORWEGISCHEN SEE (ODP LEG 104). 1994. 78 pp.
In German with English summary

34 CHRISTIAN HASS
SEDIMENTOLOGISCHE UND MIKROPALÄONTOLOGISCHE UNTERSUCHUNGEN ZUR ENTWICKLUNG DES SKAGERRAKS (NE NORDSEE) IM SPÄTHOLOZÄN. 1994. 115 pp. In German with English summary

35 BRITTA JÜNGER
TIEFENWASSERERNEUERUNG IN DER GRÖNLANDSEE WÄHREND DER LETZTEN 340.000 JAHRE / DEEP WATER RENEWAL IN THE GREENLAND SEA DURING THE PAST 340,000 YEARS. 1994. 6 + 109 pp.
In German with English summary

36 JÖRG KUNERT
UNTERSUCHUJNGEN ZU MASSEN- UND FLUIDTRANSPORT ANHAND DER BEARBEITUNG REFLEXIONSSEISMISCHER DATEN AUS DER KODIAK-SUBDUKTIONSZONE, ALASKA. 1995. 129 pp.
In German with English summary

37 CHARLOTTE M. KRAWCZYK
DETACHMENT TECTONICS DURING CONTINENTAL RIFTING OFF THE WEST IBERIA MARGIN: SEISMIC REFLECTION AND DRILLING CONSTRAINTS.1995. 133 pp. In English with German summary

38 CHRISTINE CAROLINE NÜRNBERG
BARIUMFLUSS UND SEDIMENTATION IM SÜDLICHEN SÜDATLANTIK - HINWEISE AUF PRODUKTIVITÄTSÄNDERUNGEN IM QUARTÄR. 1995. 6 + 108 pp. In German with English summary

39 JÜRGEN FRÜHN
TEKTONIK UND ENTWÄSSERUNG DES AKTIVEN KONTINENTALRANDES SÜDÖSTLICH DER KENAI-HALBINSEL, ALASKA. 1995. 93 pp. In German with English summary

40 GEOMAR FORSCHUNGSZENTRUM FÜR MARINE GEOWISSENSCHAFTEN DER CHRISTIAN-ALBRECHTS-UNIVERSITÄT ZU KIEL. JAHRESBERICHT/ANNUAL REPORT 1994. 1995. 125 pp. In German and English.
Out of print

41 FS SONNE. FAHRTBERICHT / CRUISE REPORT SO 103 CONDOR 1 B: VALPARAISO-VALPARAISO, 2-21.7.1995. Hrsg. von ERNST R. FLUEH. 1995. 140 pp. Some chapters in German, some in English

42 RV PROFESSOR BOGOROV CRUISE 37: CRUISE REPORT "POSETIV": VLADIVOSTOK-VLADIVOSTOK, September 23 - October 22, 1994. Edited by CHRISTOPH GAEDICKE, BORIS BARANOV, and EVGENY LELIKOV. 1995. 49 + 33 pp. In English

43 CHRISTOPH GAEDICKE
DEFORMATION VON SEDIMENTEN IM NANKAI-AKKRETIONSKEIL, JAPAN. BILANZIERUNG TEKTONISCHER VORGÄNGE ANHAND VON SEISMISCHEN PROFILEN UND ERGEBNISSEN DER ODP-BOHRUNG 808. II + 89 pp. In German with English summary

44 MARTIN ANTONOW
SEDIMENTATIONSMUSTER UM DEN VESTERIS SEAMOUNT (ZENTRALE GRÖNLANDSEE) IN DEN LETZTEN 250.000 JAHREN. 1995. 121 pp. In German with English summary

45 INTERNATIONAL CONGRESS: CORING FOR GLOBAL CHANGE - ICGC '95. KIEL, 28 - 30 June, 1995.
Edited by JÜRGEN MIENERT and GEROLD WEFER. 1996. 83 pp. In English

46 JENS GRÜTZNER
ZUR PHYSIKALISCHEN ENTWICKLUNG VON DIAGENETISCHEN HORIZONTEN IN DEN SEDIMENTBECKEN DES ATLANTIKS. 1995. 96 pp. In German with English summary

47 INGO A. PECHER
SEISMIC STUDIES OF BOTTOM SIMULATING REFLECTORS AT THE CONVERGENT MARGINS OFFSHORE PERU AND COSTA RICA. 1996. 159 pp. In English with German summary

48 XIN SU
DEVELOPMENT OF LATE TERTIARY AND QUATERNARY COCCOLITH ASSEMBLAGES IN THE NORTHEAST ATLANTIC. 1996. 120 pp. +7 pl. In English with German summary

49 FS SONNE - FAHRTBERICHT/CRUISE REPORT SO108 ORWELL: SAN FRANCISCO - ASTORIA, 14.4. - 23.5.1996
Edited by ERNST R. FLUEH and MICHAEL A. FISHER. 1996. 252 pp. + app. In English with German summary

50 GEOMAR FORSCHUNGSZENTRUM FÜR MARINE GEOWISSENSCHAFTEN DER CHRISTIAN-ALBRECHTS-UNIVERSITÄT ZU KIEL. JAHRESBERICHT/ANNUAL REPORT 1995. 1996. 93 pp. In German and English

51 THOMAS FUNCK
STRUCTURE OF THE VOLCANIC APRON NORTH OF GRAN CANARIA DEDUCED FOM REFLECTION SEISMIC, BATHYMETRIC AND BOREHOLE DATA. 1996.VI, 144 pp. In English with German summary

52 PETER BRUNS
GEOCHEMISCHE UND SEDIMENTOLOGISCHE UNTERSUCHUNGEN ÜBER DAS SEDIMENTATIONSVERHALTEN IM BEREICH BIOSTRATIGRAPHISCHER DISKONTINUITÄTEN IM NEOGEN DES NORDATLANTIK, ODP LEG 104, SITES 642B UND 643A. 1996. V, 73 pp. In German with Englllish summary

53 CHRISTIANE C. WAGNER
COLD SEEPS AN KONVERGENTEN PLATTENRÄNDERN VOR OREGON UND PERU: BIOGEOCHEMISCHE BESTANDSAUFNAHME. 1996. 108, XXXVI pp. In German with English summary

54 FRAUKE KLINGELHÖFER
MODEL CALCULATIONS ON THE SPREADING OF SUBMARINE LAVA FLOWS. 1996. 98 pp.
In English with German summary

55 HANS-JÜRGEN HOFFMANN
OBJEKTORIENTIERTE ANALYSE UND MIGRATION DIFFRAKTIERTER WELLENFELDER UNTER VERWENDUNG DER STRAHLENMETHODE UND DER EDGE-WAVE-THEORIE. 1996. XXI, 153 pp. In German with English summary

56 DIRK KLÄSCHEN
STRAHLENSEISMISCHE MODELLIERUNG UNTER BERÜCKSICHTGUNG VON MEHRFACHDIFFRAKTIONEN MIT HILFE DER EDGE-WAVES: THEORIE UND ANWENDUNGSBEISPIELE 1996. X, 159 pp.
In German with English summary

57 NICOLE BIEBOW
DINOFLAGELLATENZYSTEN ALS INIKATOREN DER SPÄT- UND POSTGLAZIALEN ENTWICKLUNG DES AUFTRIEBSGESCHEHENS VOR PERU. 1996. IV, 100, 17, 14 (7 pl.) pp. In German with English summary

58 RV SONNE. CRUISE REPORT SO109: HYDROTRACE ASTORIA-VICTORIA-ASTORIA-VICTORIA. MAY 23 - JULY 8, 1996. Ed. by PETER HERZIG, ERWIN SUESS, and PETER LINKE. 1997. 249 pp. In English

59 RV SONNE. CRUISE REPORT SO110: SO - RO (SONNE - ROPOS). VICTORIA-KODIAK-VICTORIA. JULY 9 - AUGUST 19, 1996. Ed. by ERWIN SUESS and GERHARD BOHRMANN. 1997. 181 pp. In English

60 RV AKADEMIK M. A. LAVRENTYEV CRUISE 27. CRUISE REPORT: GREGORY. VLADIVOSTOK-PUSAN-OKHOTSK SEA-PUSAN-VLADIVOSTOK. SEPTEMBER 7 - OCTOBER 12, 1996.
Ed. by DIRK NÜRNBERG, BORIS BARANOV, and BORIS KARP.1997. 143 pp. In English

61 GEOMAR FORSCHUNGSZENTRUM FÜR MARINE GEOWISSENSCHAFTEN DER CHRISTIAN-ALBRECHTS-UNIVERSITÄT ZU KIEL. JAHRESBERICHT / ANNUAL REPORT 1996. 1997. 169 pp.
In German and English

62 FS SONNE. FAHRTBERICHT/CRUISE REPORT SO123: MAMUT (MAKRAN MURRAY TRAVERSE - GEOPHYSIK PLATTENTEKTONISCHER EXTREMFÄLLE). Maskat - Maskat, 07.09 - 03.10.1997. Ed. by ERNST R. FLUEH, NINA KUKOWSKI, and CHRISTIAN REICHERT. 1997. 292 pp. In English with German summary

63 RAINER ZAHN
NORTH ATLANTIC THERMOHALINE CIRCULATION DURING THE LAST GLACIAL PERIOD: EVIDENCE FOR COUPLING BETWEEN MELTWATER EVENTS AND CONVECTIVE INSTABILITY. 1997. 133 pp. In English

64 FS SONNE. FAHRTBERICHT/CRUISE REPORT SO112 HIRESBAT (HIGH RESOLUTION BATHYMETRY). Victoria, B.C., Canada - Apra Harbor, Guam. 17.09 - 08.10.1996. Hrsg. von WILHELM WEINREBE. 1997. 90 pp.
Some chapters in German, some in English

65 NIELS NØRGAARD-PEDERSEN
LATE QUATERNARY ARCTIC OCEAN SEDIMENT RECORDS: SURFACE OCEAN CONDITIONS AND PROVENANCE OF ICE-RAFTED DEBRIS. 1997. 115 pp. In English with German summary

66 THOMAS NÄHR
AUTHIGENER KLINOPTILOLITH IN MARINEN SEDIMENTEN - MINERALCHEMIE, GENESE UND MÖGLICHE ANWENDUNG ALS GEOTHERMOMETER. 1997. 119, 43 pp. In German with English summary

67 MATTIAS KREUTZ
STOFFTRANSPORT DURCH DIE BODENGRENZSCHICHT: REGIONALISIERUNG UND BILANZIERUNG FÜR DEN NORDATLANTIK UND DAS EUROPÄISCHE NORDMEER. 1998. IV, 166 pp. In German with English summary

68 AMIT GULATI
BENTHIC PRIMARY PRODUCTION IN TWO DIFFERENT SEDIMENT TYPES OF THE KIEL FJORD (WESTERN BALTIC SEA). 1998. 139 pp. In English with German summary

69 RÜDIGER SCHACHT
DIE SPÄT- UND POSTGLAZIALE ENTWICKLUNG DER WOOD- UND LIEFDEFJORDREGION NORDSPITZBERGENS. 1999. 123 pp. + app. In German with English summary

70 GEOMAR FORSCHUNGSZENTRUM FÜR MARINE GEOWISSENSCHAFTEN DER CHRISTIAN-ALBRECHTS-UNIVERSITÄT ZU KIEL. JAHRESBERICHT/ANNUAL REPORT 1997. 1998. 155 pp. In German and English

71 FS SONNE. FAHRTBERICHT/CRUISE REPORT SO118 BIGSET (BIOGEOCHEMICAL TRANSPORT OF MATTER AND ENERGY IN THE DEEP SEA). MUSCAT (OMAN) - MUSCAT (OMAN). 31.03.-11.05.1997. Ed. by OLAF PFANNKUCHE and CHRISTINE UTECHT. 1998. 188 pp. In English

72 FS SONNE. FAHRTBERICHT/CRUISE REPORT SO131 SINUS (SEISMIC INVESTIGATIONS AT THE NINETY EAST RIDGE OBSERVATORY USING SONNE AND JOIDES RESOLUTION DURING ODP LEG 179). KARACHI - SINGAPORE. 04.05-16.06.1998. Ed. by ERNST R. FLUEH and CHRISTIAN REICHERT. 1998. 337 pp. In English

73 THOMAS RICHTER
SEDIMENTARY FLUXES AT THE MID-ATLANTIC RIDGE: SEDIMENT SOURCES, ACCUMULATION RATES, AND GEOCHEMICAL CHARACTERISATION. 1998. IV, 173 + 29 pp. In English with German summary

74 BARBARA MARIA SPRINGER
MODIFIKATION DES BODENNAHEN STRÖMUNGSREGIMES UND DIE DEPOSITION VON SUSPENDIERTEM MATERIAL DURCH MAKROFAUNA. 1999. 112 pp. In German

75 SABINE JÄHMLICH
UNTERSUCHUNGEN ZUR PARTIKELDYNAMIK IN DER BODENGRENZSCHICHT DER MECKLENBURGER BUCHT. 1999. 139 pp. In German

76 WOLFRAM W. BRENNER
GRUNDLAGEN UND ANWENDUNGSMÖGLICHKEITEN DER MIKRO-ABSORPTIONSPHOTOMETRIE FÜR ORGANISCH-WANDIGE MIKROFOSSILIEN. 1999. 141 pp. In German with English summary

77 SUSAN KINSEY
TERTIARY BENTHIC FORAMINIFERAL BIOSTRATIGRAPHY AND PALAEOECOLOGY OF THE HALTEN TERRACE, NORWAY. 1999. VI, 145 pp. In English with German summary

78 HEIDI DOOSE
REKONSTRUKTION HYDROGRAPHISCHER VERHÄLTNISSE IM CALIFORNIENSTROM UND IM EUROPÄISCHEN MITTELMEER ZUR BILDUNGSZEIT ORGANISCH KOHLENSTOFFREICHER SEDIMENTE. 1999. IV, 111 pp. + app. In German with English summary

79 CLAUDIA WILLAMOWSKI
VERTEILUNGSMUSTER VON SPURENMETALLEN IM GLAZIALEN NORDATLANTIK: REKONSTRUKTION DER NÄHRSTOFFBILANZ ANHAND VON CADMIUMKONZENTRATIONEN IN KALKSCHALIGEN FORAMINIFEREN. 1999. 86, XXI pp. In German with English summary

80 FS SONNE. FAHRTBERICHT/CRUISE REPORT SO129. BIGSET (BIOGEOCHEMICAL TRANSPORT OF MATTER AND ENERGY IN THE DEEP SEA). PORT SULTAN QUABOOS - DUBAI. JANUARY 30 - MARCH 9, 1998. Ed. by OLAF PFANNKUCHE and CHRISTINE UTECHT. 1999. 107 pp. In English

81 FS SONNE. FAHRTBERICHT/CRUISE REPORT SO138. GINCO-2 (GEOSCIENTIFIC INVESTIGATIONS ON THE ACTIVE CONVERGENCE ZONE BETWEEN THE EAST EURASIAN AND AUSTRALIAN PLATES ALONG INDONESIA). JAKARTA - JAKARTA. 29.12.1998 - 28.01.1999. Ed. by ERNST R. FLUEH, BERND SCHRECKENBERGER, and JÖRG BIALAS. 1999. 333 pp. In English

82 CRUISE REPORTS: KOMEX I and II (KURILE OKHOTSK SEA MARINE EXPERIMENT)
RV PROFESSOR GAGARINSKY CRUISE 22
RV AKADEMIK M. A. LAVRENTYEV CRUISE 28
VLADIVOSTOK - PUSAN - OKHOTSK SEA - PUSAN - VLADIVOSTOK. 7 JULY - 12 SEPTEMBER 1998. Ed. by NICOLE BIEBOW and EDNA HÜTTEN. 1999. 188, 89 pp. In English

83 GREGOR REHDER
QUELLEN UND SENKEN MARINEN METHANS ZWISCHEN SCHELF UND OFFENEM OZEAN. REGIONALE VARIABILITÄT UND STEUERNDE PARAMETER DER METHANVERTEILUNG UND DER AUSTAUSCH MIT DER ATMOSPHÄRE. 1999. 161, 20 pp. In German with English summary

84 SVEN-OLIVER FRANZ
PLIOZÄNE ZEITREIHEN ZUR REKONSTRUKTION DER TIEFENWASSERZIRKULATION UND DER SILIZIKLASTISCHEN AMAZONASFRACHT IM ÄQUATORIALEN WESTATLANTIK (CEARA SCHWELLE, ODP LEG 154). 1999. 183 pp. In German with English summary

85 SYLKE HLAWATSCH
Mn-Fe-AKKUMULATE ALS INDIKATOR FÜR SCHAD- UND NÄHRSTOFFFLÜSSE IN DER WESTLICHEN OSTSEE. 1999. 132 pp. In German with English summary

86 BETTINA GEHRKE
ZUSAMMENSETZUNG UND VERTEILUNG DER LITHOGENEN FEINFRAKTION IN SPÄTQUARTÄREN SEDIMENTEN DES MITTELATLANTISCHEN REYKJANES RÜCKENS (59°N) - TONMINERALE ALS INDIKATOREN FÜR LIEFERGEBIETE, TRANSPORTMECHANISMEN UND ABLAGERUNGSPROZESSE. 1999. 102 pp.
In German with English summary

87 JENS GREINERT
REZENTE SUBMARINE MINERALBILDUNGEN: ABBILD GEOCHEMISCHER PROZESSE AN AKTIVEN FLUIDAUSTRITTSSTELLEN IM ALEUTEN- UND CASCADIA-AKKRETIONSKOMPLEX. 1999. 196, XX pp.
In German with English summary

88 CRUISE REPORTS: KOMEX V and VI (KURILE OKHOTSK SEA MARINE EXPERIMENT)
RV PROFESSOR GAGARINSKY CRUISE 26
MV MARSHAL GELOVANY CRUISE 1
VLADIVOSTOK - PUSAN - OKHOTSK SEA - PUSAN - VLADIVOSTOK. 30 JULY - 5 SEPTEMBER, 1999.
Ed. by NICOLE BIEBOW, THOMAS LÜDMANN, BORIS KARP, and RUSLAN KULINICH. 2000. 296 pp. In English

89 FS SONNE. FAHRTBERICHT/CRUISE REPORT SO136. TASQWA (QUATERNARY VARIABILITY OF WATER MASSES IN THE SOUTHERN TASMAN SEA AND THE SOUTHERN OCEAN, SW PACIFIC SECTOR). WELLINGTON - HOBART. OCTOBER 16 - NOVEMBER 12, 1998. Ed. by JÖRN THIEDE, STEFAN NEES et al. 1999. 78, 106 pp. In English

90 FS SONNE. FAHRTBERICHT/CRUISE REPORT SO142. HULA (INTERDISCIPLINARY INVESTIGATIONS ON THE TIMING OF THE HAWAII-EMPEROR BEND AND THE ORIGIN OF LITHOSPHERIC ANOMALIES ALONG THE MUSICIAN SEAMOUNT CHAIN. MIDWAY - HONOLULU. MAY 30 - JUNE 28, 1999. Ed. by ERNST R. FLUEH, JOHN O'CONNOR, JASON PHIPPS MORGAN, and JOCHEN WAGNER. 1999. 224 pp. In English

91 J. HAUSCHILD, T. GINDLER, D. RISTOW, A. BERHORST, C. BÖNNEMANN, K. HINZ
DFG-FORSCHUNGSPROJEKT „*KRUSTENSPLITTER*". 3D-MAKRO-GESCHWINDIGKEITSBESTIMMUNGEN UND 3D-TIEFENMIGRATION DES SEISMISCHEN 3D-COSTA-RICA-DATENSATZES. 1999. 85 pp.
In German with English summary

92 FS AKADEMIK MSTISLAV KELDYSH. Fahrtbericht Reise Nr. 40: Norwegisch-Grönländische See, 27.6.-29.7.1998. Hrsg. von J. MIENERT, A. OMLIN, T. GÖLZ, D. LUKAS, J. POSEWANG. 1999. 65, 7 pp. In German

93 FS SONNE. FAHRTBERICHT/CRUISE REPORT SO143 TECFLUX. Ed. by GERHARD BOHRMANN, PETER LINKE, ERWIN SUESS, and OLAF PFANNKUCHE. 2000. 243 pp. In English

94 FS SONNE. FAHRTBERICHT/CRUISE REPORT SO144-1&2. PAGANINI (PANAMA BASIN AND GALAPAGOS "PLUME" - NEW INVESTIGATIONS OF INTRAPLATE MAGMATISM). SAN DIEGO - CALDERA. SEPTEMBER 7 - NOVEMBER 7, 1999. Ed. by JÖRG BIALAS, ERNST R. FLUEH, and GERHARD BOHRMANN. 1999. 437 pp. + app.
In English

95 CHRISTIAN MATTHIAS HÜLS
MILLENNIAL-SCALE SST VARIABILITY AS INFERRED FROM PLANKTONIC FORAMINIFERAL CENSUS COUNTS IN THE WESTERN SUBTROPICAL ATLANTIC. 2000. 81 pp. + app. In English with German summary

96 FS SONNE. FAHRTBERICHT/CRUISE REPORT SO146-1&2. GEOPECO (GEOPHYSICAL EXPERIMENTS AT THE PERUVIAN CONTINENTAL MARGIN - INVESTIGATIONS OF TECTONICS, MECHANICS, GASHYDRATES, AND FLUID TRANSPORT). ARICA - TALCAHUANO. MARCH 1 - MAY 4, 2000. Ed. by JÖRG BIALAS and NINA KUKOWSKI. 2000. 508 pp. In English

97 GEOMAR FORSCHUNGSZENTRUM FÜR MARINE GEOWISSENSCHAFTEN DER CHRISTIAN-ALBRECHTS-UNIVERSITÄT ZU KIEL. JAHRESBERICHT/ANNUAL REPORT 1998/1999. 2000. 261 pp. In German and English

98 RV SONNE. CRUISE REPORT SO148. TECFLUX-II-2000 (TECTONICALLY-INDUCED MATERIAL FLUXES. VICTORIA - VICTORIA - VICTORIA. 20.07.-15.08.2000. Ed. by PETER LINKE and ERWIN SUESS. 2001. 122 pp. In English

99 GEOMAR FORSCHUNGSZENTRUM FÜR MARINE GEOWISSENSCHAFTEN DER CHRISTIAN-ALBRECHTS-UNIVERSITÄT ZU KIEL. JAHRESBERICHT/ANNUAL REPORT 2000. 2001. 180 pp. In German and English

100 FS POSEIDON. FAHRTBERICHT/CRUISE REPORT POS 260 BIGSET (BIOGEOCHEMICAL TRANSPORT OF MATTER AND ENERGY IN THE DEEP SEA). LEIXOES/OPORTO (PORTUGAL) - GALWAY (IRELAND) - CORK (IRELAND). 26.04.-23.06.2000. Ed. by OLAF PFANNKUCHE and CHRISTINE UTECHT. 2001. 67 pp. In English

101 FS SONNE. FAHRTBERICHT/CRUISE REPORT SO159. SALIERI (SOUTH AMERICAN LITHOSPHERIC TRANSECTS ACROSS VOLCANIC RIDGES). GUAYAQUIL - GUAYAQUIL. AUGUST 21 - SEPTEMBER 17, 2001. Ed. by ERNST R. FLÜH, JÖRG BIALAS, and PHILIPPE CHARVIS. 2001. 256 pp. In English

102 FS SONNE. FAHRTBERICHT/CRUISE REPORT SO161-1&4. SPOC (SUBDUCTION PROCESSES OFF CHILE). ANTOFAGASTA - VALPARAISO. OCTOBER 9 - OCTOBER 15, 2001 &
VALPARAISO - VALPARAISO. NOVEMBER 30 - DECEMBER 23, 2001.
Ed. by ERNST R. FLÜH, HEIDRUN KOPP, and BERND SCHRECKENBERGER. 2002. 383 pp. In English

103 FS SONNE. FAHRTBERICHT/CRUISE REPORT SO162. INGGAS TEST (INTEGRATED GEOPHYSICAL CHARACTERISATION AND QUANTIFICATION OF GAS HYDRATES - INSTRUMENT TEST CRUISE). VALPARAISO - BALBOA. FEBRUARY 21 - MARCH 12, 2002.
Ed. by TIMOTHY JOHN RESTON and JÖRG BIALAS. 2002. In English

104 FS SONNE. FAHRTBERICHT/CRUISE REPORT SO158. MEGAPRINT (MULTIDISCIPLINARY EXAMINATION OF GALÁPAGOS PLUME RIDGE INTERACTION). ISLA DE PASCUA - GUAYAQUIL. JULY15 - AUGUST 20, 2001.
Ed. by REINHARD WERNER. 2002. 53 pp + app. In English

105 CRUISE REPORT: KOMEX (KURILE OKHOTSK SEA MARINE EXPERIMENT)
RV PROFESSOR GAGARINSKY CRUISE 32. SERENADE. SEISMO-STRATIGRAPHIC RESEARCH OFF NORTHERN SAKHALIN AND IN THE DERUGIN BASIN. VLADIVOSTOK - PUSAN - SEA OF OKHOTSK - PUSAN - VLADIVOSTOK. AUGUST 31 - SEPTEMBER 29, 2001.
Ed. by THOMAS LÜDMANN, BORIS BARANOV, and BORIS KARP. 2002. 42 pp. In English

106 FS SONNE. FAHRTBERICHT/CRUISE REPORT SO163. SUBDUCTION I. MULTI-SYSTEM ANALYSIS OF FLUID RECYCLING AND GEODYNAMICS AT THE CONTINENTAL MARGIN OFF COSTA RICA.
SO163-1. BALBOA- CALDERA. MARCH 13 - APRIL 20, 2002
SO163-2. CALDERA - BALBOA. APRIL 20 - MAY 21, 2002.
Ed. by WILLI WEINREBE and ERNST R. FLÜH. 2002. 534 pp. In English

107 GEOMAR FORSCHUNGSZENTRUM FÜR MARINE GEOWISSENSCHAFTEN DER CHRISTIAN-ALBRECHTS-UNIVERSITÄT ZU KIEL. JAHRESBERICHT/ANNUAL REPORT 2001. In prep. In German and English

108 RV METEOR. CRUISE REPORT M52/1: MARGASCH (MARINE GAS HYDRATES OF THE BLACK SEA). ISTANBUL - ISTANBUL. JANUARY 2 - FEBRUARY 1, 2002.
Ed. by GERHARD BOHRMANN and SILKE SCHENCK. 2002. 202 pp. In English

109 RV SONNE. CRUISE REPORT SO164. RASTA (Rapid Climate Changes in the Western Tropical Atlantic - Assessment of the biogenous and sedimentary record). BALBOA - BALBOA. MAY 22 - JUNE 2002. Ed. by DIRK NÜRNBERG, JOACHIM SCHÖNFELD, WOLF-CHRISTIAN DULLO, and MARCUS RÜHLEMANN. 2003. 151 pp. In English

110 CRUISE REPORT : KOMEX (KURILE OKHOTSK SEA MARINE EXPERIMENT)
RV AKADEMIK M.A. LAVRENTYEV CRUISE 29, LEG 1 and LEG 2. VLADIVOSTOK – PUSAN – OKHOTSK SEA – PUSAN – OKHOTSK SEA – PUSAN – VLADIVOSTOK. MAY 25 – AUGUST 05 2002. Ed. by NICOLE BIEBOW, RUSLAN KULINICH, and BORIS BARANOV. 2003. 190, 176 pp. In English